# DEVELOPMENT OF ELECTRONIC NOSE SYSTEM BASED ON OPTICALLY-ACTIVE ORGANIC THIN FILM SENSORS AND MOLECULAR DESIGN

**SUMANA KLADSOMBOON**

**A THESIS SUBMITTED IN PARTIAL FULFILLMENT**
**OF THE REQUIREMENTS FOR**
**THE DEGREE OF DOCTOR OF PHILOSOPHY (PHYSICS)**
**FACULTY OF GRADUATE STUDIES**
**MAHIDOL UNIVERSITY**
**2013**

Thesis
entitled

# DEVELOPMENT OF ELECTRONIC NOSE SYSTEM BASED ON OPTICALLY-ACTIVE ORGANIC THIN FILM SENSORS AND MOLECULAR DESIGN

Sumana Kladsomboon
Miss Sumana Kladsomboon,
Candidate

T. Kerdcha
Asst. Prof. Teerakiat Kerdcharoen,
Ph.D. (Physical Chemistry)
Major Advisor

Mr. Adisorn Tuantranont,
Ph.D. (Electrical Engineering)
Co-advisor

Theeraporn Puntheeranurak
Asst.Prof. Theeraporn Puntheeranurak,
Ph.D. (Molecular Genetics and Genetic Engineering)
Co-advisor

Lieberzeit
Prof. Peter Lieberzeit,
Ph.D. (Chemistry)
Co-advisor

B. Mahi
Prof. Banchong Mahaisavariya,
M.D., Dip Thai Board of Orthopedics
Dean
Faculty of Graduate Studies
Mahidol University

Narin Nuttavut
Asst. Prof. Narin Nuttavut,
Ph.D. (Physics)
Program Director
Doctor of Philosophy Program in Physics
Faculty of Science Mahidol University

Thesis
entitled

# DEVELOPMENT OF ELECTRONIC NOSE SYSTEM BASED ON OPTICALLY-ACTIVE ORGANIC THIN FILM SENSORS AND MOLECULAR DESIGN

was submitted to the Faculty of Graduate Studies, Mahidol University
for the degree of Doctor of Philosophy (Physics)
on
July 29, 2013

Sumana Kladsomboon
Miss Sumana Kladsomboon
Candidate

Mr. Sirapat Pratontep,
Ph.D. (Physics)
Chair

Prof. Peter Lieberzeit,
Ph.D. (Chemistry)
Member

T. Kerdcha
Asst. Prof. Teerakiat Kerdcharoen,
Ph.D. (Physical Chemistry)
Member

Theeraporn Puntheeranurak
Asst. Prof. Theeraporn Puntheeranurak,
Ph.D. (Molecular Genetics and Genetic Engineering)
Member

Mr. Adisorn Tuantranont,
Ph.D. (Physics)
Member

B. Maha
Prof. Banchong Mahaisavariya,
M.D., Dip Thai Board of Orthopedics
Dean
Faculty of Graduate Studies
Mahidol University

Prof. Skorn Mongkolsuk,
Ph.D. (Biological Science)
Dean
Faculty of Science
Mahidol University

# ACKNOWLEDGEMENTS

I would like to express my deep and sincere gratitude to my advisors, Asst. Prof. Dr. Teerakiat Kerdcharoen, Asst. Prof. Dr. Theeraporn Puntheeranurak and Dr. Adisorn Tuantranont, for their advice, idea, suggestion and encouragement throughout. I am deeply grateful to my co-advisor Univ. Prof. Dr. Peter Lieberzeit from department of analytical chemistry at University of Vienna who gave the idea about the molecular imprinted polymer (MIP).

I gratefully acknowledge the ACHE-Ph.D.-SW-INV scholarship from the Commission of Higher Education for the financial support. I also thank the National Science and Technology Development Agency (NSTDA) and their staff for general supports.

I also wish to thank Dr. Chatchawal Wongchoosuk and Dr. Panida Lorwongtragool for their guidance in electronic nose system. Additionally, I want to thanks to my friends and members of Center of Intelligent Materials and Systems, particularly, Thara, Songpun, Treenet, Mario, Chayanin and Arunee, for their helps and suggestions during this thesis. Moreover I wish to thanks to the Center of Intelligent Materials and Systems (CIMS) and the Center of Nanoscience and Nanotechnology, Mahidol University for generously supplying computation and laboratorial stations.

Finally, I greatly respect my parent and my family, who gave me many chances to study and kindly help me throughout my whole life.

Sumana Kladsomboon

DEVELOPMENT OF ELECTRONIC NOSE SYSTEM BASED ON OPTICALLY-ACTIVE ORGANIC THIN FILM SENSORS AND MOLECULAR DESIGN

SUMANA KLADSOMBOON 5237031 SCPY/D

Ph.D. (PHYSICS)

THESIS ADVISORY COMMITTEE: TEERAKIAT KERDCHAROEN, Ph.D. (PHYSICAL CHEMISTRY), ADISORN TUANTRANONT, Ph.D. (ELECTRICAL ENGINEERING), THEERAPORN PUNTHEERANURAK, Ph.D. (MOLECULAR GENETICS AND GENETIC ENGINEERING), PETER LIEBERZEIT, Ph.D. (CHEMISTRY)

## ABSTRACT

The sense of smell is an important sense for human in daily life. Many researchers have been trying to fabricate a device that mimics the human olfactory system, called “Electronic nose” (e-nose). This instrument comprises an array of gas sensor, a transducer and a pattern recognition analysis. In this thesis, organic thin film gas sensors have been fabricated from organic dyes, namely, metallo-porphyrin (MP) and metallo-phthalocyanine (MPc). Both compounds have been used as sensing materials for volatile organic compounds (VOC) based on optical detection. The interaction energy and the charge transfer between sensing materials and VOC molecules were investigated by the density functional theory (DFT) with the B3LYP 6-31G* basis set. The objective of this thesis is to investigate various kinds of optical gas sensors, for example, mixtures layer of MP and MPc, nanocomposite between MP and multiwall carbon nanotube (MWCNT) and molecularly imprinted polymer (MIP) mixed MPc. Optical technique was used as the transducer to transform the physical properties of sensing material to the electronic signal. Two types of optical e-nose have been explored. The first type employed the UV-vis spectrophotometer to monitor optical spectral changes of the area integral under absorption spectrum. The second type employed light-emitting diodes (LEDs) as the light source and CMOS photodetector was as transducer. The latter e-nose system was invented as a portable device. Finally, the principal component analysis (PCA) was performed as the pattern recognition to investigate the performance of our e-nose systems. The results confirmed that both e-noses successfully classified VOCs vapor based on optically-active organic thin films.

KEY WORDS: PORPHYRINS / PHTHALOCYANINES / OPTICAL GAS SENSOR/ E-NOSE/ DENSITY FUNCTIONAL THEORY

104 pages

การพัฒนาระบบจมูกอิเล็กโทรนิกส์โดยใช้ฟิล์มบางของสารอินทรีย์ชนิดที่ไวต่อแสง
และการสร้างแบบจำลองโมเลกุล
DEVELOPMENT OF ELECTRONIC NOSE SYSTEM BASED ON OPTICALLY-ACTIVE
ORGANIC THIN FILM SENSORS AND MOLECULAR DESIGN

สุมนา กลัดสมบูรณ์ 5237031 SCPY/D

ปร.ด. (ฟิสิกส์)

คณะกรรมการที่ปรึกษาวิทยานิพนธ์: ธีรเกียรติ์ เกิดเจริญ, Ph.D. (PHYSICAL CHEMISTRY), อดิสร เตือนตรานนท์, Ph.D. (ELECTRICAL ENGINEERING), ธีราพร พันธุ์ธีรานุรักษ์, Ph.D. (MOLECULAR GENETICS AND GENETIC ENGINEERING), PETER LIEBERZEIT, Ph.D. (CHEMISTRY)

## บทคัดย่อ

ประสาทสัมผัสการรับรู้กลิ่นเป็นสิ่งสำคัญสำหรับชีวิตประจำวันของมนุษย์ นักวิจัยพยายามที่จะประดิษฐ์อุปกรณ์เลียนแบบระบบรับรู้กลิ่นของมนุษย์ ที่เรียกว่า “จมูกอิเล็กทรอนิกส์” (e-nose) เครื่องมือนี้ประกอบด้วย อะเรย์ของเซ็นเซอร์ตรวจวัดก๊าซ, ตัวแปลงสัญญาณ และส่วนวิเคราะห์จดจำรูปแบบของกลิ่น ในวิทยานิพนธ์เล่มนี้เซ็นเซอร์ตรวจวัดก๊าซเชิงแสงแบบฟิล์มบางได้ถูกประดิษฐ์ขึ้นจากสีย้อม (dye) อินทรีย์ คือ เมทัลโลพอร์ไฟริน (MP) และ เมทัลโลพทาโลไซยานีน (MPc) ซึ่งสารประกอบทั้งสองมีคุณสมบัติในการตรวจจับไอระเหยโดยใช้วิธีการทางแสง อันตรกิริยาและการเปลี่ยนแปลงของประจุไฟฟ้าระหว่างโมเลกุลของวัสดุที่ใช้ตรวจจับกับโมเลกุลของไอระเหยได้ถูกตรวจสอบโดยวิธีของทฤษฎีเดนซิติฟังก์ชัน (DFT) ใช้เบซิสเซต B3LYP 6-31G* วัตถุประสงค์ของวิทยานิพนธ์นี้คือการประดิษฐ์เซ็นเซอร์ตรวจวัดก๊าซเชิงแสงหลากหลายชนิด ตัวอย่างเช่น การใช้เมทัลโลพอร์ไฟริน และเมทัลโลพทาโลไซยานีน แบบผสมผสานกัน, การใช้สารผสมระหว่าง MP กับท่อนาโนคาร์บอน (MWCNT) และ การใช้สารผสมของพอลิเมอร์ที่มีรอยพิมพ์ประทับโมเลกุล (MIP) กับ MPc โดยที่เทคนิคทางแสงถูกนำมาใช้ในการแปลงจากคุณสมบัติทางกายภาพของวัสดุเซ็นเซอร์มาเป็นสัญญาณทางอิเล็กทรอนิกส์ จมูกอิเล็กทรอนิกส์ทั้งสองชนิดได้ถูกศึกษา ชนิดแรกคือจมูกอิเล็กทรอนิกส์ที่ใช้เครื่องวัดค่าการดูดกลืนแสงในการตรวจสอบพื้นที่ใต้กราฟของสเปกตรัมการดูดกลืนแสงที่เปลี่ยนไป ส่วนชนิดที่สองนั้นใช้ไดโอดเปล่งแสง (LED) เพื่อเป็นแหล่งกำเนิดแสง และใช้ตัวตรวจจับทางแสง (Photodetector) สำหรับอ่านค่าการเปลี่ยนแปลงความเข้มแสง จมูกอิเล็กทรอนิกส์เครื่องหลังนี้ได้ถูกสร้างขึ้นให้เป็นอุปกรณ์ที่พกพาได้ สุดท้ายนี้ได้ใช้การวิเคราะห์การจำแนกกลิ่นด้วยวิธีวิเคราะห์องค์ประกอบหลัก (PCA) พบว่าเครื่องจมูกอิเล็กทรอนิกส์ที่ใช้ก๊าซเซ็นเซอร์ฟิล์มบางทั้งสองแบบ ประสบความสำเร็จในการจำแนกกลิ่นของไอระเหยต่าง ๆ

104 หน้า

# CONTENTS

# CONTENTS (cont.)

# CONTENTS (cont.)

# CONTENTS (cont.)

# LIST OF TABLES

# LIST OF FIGURES

# LIST OF FIGURES (cont.)

# LIST OF FIGURES (cont.)

# LIST OF FIGURES (cont.)

# LIST OF FIGURES (cont.)

# LIST OF FIGURES (cont.)

# CHAPTER I
# INTRODUCTION

## 1.1 Overview and Outline

Sensory perception has been the important sensing systems in human, especially for smell or scent. Human uses their odorant receptors in the nasal cavity to recognize up to 10,000 kinds of odors. Scent plays a major role in our daily life, such as detection of harmful conditions and food selection. Many research studies have been developed scent technology to facilitate human activities. Electronic nose (e-nose) is a scent technology for odor classification that resembles the natural olfactory system. In the olfactory system, there are millions odorant receptors working for odor detection. Signals from the odorant receptors are accumulated and transmitted to the brain by the olfactory bulb. Then, the brain classifies the odor types using pattern recognition based on past memory. In turn, the e-nose system consists of a gas sensor array, signal processing and pattern recognition, reflecting the biological odorant receptors, olfactory bulb and brain, respectively [1]. In contrast to biological nose that involves very complex biological and neural process, odor sensing in e-nose is based on much simpler transduction techniques, such as electrochemical, gravimetric and optical approaches. Electrochemical transduction, as often implemented in the metal-oxide semiconductor gas sensor, is the most popular technology. The most used sensing material in the metal-oxides gas sensors is $SnO_2$ thin film, as reported to detect several industrial gases such as methane, $H_2$, CO, $H_2S$ and alcohols [2-3]. But Metal-oxide gas sensors have to work at high temperature using additional electrical power to supply the heater. Another electrochemical technology based on poly polymer/carbon nanotube nano-composites was introduced to allow measurement at room temperature [4]. Gravimetric transduction employs piezoelectric technique, usually known as the quartz crystal microbalance (QCM), for sensitive mass measurement by observing the change of oscillating frequency upon adsorption of the odorants on the crystal surface. For example, Ding et al. reported a QCM-based device coated with copper(II) tetra-tert-butyl-5,10,15,20-tetraazaporphyrin that was sensitive to hydrocarbon gases, i.e., hexane, benzene and toluene [5]. Optical transducer is an interesting choice for developing e-nose technology. General optical instrument can be used in e-nose setups, such as UV-Vis spectrophotometer, charge coupled device (CCD) cameras and photo detector [6]. Moreover, new light sources have been developed, for examples, solid-state lasers, laser diodes, and light-emitting diodes (LEDs) [7]. LED technology was developed by Holonyak Jr. et al. based on GaAsP layers, which emits red light [8]. Then LED has been applied to several problems in chemical analysis such as absorbance, fluorescence and special analytical applications measurement [9]. Most optical devices are easy to obtain because they have been developed for several purposed such as telecommunications, entertainment and computer. Therefore, optical devices are of reasonable price. In the first part, optical e-nose based on using UV-Vis spectrophotometer was developed in this thesis. Then, LED and CMOS photo detector were used as light source and detector, respectively. Finally, optical e-nose was developed in the form of portable briefcase.

Organic semiconductor materials such as Metallo-porphyrin (MP) and metallo-phthalocyanine (MPc) can work as gas sensor based on the change in electrical or optical properties via charge transfer on their surface upon interactions with volatiles. It was found that MP and MPc are very versatile sensing materials for detection of a wide range of gases. For examples, metallo-octaethyl porphyrins thin films were tested with 2-propanol, ethanol, acetone and cyclohexane by recording the reflected light intensity change [10]. Blending of MP and MPc also lead to enhancement of the sensor, as reported by Spadavecchia and co-workers [11]. They blended phthalocyanine and porphyrin to fabricate the sensing materials for methanol, ethanol and isopropanol detection. They also proposed a very novel technique based on optical absorption using MP and MPc as sensing materials, in which it employs only one sensor film to detect and classify several gases depending on their selectivity on specific wavelength regions. Many research works have reported that MP and MPc are very effective sensing materials for optical sensing due to their versatile and tunable spectra based on variation of central metal and substituent of the molecules [12-13]. Density functional theory (DFT) based on basis set of B3LYP 6-31G*was used to optimize molecular structure of the MP and MPc compounds which compose of carbon, hydrogen and nitrogen atoms. Geometry and electronic structure of sensing molecule was optimized. Charge transfer between sensing molecule and analyte molecule was found by this calculation [14-15].

MP and MPc were chosen to prepare sensing layer based on optical detection in this thesis. In chapter III, we prepared sensing material by mixing three types of organic compounds which possess different absorption regions. The UV-Vis spectrophotometer was modified to function in e-nose system. DFT calculation was used to interpret the ground state molecular structure and charge transfer between sensing molecule and analyte molecule. In chapter IV, optical e-nose was developed by using LED as light source and photo detector as light intensity detector. And mixed layer of MP and MPc was developed by thermal annealing. This sensing material was tested with alcohol, dried seafood and beers. In chapter V, the enhancement of an e-nose system based on combined optical and electrochemical transduction was reported. Porphyrin and multi-walled carbon nanotube (MWCNT) composite was used as the sensing materials based on its good optoelectronic properties. Finally, optical gas sensors were developed by using molecular imprinted polymer (MIP) technique based on polyurethane (PU) and phthalocyanine composite as presented in chapter VI. This gas sensor was tested by using the optical e-nose based on LED arrays and quartz crystal microbalance (QCM) measurement. All types of optical gas sensor (chapter III - VI) were analyzed by pattern recognition, namely, principal component analysis (PCA). PCA is a linear transformation that can efficiently reduce data dimension into a more comprehensible visualization. This calculation has been usually used to classify data in e-nose technology [16]. The flow chart of this thesis is shown in Figure 1.1.

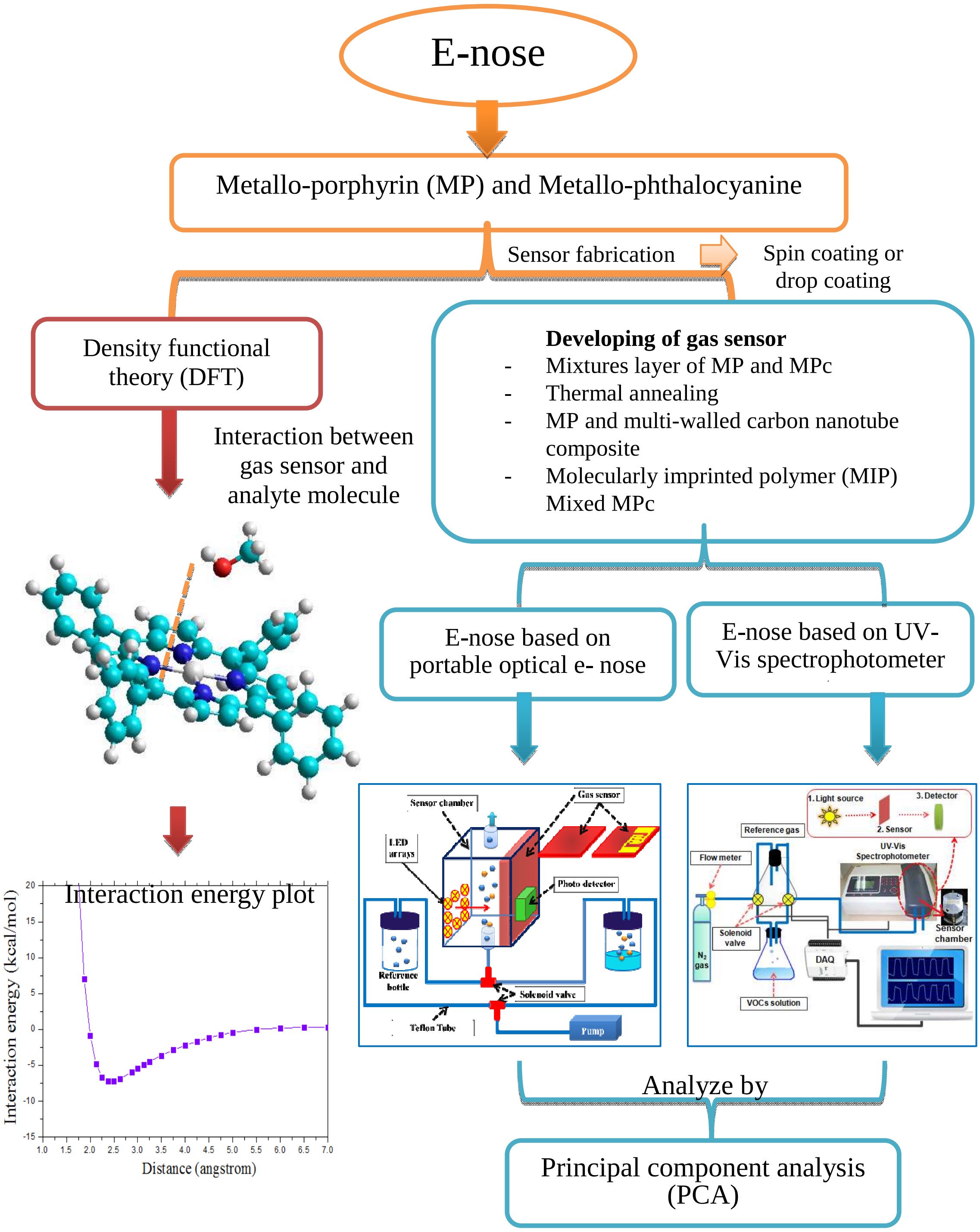

**Figure 1.1** The flow chart of this thesis.

## 1.2 Objectives

1. To develop the sensitivity of optically-active organic thin film gas sensors based on porphyrin and phthalocyanine compounds.
2. To study the molecular structure and interaction mechanism between the sensing materials and analyte molecules.
3. To develop the portable optical electronic nose system based on a LED array.
4. To apply a portable optical electronic nose in the areas of food and agriculture product.
5. To fabricate gas sensors by using molecularly imprinted technology.
6. To integrate the new sensors into portable optical e-nose.

## 1.3Methodology

1. Searching for efficient optical gas sensor materials based on porphyrin and phthalocyanine structures which are active with volatile organic compounds (VOCs) vapor based on spin-coating or drop-coating technique.
2. Studying the molecular structure and electronic properties of sensing molecule by using density functional theory (DFT) calculation.
3. Developing a new portable optical electronic nose system by using the array of light emitting diode (LED) and photo-detector.
4. Applying the portable optical electronic nose in the areas of food and agriculture, such as beer and seafood food.
5. Searching for efficient optical gas sensor materials based on molecular imprinted polymer which is active with specific volatile organic compounds vapors.
6. Applying molecular imprinted polymer gas sensor in the portable optical electronic nose.

# CHAPTER II

# ELECTRONIC NOSE SYSTEM AND GAS SENSOR

## 2.1 Background of Electronic Nose System

The olfaction system has been the important system for the living things. Especially, human need this sense for several activities such as feeding and detecting of potentially harmful conditions to get the good quality of life. Therefore, the sense has been the important parameter for producing food and beverage products. However, our olfaction system has a limit of detection to the complex aroma which is generated from multi volatile molecules. The limit of detection in human depends on individual experience and training [17]. The organic chemist tried to analyze the odor by using the analyzed instrument. For example in wine product, the storage method of aroma in wine bottle had been investigated by gas chromatography (GC) and GC-mass spectrometry (MS) based on principal component analysis (PCA) calculation [18]. But this method takes a long time and complicates to analyze the data. Therefore, an e-nose has become a new technology for odor classification by mimicking the functions of the olfactory system in human. In the olfactory system, there are millions odorant receptors in the nasal working for odor detection. The size of odorant receptor is specific to the target molecule. Signals from the odorant receptors are accumulated and transmitted to the brain by the olfactory bulb. Then, the brain classifies the odor types using pattern recognition based on past memory. In the e-nose system, there are gas sensor array, signal processing and pattern recognition as shown in Figure 2.1 [1]. The volatile odorant is detected by the gas sensor array in the interaction process. Then the electronic signal is generated by the transducer that depends on the type of gas sensor such as mass, optical and electrical transducers. Finally, pattern recognition (database) based on statistical calculation is used to identify the volatile odorant. Therefore, the first step to develop the e-nose is the fabrication of sensitivity and stability of the chemical gas sensors that represent in the topic of chemical gas sensor.

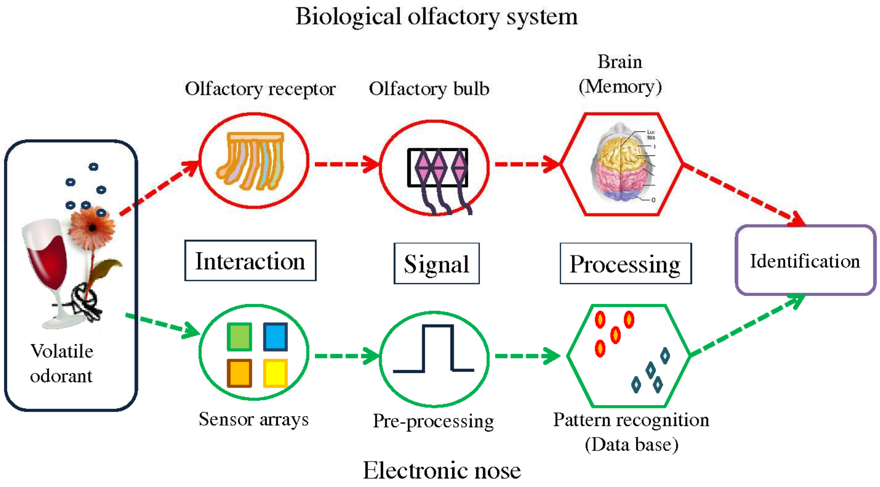

Figure 2.1 The basic diagram of the comparing between biological and electronic noses.

## 2.2 Chemical Gas Sensor

In contrast to biological nose that involves very complex biological and neural process, odor sensing in e-nose is based on much simpler transduction techniques such as electrochemical, gravimetric and optical approaches. The details of each technique are presented in this section.

### 2.2.1 Electrochemical Technique

Electrochemical transduction, as often implemented in the metal-oxide semiconductor gas sensor, is the most popular technology due to its established advantages such as low cost, compactness and easy integration with integrated circuit technology. The most used sensing material in the metal-oxides gas sensors is $SnO_2$ thin film, as reported to detect several industrial gases such as methane, $H_2$, CO, $H_2S$ and methanol [2-3]. Metal-oxide gas sensors work at high temperature using additional electrical power to supply the heater. Another electrochemical technology based on polymer/carbon nanotube nanocomposites was introduced to allow measurement at room temperature [4]. This carbon nanotube was dispersed in the matrix of different polymers such as polyvinyl chloride (PVC), cumene terminated polystyrene-co-maleic anhydride (cumene PSMA), poly(styrenecomaleic acid) partial isobutyl/methyl mixed ester (PSE) and polyvinylpyrrolidon (PVP). The polymer/carbon nanotube was tested with the sample in real life which was dried seafood.

### 2.2.2 Gravimetric Technique

Gravimetric transduction employs piezoelectric technique, usually known as the quartz crystal microbalance (QCM), for sensitive mass measurement by observing the change of oscillating frequency upon adsorption of the odorants on the crystal surface. For example, Ding et al. reported a QCM-based device coated with copper (II) tetra-tert-butyl-5,10,15,20-tetraazaporphyrin that is sensitive to hydrocarbon gases, i.e., hexane, benzene and toluene.

The principle of mass measurements is the relationship between the changing of the quartz frequency and the added mass of on quartz surface [19]. The calculation of this relationship is shown in equation (1)

$$\Delta f = \frac{-f_q{}^2 M_f}{N\rho_q S} = \frac{-f_q{}^2 m_f}{N\rho_q} \qquad (2.1)$$

where $f_q$ is the fundamental resonant frequency of the quartz.

$N$ is the frequency constant of the specific crystal cut ( $N_{AT}$ = 1.67 x $10^5$ Hz . cm).

$\rho_q$ is the quartz density (2.65 kg/$dm^3$ ).

$S$ is the surface area of the deposited film.

$M_f$ is the mass of deposited film.

$m_f$ is the areal density $M_f/S$ (the area density).

The gold electrodes are coated on both side of quartz template as shown in Figure 2.2. Therefore, the thickness of the film ( $l_f$ ) is calculated by equation (2)

$$l_f = \frac{m_f}{\rho_f} \qquad (2.2)$$

where $\rho_f$ is the density of the deposited film.

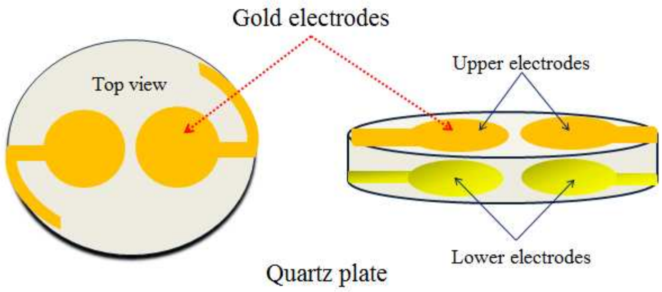

Figure 2.2 The gold electrodes on quartz template for mass measurement.

Molecularly imprinted polymers (MIPs) have been one popular method to prepare specific sensing layer. The main idea of this method is the cavity for the specific analyte or template molecule in the sensing polymer [20]. The analyte molecules which do not have interaction with the polymer in the polymerization process are added to the initial monomer and suitable cross-linking monomers. Then the analyte molecules are removed by evaporation method in the polymerization process. The cavities in the shape of analyte molecule are used to detect the specific molecule as shown in Figure 2.3. The advantage points of molecularly imprinted polymers are the selective sensing material similar to the natural receptor, the straightforward transducer and the inexpensive materials with high thermally and mechanically stable. The details about MIPs are discussed in the section 2.4.

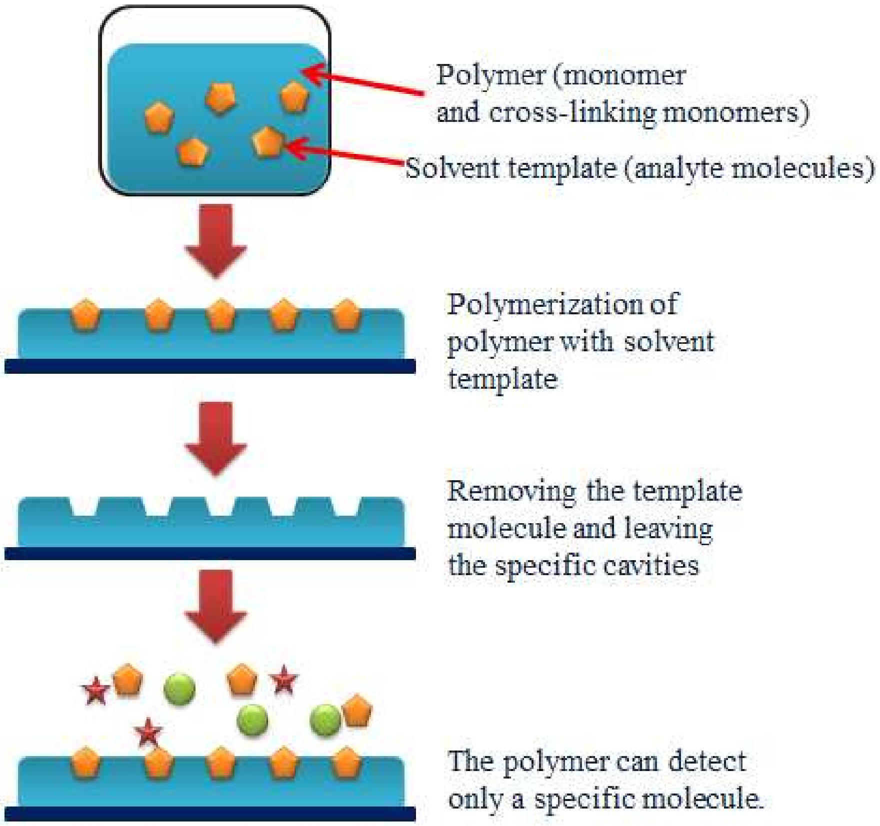

Figure 2.3 Molecularly imprinting process with solvent template.

MIP gas sensors based on the QCM method have been investigated. For example, the QCM arrays of polyurethane were used to detect water, 1-propanol, 1-butanol and ethyl acetate vapors [21]. The modification of QCM surface for gas detection has been an interesting topic according to Serhiy Korposh and coworker [22]. They tried to enhance the sensing layers for humidity monitoring based on polymer and dye molecule. Two porphyrin derivatives (Tetrakis-(4-sulfophenyl)-porphine and 5,10,15,20 Tetrakis-(4-sulfophenyl)-21H,23H-porphine manganese (III) chloride were used to enhance the surface of poly (sodium 4-styrenesulfonate) and poly (diallyldimethylammonium chloride) which were deposited on QCM plate. Porphyrin based polymer thin films presented higher sensitivity with water molecule in gas phase as compared with pure polymer thin film.

### 2.2.3 Optical Technique

More recently, the optical gas sensors have been developed by various methods such as wave guide, luminescent, surface plasmon resonance and colorimetric methods. All of them have been applied in different applications, for example, food, healthcare and industrial safety process control. The advantage of the optical technique is the rich availability of transduction methods because optical instruments have been fabricated for the various applications before. Therefore, the light sources, optics, and detectors, which are the principle composition of this instrument have been continually developed. The optical instruments have been found in every principle laboratory. But there are disadvantages for optical techniques, for example, optical measurements need more complicated data processing than other transducing methods. In this topic, optical methods that used MP and MPc as the sensing material were discussed.

#### 2.2.3.1 Microwave Gas Sensor

Microwave gas sensor is one type of gas sensor based on microwave transducer. Guillaume Barochi and coworkers studied the gas sensing properties of cobalt phthalocyanines by using the wave guide technique in the frequency of microwave region [23]. The principle concept of microwave transducer is presented in Figure 2.4. The permittivity of semiconductor material such as phthalocyanines compound is measured by vectorial network analyzer during the gas absorption. The permittivity change under electromagnetic wave in microwave frequency range (300 MHz to 300 GHz) is recorded in the ratio between reflected wave and incidental wave (Γ(f)).

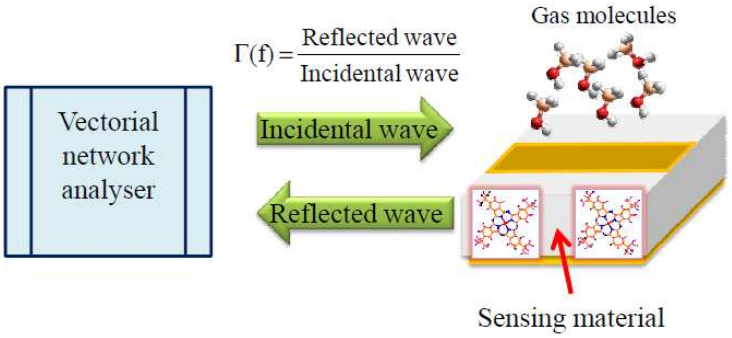

Figure 2.4 The principle diagram of microwave gas sensor based on organic sensing material (phthalocyanine molecule)

#### 2.2.3.2 Colorimetric

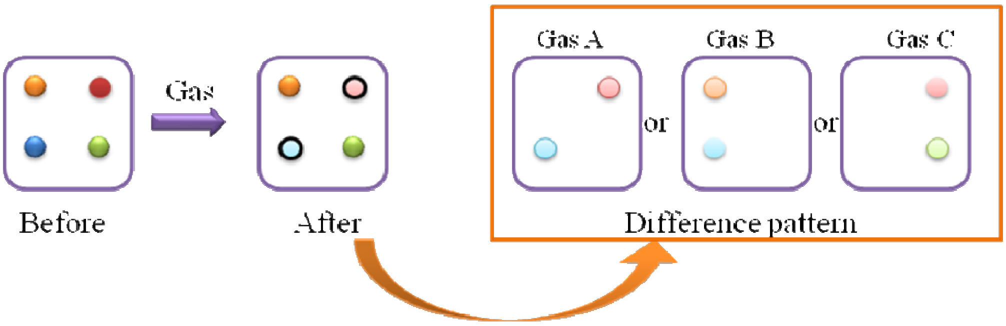

Figure 2.5 The duplicate diagram of sensing arrays in colorimetric technique. Proposed by Chen Zang et al. [24].

The colorimetric sensor arrays have been developed for identification and quantification in food and beverages based on gas or liquid phase. The idea of this method is the color change of organic dye after interacts with VOCs in gas or liquid phase. Figure 2.5 presents the diagram of colorimetric sensor arrays in three steps. At the initial step, the sensor arrays are prepared from the color organic molecule such as porphyrin and phthalocyanine, which are represented in several colors. Then the sensor arrays are exposure to the analyst gas. Therefore, the color of some dye are changed in the different pattern depending on the VOCs types. The color changes of dye are observed by eyes or flatbed scanner [25]. There is some disadvantage point for this method, especially the number of sensing array that should be enough to separate the various kinds of analyze gas. It means that this system needs several kind of dye for data processing and analysis. For example, Chen Zang and coworkers generated the sensing arrays from 36 dyes for water classification [26].

### 2.2.4 Metal Oxide Gas Sensor

Metal oxide gas sensors are fabricated from the n-type or p-type semiconductors. For example, $SnO_2$, ZnO and $Fe_2O_3$ are the n-type semiconductors and CuO, NiO and CoO are the p-type semiconductors. These gas sensors have to function at high temperature between 150-400 $^{o}$C by using heater (see in Figure 2.6). The free electron charges are found in n-type material and charge carriers or holes are found in p-type material. These sensing materials respond to oxidizing gases such as $O_2$ that is absorbed on material surface by trapping electron from semiconductor surface. Therefore, the resistances of sensing material decrease for p-type material and the resistances of sensing material increase for n-type material [27-28].

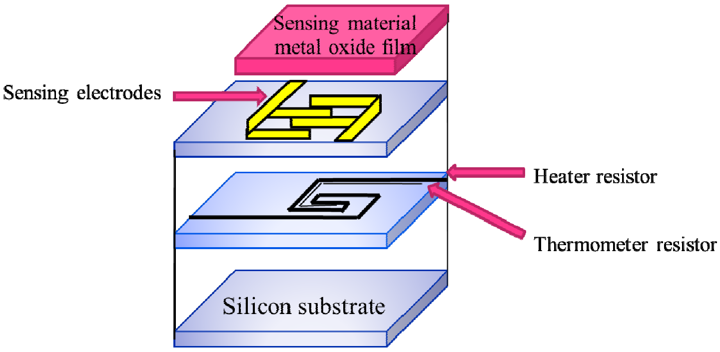

Figure 2.6 Diagram of Metal oxide gas sensors.

## 2.3 Porphyrin and Phthalocyanine Compounds

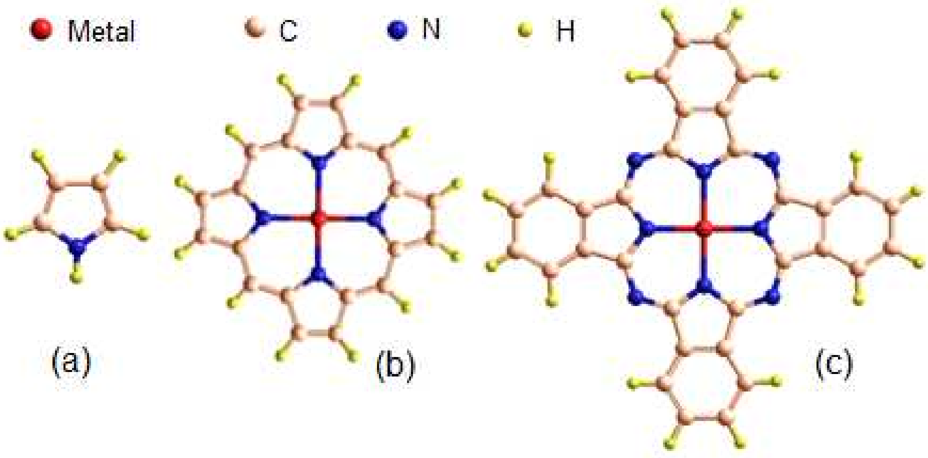

Figure 2.7 Molecular structures of (a) pyrrole, (b) porphyrin and (c) porphyrazine.

Metal porphyrin (MP) and metal phthalocyanine (MPc) are the organic compounds that present the strong absorption spectra in the UV-Visible regions. Both compounds are used as common coloring dyes in the industry. The structures of porphyrin and phthalocyanine basically consist of four pyrrole units that produce a macro cycle as shown in Figure 2.7 (a). The electronic structures of both organic compounds can be varied by substitution of some peripheral positions with side chains or replacement to the central atom with other metallic atoms (see Figure 2.7 (b)-(c)). MP and MPc present different electronic properties because of a central metal atom in core molecular structures and a peripheral skeleton around molecular structures. The skeleton of MP has an extended conjugation system with 24-π electrons leading to a wide range of wavelengths for light absorption. MP presents the strong absorption spectra in a region around 400 nm so called Soret band or B band. The strong absorption band in visible wavelength region is generally interpreted in terms of π-π* transition between bonding and anti-bonding molecular orbital [29]. MPc presents the absorption in two regions, e.g., around 300 nm and 700 nm. The first absorption band (around 300nm) is described as the transition of π-electron from the highest occupied energy level to the lowest unoccupied level. The maximum absorption band (around 700nm) is produced from the resonating of π-electrons, which is the free electron gas between two equivalent limiting structures [30].

MP and MPc have been used in many field of research, i.e., dye sensitized solar cells (DSSCs) [31], metal-organic frameworks (MOFs) [32], bioelectronics tongue [33], organic thin-film transistors (OTFTs) [34], photo-sensitizer for healthcare technology [35] etc. MP and MPc have been used as chemical gas sensors in e-nose applications because their optical properties can be changed when interacting with VOCs. Such interactions introduce charges transfer between the sensing materials and VOCs molecule, for example, the electrons in oxygen atom of some gases such as $C_2H_5OH$ and $NO_2$ transferred to the sensing molecules while the gas molecules were adsorbed at the central metal atom or the conjugated π-electron system of the sensing molecules [36].

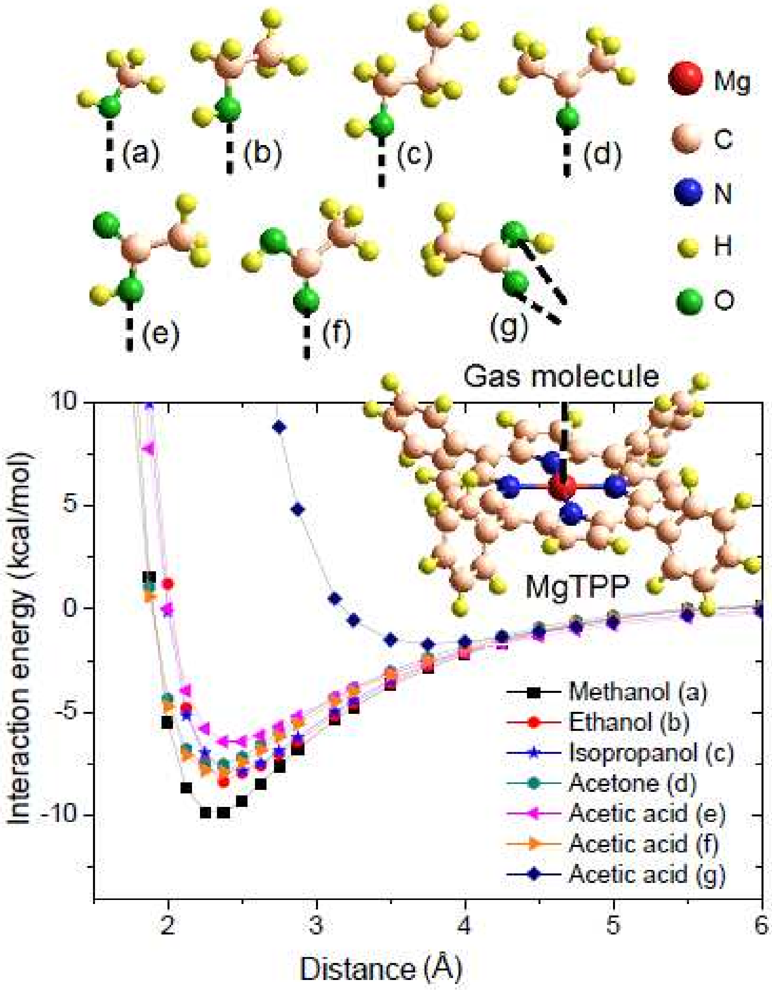

Figure 2.8 Plot of interaction energies versus distance between oxygen atom in gas molecule and Mg atom in MgTPP molecule.

Computational method based on density functional theory (DFT) at the B3LYP/6-31G* level of theory was used to described the interaction energies between magnesium-tetra-phenyl-porphyrin (MgTPP) and gas molecules such as methanol, ethanol, isopropanol, acetone and acetic acid molecules. Figure 2.8 plots the interaction energies between gas molecules and MgTPP versus varying distance between the oxygen atom in gas molecule and the Mg atom in porphyrin molecule. The interaction energies at the optimized distance indicate that MgTPP presents the stable structure with gas molecules. The results reveal that MgTPP has stronger interaction with methanol molecule at the optimized distance of 2.375 Å than other molecules.

**Table.2.1** The interaction energies; $E_{Int}$ (kcal/mol) at the optimized distance; $D$ (Å), change in energy gap of MgTPP = 2.82 eV; $\Delta E_g$ (eV), and the change in NBO charge: for MgTPP at magnesium (1.70153 a.u.), nitrogen (-0.73441 a.u.); for VOCs at oxygen atomic site (methanol; O -0.741 a.u., ethanol; O -0.759 a.u. and isopropanol; O -0.753 a.u., acetone; O -0.540 a.u.and acetic acid; O -0.591 a.u.) atomic site.

| **Interaction of MgTPP with** | ***D*** **(Å)** | **$E_{Int}$ (kcal/mol)** | **$\Delta E_g$ (eV)** | **Delta NBO charge of** | | |
|---|---|---|---|---|---|---|
| | | | | **Metal** | **O** | **N** |
| Methanol | 2.375 | -9.92 | 0.105 | +0.001 | -0.045 | +0.024 |
| Ethanol | 2.50 | -8.37 | 0.098 | +0.002 | -0.041 | +0.022 |
| Isopropanol | 2.25 | -7.83 | 0.102 | +0.003 | -0.040 | +0.023 |
| Acetone | 2.375 | -7.61 | 0.117 | +0.001 | -0.065 | +0.028 |
| Acetic acid (Figure 2.8(f)) | 2.375 | -7.91 | 0.099 | +0.004 | -0.060 | +0.026 |

Effect from the substitution on the central metal atom in porphyrin was tested by DFT calculation. The interaction energies *($E_{Int}$)*, changes in energy gap ($\Delta E_g$) and changes in NBO charges of MgTPP were investigated as presented in Table.2.1. The interactions between porphyrin and VOC molecules are determined by the metal atom site via the interactions of the π-electrons and the free electrons of the metal atom in porphyrin with the electrons of the VOC molecules. Hence, electron transfer from the metal atom in porphyrin to an oxygen atom of the VOCs molecule occurs when MgTPP is in contact with the VOC molecule at the optimized distance [37].

To use MP and MPc as optical gas sensor, sensing materials have been fabricated as the thin solid film on glass substrate. Measuring changes in the absorption or emission spectra of the thin film is a convenient technique for the optical gas sensor. Various derivatives of MP and MPc compounds have been fabricated to use as the gas sensors. For instances, Zinc-5,10,15,20-tetra-phenyl-21H,23H-porphyrin (ZnTPP), manganese(III)-5,10,15,20-tetraphenyl-21H,23H-porphyrin chloride (MnTPPCl) and Zinc-2,9,16,23-tetra-tert-butyl-29H,31H-phthalocyanine (ZnTTBPc) were widely used to detect $NO_2$ [38-39], VOCs [40] and foods [41]. Figure 2.9 illustrates the molecular structure of (a) ZnTPP, (b) MnTPPCl and (c) ZnTTBPc.

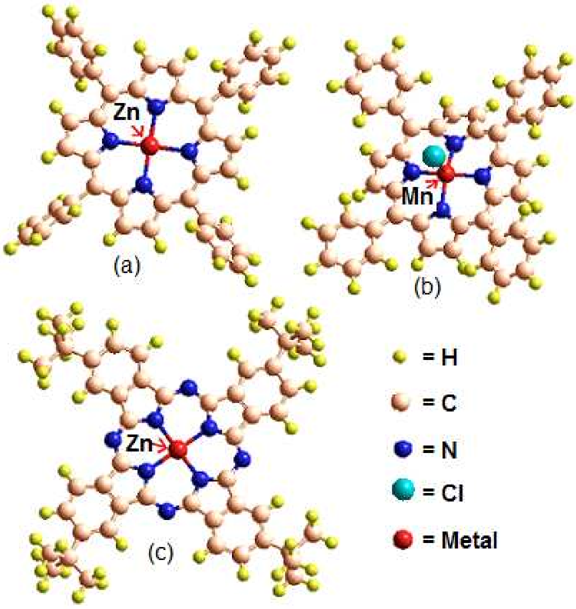

Figure 2.9 Molecular structures of (a) ZnTPP, (b) MnTPPCl and (c) ZnTTBPc.

## 2.4 Molecularly Imprinted Polymer (MIP)

There are two ways to fabricate the molecularly imprinted polymers i.e. surface imprinting and bulk imprinting. Surface imprinting is used for imprinting the large templates such as proteins, cells and microorganisms but bulk imprinting is used for imprinting the small templates such as volatile organic compound (VOC), polycyclic aromatic hydrocarbons, pharmaceutically active compounds and environmental contaminants [42]. Therefore, the bulk imprinting process is more interested in the gas sensor problem. This imprinting process starts by adding the initial monomer, cross-linking monomers and the specific VOC template. After removing the VOC molecule the active sites for VOC detection are presented in the whole bulk material as shown in Figure 2.10. The adsorbed gases on the polymer are observed by frequency counter and reported in the term of frequency changes. In the measurement system, there is the molecularly imprinted polymer (MIP) electrode and non-molecularly imprinted polymer (Non-MIP) or empty electrode. MIP electrode must present more frequency change than Non-MIP electrode to confirm that the target gas was imprinted by this polymer. The frequency of quartz electrode is decrease when the target gas absorbed on MIP layer.

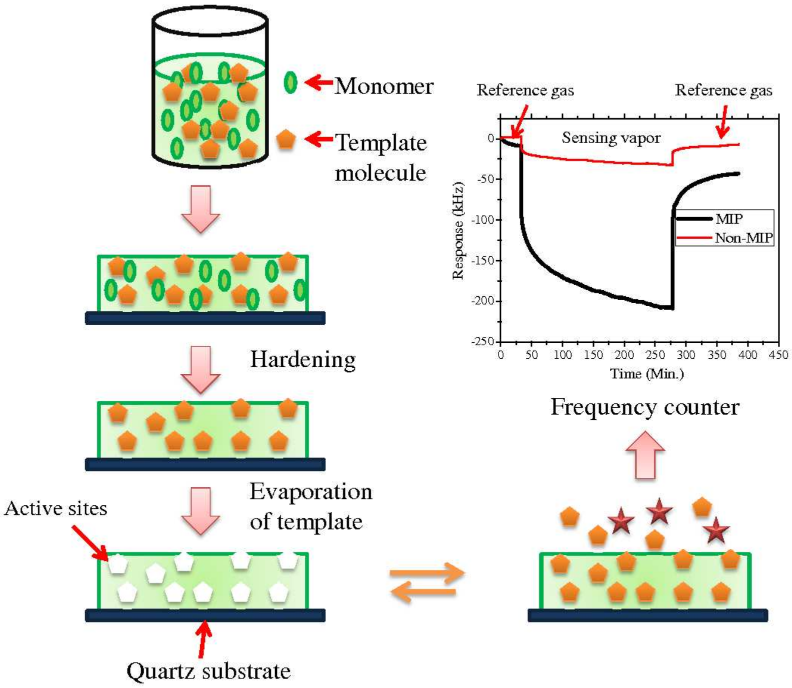

Figure 2.10 Bulk imprinting process with VOC template.

## 2.5 E-nose System based on UV-Vis Spectrophotometer

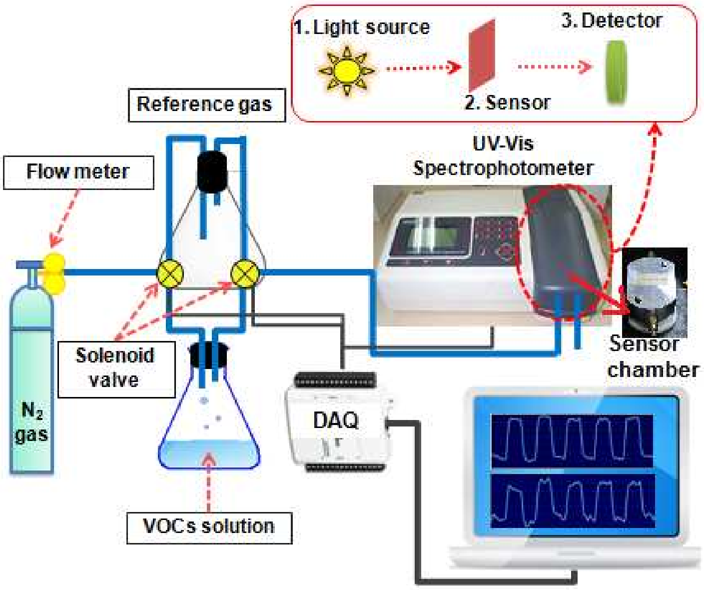

Figure 2.11 Schematic diagram of gas flow system based on the UV-Vis spectrophotometer measurement.

An optical e-nose system consists of three basic components: gas sensor, transducer, data processing and pattern recognition. In this system, a UV-Vis spectrophotometer was used as the transducer (light source and detector). All measurements were performed at room temperature and at the normal incidence of the light beam. The gas sensors are fabricated from the spin-coating of organic dyes solution (MP and MPc). These sensing thin films are measured under the dynamic gas flow through a home-built stainless steel chamber, equipped with quartz windows for optical measurements as shown in Figure 2.11. The carrier gas (in this case 99.9% nitrogen) was supplied into the sample bottle that was immersed in a heat bath. The sample vapor was evaporated from the surface of the liquid sample and carried by the nitrogen gas. The gas flow was controlled by solenoid valve to switch between the reference gas and the sample gas. The rate of gas flow was controlled by the flow meter. The absorption spectra of the organic thin film were collected by the UV-Vis spectrometer for every 1 second based on the function of the DAQ card.

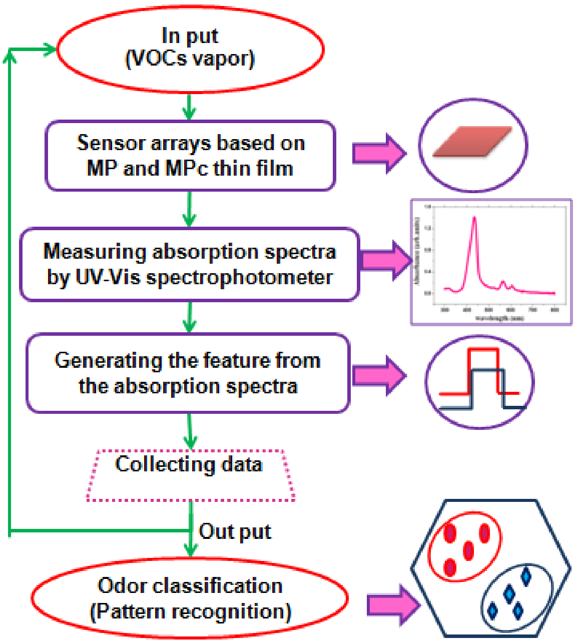

Figure 2.12 The flow chart of the optical e-nose system based on UV-Vis spectrometer.

Figure 2.12 shows the flow chart of the optical e-nose system, starting with a flow of different VOC vapor into the gas sensor that fabricated from MP and MPc compounds. Then the data processing starts from absorption spectra that are collected by the UV-Vis spectrophotometer. The absorption spectra were collected for different sample vapors, comparison with the spectra of the unexposed films. The features extracted from the sensing signal were prepared for further pattern recognition process (in this case, PCA). Then the new data set was presented in the new orthogonal axes or principal components (PCs) such as the first PC (PC1) and the second PC (PC2), which are linear combinations of the original axes. The first PC carries most of the data variance, hence the most important information about the data.

## 2.6 Analytical Techniques

### 2.6.1 UV-Vis Spectrophotometer

In this thesis the absorption spectrum changes of the thin film was recorded by UV-Vis spectroscopy instrument. This instrument is routinely used in the quantitative determination of solutions of transition metal ions and highly conjugated organic compounds. This technique records the UV-Vis region of electromagnetic spectrum at 300-800 nm. The solutions of transition metal ions can be colored (i.e., absorb visible light) because electrons of the metal atoms can be excited from one electronic state to another state. The color of metal ion solutions is strongly affected by the presence of other species. Some of the emitted radiation is absorbed at certain characteristic wavelength, causing a decrease in the intensity of the beam at the wavelength.

$T$ is the “transmittance” value which is the ratio of $I/I_0$, where $I$ and $I_0$ are the transmitted and initial beam intensities, respectively. Then the photo spectrometer calculated the absorbance $A$ from the definition [2]:

$$A = -\log T = -\log \frac{I}{I_0} \tag{2.3}$$

$A$ is usually expressed as a percentage of transmittance (%$T$).

$$\%T = 100 \times T$$

$$T = \frac{\%T}{100}$$

$$A = -\log\frac{\%T}{100} = \log 100 - \log\%T$$

$$A = 2 - \log\%T \tag{2.4}$$

The basic components of a spectrophotometer are a light source, a holder for the sample, a diffraction grating or monochromator to separate the different wavelengths of light, and a detector. A Tungsten filament (350-2500 nm) is used as the radiation source. The detector is typically a photodiode or a CCD. Photodiodes are used with a monochromator which filters the light to produce of a single wavelength reaches the detector. Diffraction gratings are used with CCDs which collects light of different wavelengths on different pixels.

### 2.6.2 Atomic Force Microscope (AFM)

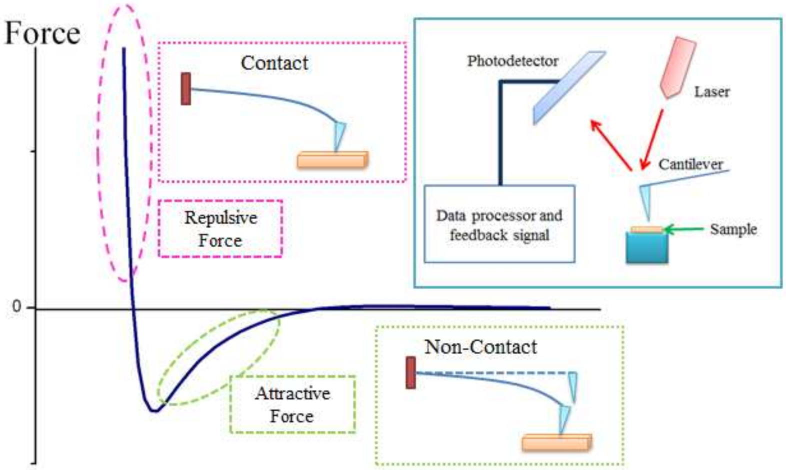

Figure 2.13 Schematic representation of AFM setup and the Lennard-Jones atomic interaction force distance curve between the probe tip and sample surface.

AFM is the one type of microscope technique that use to investigate very small area based on high-resolution scanning probe. The resolution AFM is in the range of nanometer and more than 1,000 times better than the optical diffraction limit. The AFM consists of a cantilever with a sharp tip (probe) at its end that is used to scan the specimen surface. The cantilever is typically silicon or silicon nitride with a tip radius of curvature on the order of nanometers. When the tip is brought into proximity of a sample surface (see Figure 2.13), forces between the tip and the sample lead to a deflection of the cantilever according to Hooke's law [43]. Laser beam is used deflection system to generate the feedback signal.

There are two modes of AFM namely contact mode and non-contact mode. For the contact mode, attractive forces can be quite strong, causing the tip interact close to the surface of the sample. Thus contact mode AFM is always done in contact where the overall force is repulsive [44]. For the non-contact mode, the cantilever is driven to oscillate up and down at near its resonance frequency by a small piezoelectric element mounted in the AFM tip holder. The amplitude of this oscillation is greater than 10 nm, typically 100 to 200 nm depending on the interaction of forces acting on the cantilever when the tip comes close to the surface such as Van der Waals force or dipole-dipole interaction, electrostatic forces. The amplitude of the oscillation decreases when the tip gets closer to the sample surface [45].

### 2.6.3 Density Functional Theory (DFT)

The quantum mechanical theory based on DFT calculation is useful to investigate the electronic structure in ground state of particular molecule. This calculation is the most popular and versatile methods to calculate the electronic structure for instance bond distance, bond angles, interaction energy, atomic charge, transition states and etc. for the porphyrin and phthalocyanine compound. From the previous theoretical studies based on DFT, porphyrin complex have been calculated energy-minimized structure at density functional B3LYP level using the 6-31G(d) basis set [46].

In this thesis the interaction energy and atomic charges between porphyrin molecule and volatile organic compound molecule were calculated by density functional theory at the B3LYP/6-31G* level of theory, using the GAUSSIAN 03 program. The geometries of MP and MPc were optimized based on the semi-empirical quantum chemistry PM3 Techniques [47]. Then the atomic charges and total energies were computed by density functional theory at the B3LYP/3-21G* and B3LYP/6-

31G* level of theory, respectively, using the GAUSSIAN program. In addition, B3LYP/6-31G* was also used to compute electronic properties and the interaction energies between sensing molecule and metallo-porphyrins by varying the distance between oxygen atom in analyte molecule and the metal center atom in sensing molecule. Finally the comparison of the interaction energies between the calculation method and the gas sensing in the experimental was investigated.

### 2.6.4 Principal Component Analysis (PCA)

The principal components analysis (PCA) is a multi-variate data analysis method that has been widely used as a pattern recognition algorithm in most e-nose systems to discriminate different VOCs, e.g., alcohols, toluene, methylethylketon, soft drink and alcoholic beverages [48].

PCA which is the one of chemical pattern recognition had been used to determine the data pattern, for examples, classifying the types of wine, whisky and food in electronic nose analysis. In this thesis, PCA technique is mainly used to verify the data set from e-nose. PCA is the statistical technique that translates and reduces the dimensions of data in the experiment. By using this technique, we can transform a number of possibly correlated variables into a smaller number of uncorrelated variables. PCA is the simplest of the true eigenvector-based multivariate analyses. Often, its operation can be thought of as revealing the internal structure of the data in a way which best explains the variance in the data [49]. The main advantage of PCA is that you can found these patterns in the data, and you compress the data, i.e. by reducing the number of dimensions, without much loss of information. This section presents the process to perform a PCA calculation [50].

#### 2.6.4.1 Data Collection

In this thesis, the data set was calculated from the difference of the average gas sensing response between sensing vapor and reference gas ($x_{ij}$). The number of sensor (j) and number of experiment (i) are depended on the electronic nose system.

**Table.2.2** The PCA original data for gas sensor array.

| Number of experiments | Sensor number | | | | | |
|---|---|---|---|---|---|---|
| | 1 | 2 | 3 | 4 | 5 | …j |
| 1 | $x_{11}$ | $x_{12}$ | $x_{13}$ | $x_{14}$ | $x_{15}$ | $x_{1j}$ |
| ↓ | ↓ | ↓ | ↓ | ↓ | ↓ | ↓ |
| i | $x_{i1}$ | $x_{i2}$ | $x_{i3}$ | $x_{i4}$ | $x_{i5}$ | $x_{ij}$ |

#### 2.6.4.2 Mean Centering ( $^{cen}x_{ij}$ )

The columns is subtracted the mean of each column by $^{cen}x_{ij} = x_{ij} - \overline{x_j}$ . After that the sum of each column is equal to zero so now the data plot is centered on the origin. The mean of the sample ( $\bar{x}$ ) was calculated by $\bar{x} = \frac{\sum_{j=1}^{n} x_j}{n}$

#### 2.6.4.3 Calculate Covariance Matrix

The calculation of the covariance between one dimension and itself is the variance. So if there is a 3-dimensional data set (x, y, z), then compute the covariance between the x and y dimensions, the x and z dimensions, and the y and z dimensions. To Measure the covariance between x and x or y and y or z and z would get the variance of the x, y and z dimensions, respectively. The formula for covariance is very similar to the formula for variance. The formula for variance could also be written as “ $\mathrm{var}(x) = \frac{\sum_{i=1}^{n}(x_i - \bar{x})(x_i - \bar{x})}{n-1}$ ”.

The formula for covariance denote by “ $\mathrm{cov}(x, y) = \frac{\sum_{i=1}^{n}(x_i - \bar{x})(y_i - \bar{y})}{n-1}$ ”.

In this thesis, there were more than one covariance measurements that can be calculated. For example, for a 3 dimensional data set (dimensions x,y,z) the $\mathrm{cov}(x, y)$ , $\mathrm{cov}(x, z)$ and $\mathrm{cov}(y, z)$ were calculated. Therefore, an n-dimensional data set, different covariance values were calculated at $n![(n-2)!\times 2]$ times. The way to get all the possible covariance values between all the different dimensions is to calculate them all and then put them in a matrix. The definition for the covariance matrix for a set of data with dimensions is "$c^{nxn} = \left(c_{ij}, c_{ij} = \operatorname{cov}(Dim_i, Dim_j)\right)$".

#### 2.6.4.4 Calculate the Eigenvectors and Eigenvalues of Covariance Matrix

The eigenvectors and eigenvalues for this matrix were calculated by "$AX - \lambda IX = 0$", where A is a covariance matrix, X is the eigenvector and λ is the eigenvalue.

#### 2.6.4.5 Choosing Components and Forming a Feature Vector

The eigenvector with the highest eigenvalue is the first principal component (PC1) of the new data set. The eigenvectors are ordered by eigenvalue from highest to lowest eigenvalue. If the original matrix has n dimensions, first calculate eigenvectors and eigenvalues, next choose only the first *p* eigenvectors, then the dimension of final data set is equal to the dimension of *p* eigenvectors. Finally, take the eigenvectors which keep from the list of eigenvectors, and then form a matrix with these eigenvectors in the columns called *"Feature Vector"* $(\text{Feature Vector} = (\text{eig}_1 \quad \text{eig}_2 \quad \text{eig}_3 \ldots\text{eig}_n))$

#### 2.6.4.6 Deriving the New Data Set

After a feature vector is formed, the transpose of the eigenvector is taken and multiply it on the left of the original data set, transposed (see equation 2.5).

$$Final\,Data = Row\,Feature\,Vector \ x \ Row\,Data\,Adjust \qquad (2.5)$$

Where $Row\,Feature\,Vector$ is the matrix with the eigenvectors in the columns transposed so that the eigenvectors are now in the rows, with the most significance eigenvector at the top and $Row\,Data\,Adjust$ is the mean-adjusted data transposed, i.e. the data items are in each column, with each row holding a separate dimension.

# CHAPTER III

# THE MIXED LAYER OF PORPHYRIN AND PHTHALOCYANINE SPIN-COATED THIN FILMS FOR AN OPTICAL ELECTRONIC NOSE

## 3.1 Synopsis

Metallo-porphyrin (MP) and metallo-phthalocyanine (MPc) have recently become very attractive and practically alternative because MP and MPc present versatile and tunable optical spectra by changing the central metal atom such as zinc and manganese. Both compounds have been used as sensing material to detect various volatile organic compounds (VOCs) based on optical detection. Therefore, MP and MPc are selected to fabricate the gas sensor array for the optical e-nose. In this chapter, we prepared sensing material by mixing three types of organic compound which are present the different absorption region. The spin-coating technique was used to prepare the sensing layer thin film. The UV-Vis spectrophotometer was used as transducer to measure the absorption spectra changes of organic thin film in dynamic gas flow system. The efficiency of this sensing layer was tested by methanol, ethanol, isopropanol, acetone (5% eq.) and acetic acid (5% eq.) vapor. Atomic force microscope (AFM) and x-ray diffraction (XRD) were used to investigate the surface morphological and nanocristalline structure of this sensing layer. The electronic structure and interaction energies between sensing molecules and analyte molecules were calculated by density functional theory (DFT) at the basis set of B3LYP 6-31G*. Finally, principal components analysis (PCA) was used as the pattern recognition to classify the various vapors.

## 3.2 Introduction

The chemical gas sensor is a device that converts the chemical properties of the odorant into electronic signal. There are many types of chemical gas sensor, for instance, conductometric, gravimetric (piezoelectricity), chemoresistor and optical sensor. Among these transduction techniques, optical measurement has been one of the most popular choices due to it variety in the measurement of optical modes, for example absorbance, fluorescence, polarization, refractive index and reflectance [51-52]. The absorption or emission spectra of sensing material have been used to investigate the interaction between sensing material and analyte molecule. Therefore, UV-Vis spectrophotometer is the convenient instrument for the optical gas sensor analysis. This method is usually called as “optical electronic nose” [53]. The e-nose is a promising technique for discrimination product from odor and volatile chemicals associated with the aroma of products. This e-nose system composes of chemical gas sensor, signal transducing and data analysis or pattern recognition [1]. Therefore, chemical gas sensor based on optical detection has been studied in several sensing material such as phthalocyanine and porphyrin compounds. Metallo-phthalocyanine (MPc) and metallo-porphyrin (MP) are the semiconductor materials that present the strong absorption spectra in visible light region. Both compounds present the different electronic properties that correspond to the central metal atom and peripheral ring [54]. MP and MPc such as Zinc-2,9,16,23-tetra-tert-butyl- 29H,31H- phthalocyanine (ZnTTBPc), Zinc-5,10,15,20-tetra-phenyl-21H,23H-porphyrin (ZnTPP) and manganese(III)-5,10,15,20-tetraphenyl-21H,23H-porphyrin chloride (MnTPPCl) were widely used as optochemical sensing materials to detect the different odorant such as VOCs [37] and foods [41]. Moreover, the active regions for optical gas sensor based on MP and MPc were found near the absorption peak [55].

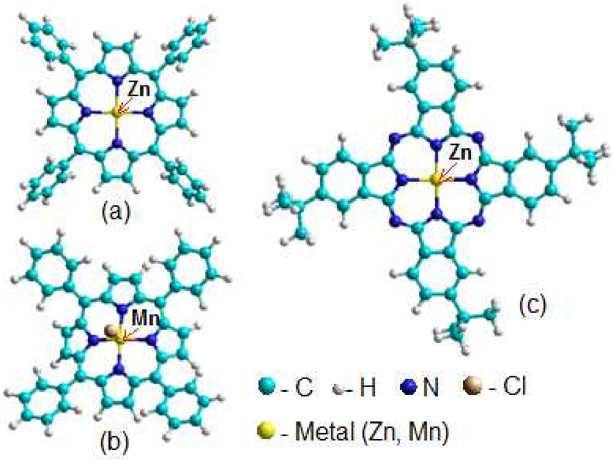

**Figure 3.1** The molecular structure of (a) Zinc-5,10,15,20-tetra-phenyl-21H,23H-porphyrin, (b) manganese(III)-5,10,15,20-tetraphenyl-21H,23H-porphyrin chloride and (c) Zinc-2,9,16,23-tetra-tert-butyl-29H,31H- phthalocyanine.

In this work, the optical gas sensor was developed by using the three types of organic compounds, namely, ZnTTBPc, ZnTPP and MnTPPCl as shown in Figure 3.1. The structure of MP and MPc are formed of the macro-cyclic organic compounds that contain the four-pyrrole groups. The electronic properties of both organic compounds can be varied by substitution of some peripheral group or replacement to the central atom with other metallic atoms such as Zn and Mn atoms [30]. The sensing response toward various VOCs in food and beverage, for instance, methanol, ethanol, isopropanol, acetone (5% eq.) and acetic acid (5% eq.) were tested in this chapter. Optical absorption changes of the sensing materials in the presence of VOC vapor were measured by UV-Vis Spectrometer in the range of 300-800 nm. The effect from flow rate of nitrogen gas in the dynamic flow system was tested by varying the flow rate of nitrogen gas from 200 to 600 ml/min. The atomic force microscope (AFM) and x-ray diffraction (XRD) were used to investigate the surface morphological and nanocrystalline structure of spin coated thin film.

In addition, the computational method has been widely used to understand the organic sensing material mechanism. Charges transfer between organic compound and alcohol molecules were used to identify the absorption spectra changes when organic compounds interact with alcohol vapor. The electrons in oxygen atom of sensing gas such as $C_2H_5OH$, $NH_3$ and $NO_2$ transferred to the porphyrin molecules while gas molecules were adsorbed at the central metal atom or the conjugated π-electron system of porphyrin molecules [36]. Many research tried to investigate the mechanism of phthalocyanine and porphyrin for gas sensor application. The quantum mechanical theory has been chosen for investigating the electronic structure at the ground state of the particular atoms and molecules especially predict the gas sensing behavior of the organic molecule. Density Functional Theory (DFT) with B3LYP level using the 6-31G* basis set (for carbon, hydrogen, and nitrogen) has been among the most popular and versatile methods to calculate the electronic structure of the porphyrin and phthalocyanine compound, for instance bond distance, bond angles, interaction energy, atomic charge, transition states and etc. The energy gaps between the highest occupied molecular orbital (HOMO) and the lowest unoccupied molecular orbital (LUMO) in the MP and MPc were calculated by DFT [56]. Therefore, DFT based on B3LYP level was prepared for analyze the charge transfer and interaction energies between organic compound and alcohol molecules in this chapter.

Moreover, the significant step for classify the odor in e-nose system is the pattern recognition. The statistical technique namely principal components analysis (PCA) is a multi-variant data analysis method that has been widely used as a pattern recognition algorithm in an e-nose system [3]. This method has been used to discriminate various volatile organic compounds (VOCs), e.g., alcohols, toluene, methylethylketon, soft drink and alcoholic beverages [48, 57]. Therefore, in our optical e-nose system, PCA was used to analyze the sensing signal from the UV-Vis spectrophotometer. The result indicated that the mixed layer gas sensor based on ZnTTBPc/ZnTPP/MnTPPCl has more efficiency than the single layer gas sensor for VOCs discrimination.

## 3.3 Experimental

### 3.3.1 Instrumentation

The optical e-nose set up comprised three basic components: 1) UV-Vis spectrophotometer; 2) sensing materials or gas sensor; and 3) gas flow system. Jenway 6405 UV-Visible spectrophotometer was used to collect the absorption spectra of spin-coated thin at room temperature and at the normal incidence of the light beam. The home-built stainless steel chamber that equipped with quartz windows for optical measurements under the spectrophotometer was used to investigate the gas sensing capability of the organic thin films in dynamic gas flow system. The carrier gas or nitrogen (99.9%) gas was supplied at the liquid sample bottle that was immersed in a heat bath. The sensing vapor was evaporated from the surface of the liquid sample and carried by the nitrogen gas. The concentration of VOCs vapor in reference gas was controlled by varying the temperature of solvent in the sample bottle. The concentration was calculated from the lost weight of solvent after measurement. The gas flow was controlled by solenoid valve to switch between the reference gas and sample gas in every 10 minutes. These solenoid valves were contacted with computer by using data acquisition or DAQ card to switch between reference gas and sensing vapor. The absorption spectra of the organic thin film were collected by UV-Vis Spectrometer for every 1 minute. Each measurement consists of 5 cycles of switching between the references and sensing vapor.

### 3.3.2 Film Preparation

ZnTTBPc, ZnTPP and MnTPPCl were obtained from Sigma-Aldrich. The ZnTTBPc, ZnTPP and MnTPPCl were dissolved in chloroform solution at the concentration of 12, 5 and 15 mg/ml while the mixed solution of ZnTTBPc/ZnTPP/MnTPPCl was obtained from a 3 ml of chloroform solution that was composed of 12 mg of ZnTTBPc, 5 mg of ZnTPP and 15 mg of MnTPPCl. Then the spin-coated thin films were obtained by spinning the solution on the clean glass substrate at 1,000 rpm for 30 s.

### 3.3.3 Sensing Analysis

This process started with a flow of the different VOCs vapor into the sensing layers. Then the absorption spectra from UV-Vis spectrophotometer were collected for the different vapors, in comparison to the spectra of the unexposed films. Finally, the PCA method projected the collected data from five wavelength regions of the spectra in a new vector space of lower dimensionality. These new data set are presented in the new orthogonal axes or principle components (PC) such as first PC

(PC1) and second PC (PC2) which are linear combinations of the original axes. The first PC carries most of the data variance, hence the most important information about the data.

### 3.3.4 Computational Method

The geometries of ZnTTBPc, ZnTPP, MnTPPCl, methanol, ethanol and isopropanol molecules were optimized based on the semi-empirical quantum chemistry PM3 techniques. Then the energy-minimized structure of these molecules were calculated by the DFT at B3LYP/3-21G* and B3LYP/6-31G* level of theory, respectively, using the GAUSSIAN 03 program. The interaction energies and atomic charges when sensing molecule interacted with alcohols molecule were calculated by DFT at the B3LYP/6-31G* level of theory. The interaction energy or binding energy ($E_{Int}$) between sensing materials and alcohols molecule were calculated by equation (3.1).

$$E_{Int} = E_{SM+Alc} - (E_{SM} + E_{Alc}) \tag{3.1}$$

Where $E_{SM}$ and $E_{Alc}$ is the total energy of isolated sensing molecule and alcohol molecule, respectively. $E_{SM+Alc}$ is the total energy of system when sensing molecule interacted with alcohol molecule.

## 3.4 Results and Discussion

### 3.4.1 Optical Measurements and Sensing Characteristics

The optical properties of spin-coated thin films were measured by the UV-Visi spectrophotometer. Figure 3.2 (a) shows the absorption spectra of the ZnTTBPc, ZnTPP and MnTPPCl spin-coated thin films. The main peaks of ZnTTBPc are located around 342 nm, corresponding to the Q band, and 635 and 688 nm, corresponding to the B band in phthalocyanine compounds. The $Q_I$ band peak at 688 nm is attributed to the monomer and occurred from the $\pi$-$\pi$* transition from the highest occupied molecular orbital (HOMO) to the lowest unoccupied molecular orbital (LUMO) of the phthalocyanine ring. The $Q_{II}$ band at 635 nm is attributed to the neutral dimer form or higher aggregates. The B band in the 300-400 nm is attributed to the transitions from deeper π levels to the LUMO [58]. ZnTPP thin film exhibits the B band at 433 nm and the Q band at 570 and 610 nm. The absorption spectrum of MnTPPCl film consists of the two Soret bands (376 and 483 nm) and the two Q bands (590 and 630 nm) [59]. The absorption spectra of MP with the difference central metal atom exhibit difference in absorption peak specially MnTPPCl and ZnTPP film show the strongest absorption spectra in separated area that are related to π-π* transition from HOMO to the LOMO.

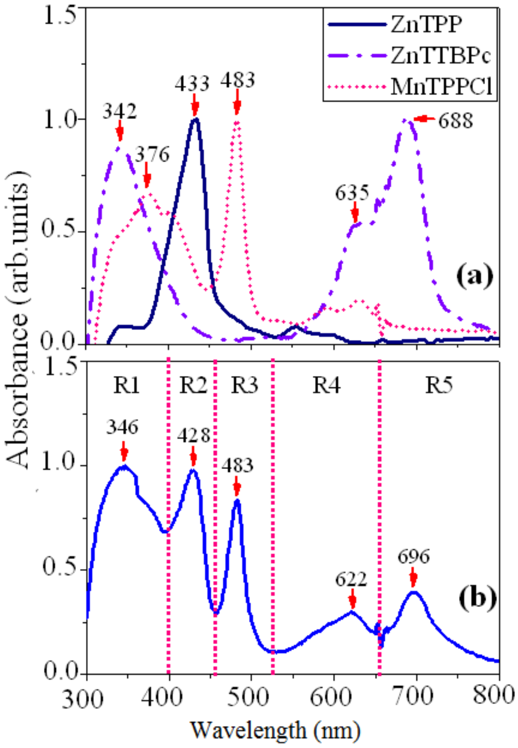

**Figure 3.2** Optical absorption spectra of (a) the ZnTTBPc, ZnTPP and MnTPPCl spin-coated film and (b) the mixed layer of ZnTTBPc/ZnTPP/MnTPPCl spin-coated film.

The absorption spectrum of the blended ZnTTBPc/ZnTPP/MnTPPCl spin-coated thin films is shown in Figure 3.2 (b). The mixed layer thin film shows the main peak at 346, 428, 483, 622 and 696 nm, in accordance with the strongest absorption peaks of the MPc and the MP. In case of the e-nose based on colorimetric, various organic dyes based on MP or MPc were selected to produce the sensor arrays. This technique need more organic compounds for preparing sensor arrays such as MP (M = Mn, Fe, Co, In, Cu, Eu, $H_2$, Fe and Zn) for $NH_3$ classification [60]. In this chapter, gas sensor arrays were generated from the whole spectrum of ZnTTBPc/ZnTPP/MnTPPCl thin film by dividing the absorption spectra into 5 regions (R1-R5) around each of the main absorption peaks: 300-400 nm (R1), 400-460 nm (R2), 460-530 nm (R3), 530-655 nm (R4) and 655-800 nm (R5) because the active regions for optical detection were observed near the main peak of absorption spectra. From the previous research, the area integral under the absorption spectra were corresponded to the sensing molecule and binding gas molecule for example percentage change in area integral under the absorption spectra of 2-nitro-5,10,15,20-tetraphenylporphyrinato zinc (ZnTPP-$NO_2$) thin film presented the different pattern with various chemical vapor. Therefore, the changes of area integral under the absorption spectra for specific wave length region of ZnTTBPc/ZnTPP/MnTPPCl thin film (R1 - R5) were investigated in the term of “gas-sensing response”. The gas-sensing response ($S$) is calculated by equation (3.2):

$$S = \Delta A / A_{Base} \tag{3.2}$$

Where $A_{Base}$ is the total area integral of absorption spectra before flowing gas and $\Delta A$ is the absolute value of the difference between the absorption spectrum area integrals under VOC vapor flow and those under the reference gas (nitrogen gas).

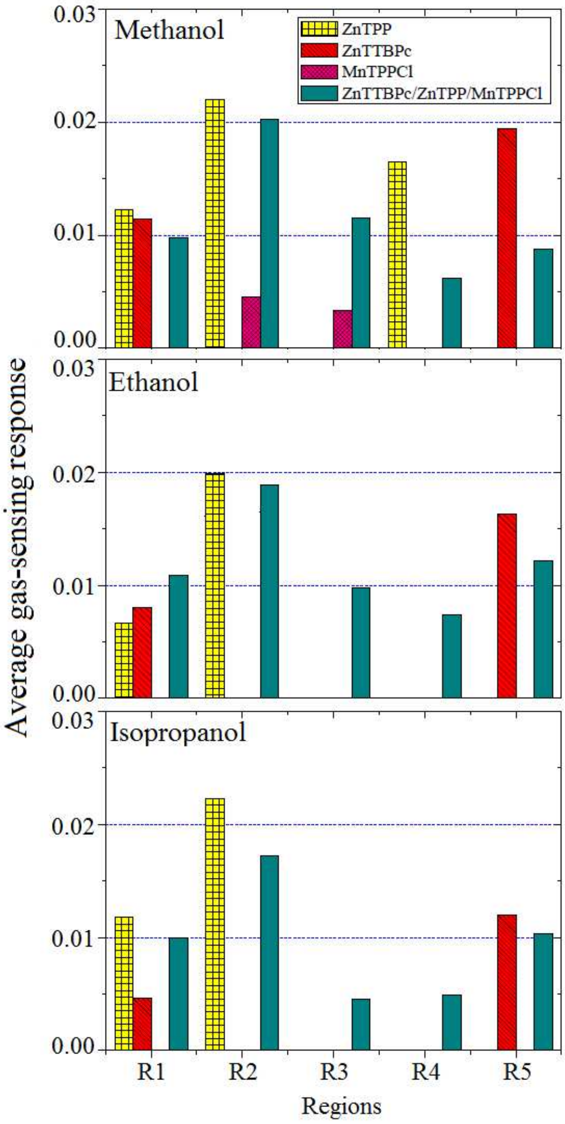

**Figure 3.3** The average gas sensing of ZnTTBPc, ZnTPP, and MnTPPCl and mixed layer of ZnTTBPc/ZnTPP/MnTPPCl spin coated thin film.

The effect of mono-layer and mixed layers of MP and MPc were investigated by using alcohols vapor. Figure 3.3 shows the average gas sensing response (*S*) of ZnTTBPc, ZnTPP, MnTPPCl and ZnTTBPc/ZnTPP/MnTPPCl mixed layers thin films toward 10 mol% of alcohols vapor in nitrogen gas. The concentration of alcohols vapor was controlled by the heat bath and calculated from the weight loss of the alcohols solution. The average gas sensing responses of ZnTTBPc, ZnTPP and MnTPPCl spin-coated films present the strong average gas sensing responses that were observed from the absorption peak of ZnTTBPc (R1:300-400 nm and R5: 655-

800 nm), ZnTPP (R1:300-400 nm, R2:400-460 nm and R4: 530-655nm) and MnTPPCl (R2:400-460 nm and R3:460-530 nm). Methanol shows the highest average gas sensing amongst the alcohols for all five regions even though ZnTPP and MnTPPCl exhibit no response to ethanol and isopropanol vapor in the region R3 and R4. Nevertheless, the mixed layer film displays gas-sensing responses to all types of alcohol in five regions especially this mixed layer film shows the average gas sensing for ethanol and isopropanol vapor in R3-R4. Therefore, the mixed layer film of MP and MPc presented more characteristic of gas sensor than mono-layer of their compound such as the previous work about zinc-phthalocyanine mixed copper-porphyrin [61]. The interactions between ZnTTBPc, ZnTPP and MnTPPCl compounds may induce some variation of the central metal atom coordination to detect the testing gas. In addition, there are the transformations of the free electron density for $\pi$ transition corresponding to the Q and Soret bands in absorption spectra when MP and MPc adsorb gas molecule [62]. Therefore, the gas-sensing properties of ZnTTBPc/ZnTPP/MnTPPCl thin films were investigated in this work such as the gas-sensing response (*S*), the effect of flow rate in e-nose system and the surface morphology of sensing material.

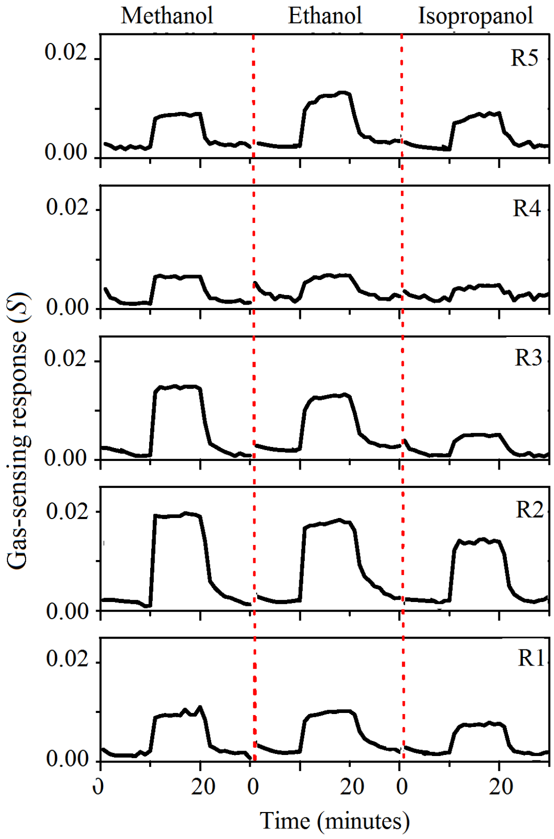

**Figure 3.4** The dynamic gas-sensing response (*S*) of mixed layer of ZnTTBPc/ZnTPP/MnTPPCl spin coated thin film for methanol, ethanol and isopropanol at the concentration of 10 mol% of alcohols vapor in nitrogen gas.

In Figure 3.4, a closer look on the results indicate that the mixed ZnTTBPc/ZnTPP/MnTPPCl spin coated film shows the stronger response to methanol than ethanol and isopropanol vapor in R1, R2 and R3 regions. The R2 region correlates mostly to the Soret band of ZnTPP (400-460 nm), corresponding to the π-π* transition between bonding and anti-bonding molecular orbital in porphyrin compound [63]. The typical dynamic response (S) of mixed layer thin film with methanol is faster than ethanol and isopropanol vapors.

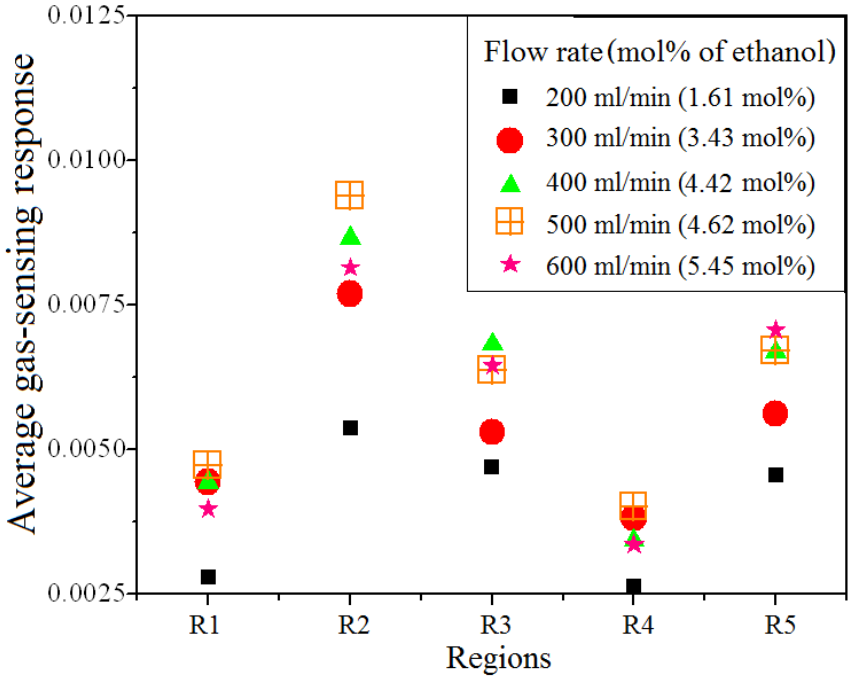

**Figure 3.5** The average gas sensing response of ZnTTBPc/ZnTPP/MnTPPCl spin coated thin film with ethanol vapor by varying flow rate of nitrogen gas from 200-600 ml/min at 25 °C.

The effect from the flow rate of nitrogen gas in the dynamic flow system was investigated by varying the flow rate of nitrogen gas from 200 to 600 ml/min. Figure 3.5 shows that the low flow rate of gas effect to the average gas-sensing response of spin-coated thin film. The flow rate from 400 to 600 ml/min presents the similar average gas-sensing response in five wavelength regions and the flow rate lower than 300 ml/min presents the less average gas sensing. The mol% of ethanol vapor in nitrogen was calculated by weight loss of ethanol solution (see in Figure 3.5). There are low evaporation rate of ethanol about 1.61 mol% at flow rate of 200 ml. This sensing material presents nearly average gas sensing response in concentration about 4-5 mol%. Therefore, the efficiency of optical gas sensor depends on the pressure of nitrogen gas because the low flow rate effects to the evaporation of the alcohol vapor. To make a stable gas sensor system, we need to control the flow rate in the range of 400-600 ml/min.

### 3.4.2 Surface Morphological Studies

Figure 3.6 shows the AFM image of mixed layer of ZnTTBPc/ZnTPP/MnTPPCl spin coated thin film on the glass substrate. The surface structure was reported as the size of 1μm x 1μm in 2D and 3D views of the thin film. The nano structure of this film was obtained by the average roughness about 6 nm. The mixed layer thin film shows the smooth surface. The thickness of spin-coated film was about 200 nm.

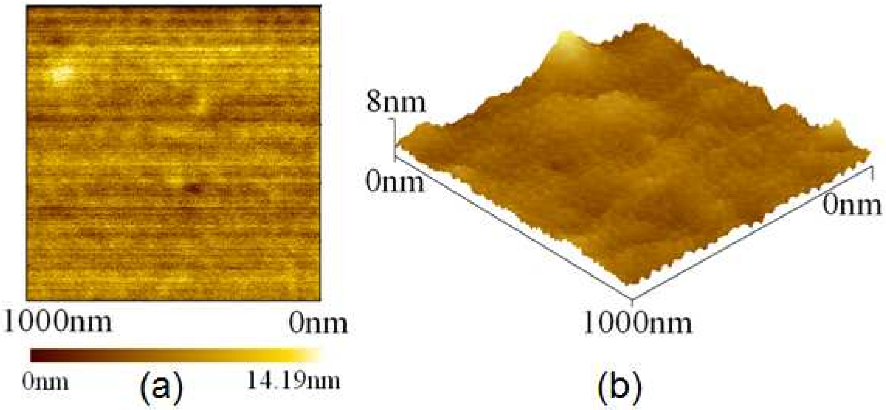

**Figure 3.6** The AFM images in (a) 2D and (b) 3D of mixed layer of ZnTTBPc/ZnTPP/MnTPPCl spin coated thin film.

The structure of ZnTTBPc, ZnTPP and MnTPPCl powders and films were investigated by using XRD (Cu Kα radiation, λ=1.5418 nm). The low thickness of ZnPc film based on thermal evaporation method was not presents the intensity of XRD peak in the range of 10-250 nm [64]. Therefore, the low spin speed of spin-coated film was used to prepare the sensing layer in XRD measurement. The spin-coated films were prepared at the spin speed of 500 rpm on a glass substrate at room temperature.

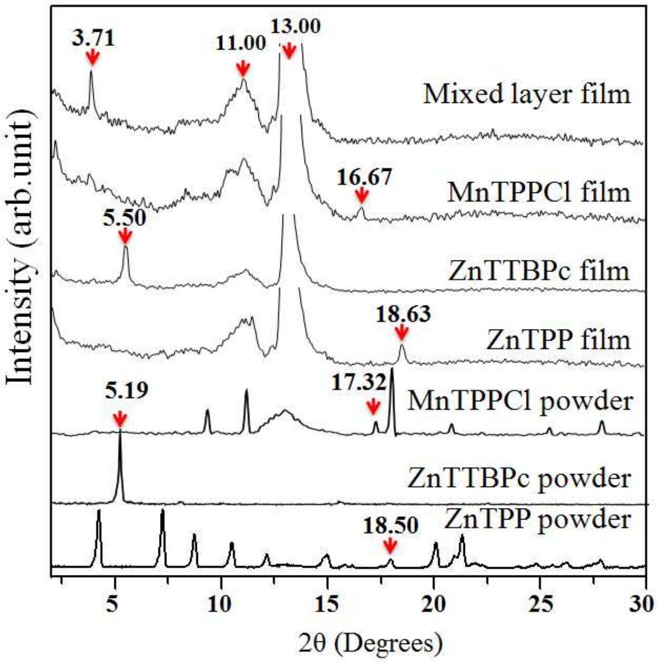

**Figure 3.7** The XRD patterns of powders and spin-coated film for ZnTTBPc, ZnTPP, MnTPPCl and mixed layer of ZnTTBPc/ZnTPP/MnTPPCl film.

Figure 3.7 shows the corresponding intensity peaks between powders and spin-coated films by observing a broad diffraction band from $2^{o}$ to $30^{o}$. The intensity peaks at 2θ equal to $11^{o}$ and $13^{o}$ for all films are the effect from the glass slide substrate. The intensity peaks of ZnTPP compound presents at 2θ equal to $18.50^{o}$ for powder and $18.63^{o}$ for spin-coated film which correspond to the interplanar distance (d) of 4.76 and 4.78 Å, respectively. XRD pattern of ZnTPP spin-coated film agreed with the result of Takeo Oku and coworkers [65]. The intensity peaks of porphyrin thin film were found in the same area of the intensity peaks in porphyrin powder. For example, NiTPP presented two intensity peaks for spin-coated film but NiTPP presented five intensity peaks in the form of powder [66]. The intensity peaks of ZnTTBPc compound presents at 2θ equal to $5.19^{o}$ for powder and $5.50^{o}$ for spin-coated film which correspond to the d value = 17.03 and 16.06 Å, respectively. The intensity peak of ZnTTBPc spin coated film was different from ZnTTBPc thermal evaporation that was observed at 2θ equal to $7.34^{o}$ [67]. The intensity peaks of MnTPPCl compound presents at 2θ equal to $17.32^{o}$ for powder and $16.67^{o}$ for spin-coated film which correspond to the d value = 5.12 and 5.32 Å, respectively. The XRD patterns of ZnTTBPc, ZnTPP, MnTPPCl spin-coated thin films confirm that each film shows the individual crystalline structure. From the result, the intensity peaks of mixed layer of ZnTTBPc/ZnTPP/MnTPPCl film that is observed at 2θ equal to 3.71° located near the main peak of ZnTTBPc film. The interplanar distance that is corresponding to 2θ equal to 3.71° is 23.79 Å. This peak indicates that the interplanar distance of mixed layer film is bigger than the value in all types of mono-layer films. Therefore, mixed layer film from various central metal atom (Zn and Mn) and different molecular skeleton (porphyrin and phthalocyanine) is arranged to form nanocrystalline with the different structure from mono-layer film. The effect of different nanocrystalline structure was observed by changing the central metal atom such as Al and Zn atom in phthalocyanines thin layers [68].

### 3.4.3 Computational Results

The theoretical work has been widely used for studying about the electronic structure of organic dye molecule. Therefore, the previous experiment results should be explained and compared with the computational results based on DFT method. The electronic structure at ground state of MP, MPc, methanol, ethanol and isopropanol were calculated by in basis set of B3LYP 6-31G* level that is usually used to calculate the structure that compost of H, C, N, Cl and O atom.

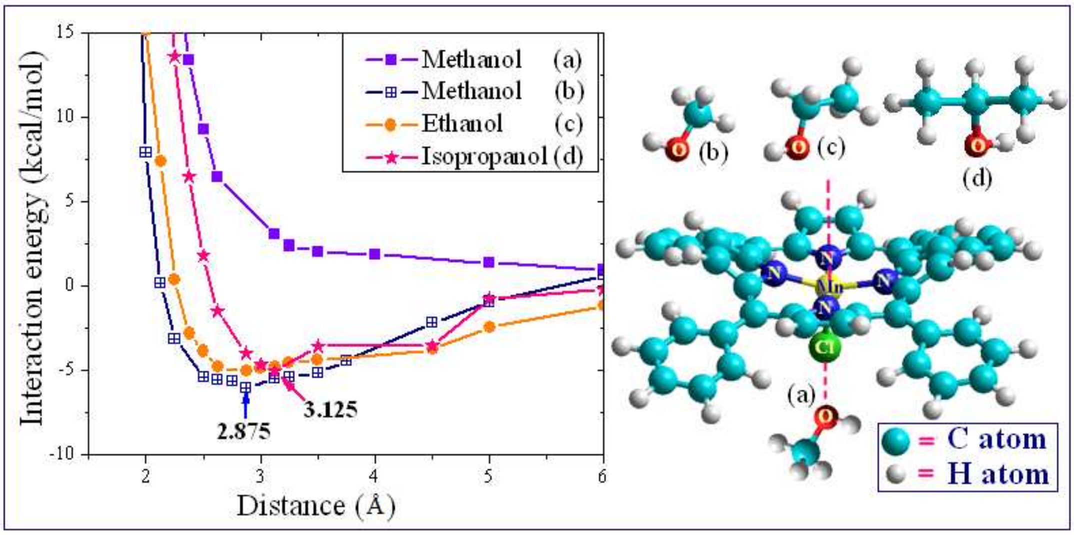

**Figure 3.8** Plot of interaction energies versus distance between oxygen atom in alcohols molecule and manganese (Mn) or chloride (Cl) atom in MnTPPCl molecule.

In case of MnTPPCl, there are two possible sites for gas interaction, namely, Mn and Cl atomic sites. The interaction energy between MnTPPCl and methanol molecule was studied in 2 conditions: 1) varying distance between chloride atom and oxygen atom (see Figure 3.8(a)) and 2) varying distance between manganese atom and oxygen atom (see Figure 3.8(b)). Figure 3.8 shows that the interaction energy plot of MnTPPCl with methanol in pattern (b) is higher than pattern (a). Therefore, the optimized site for gas absorption was observed at the metal atomic site in porphyrin and porphyrin derivative such as chlorophyll a and pheophytin a [69]. MnTPPCl has higher interaction energy with methanol than ethanol and isopropanol at the distance of 2.875 Å. This computational result shows an agreement with the experimental result that MnTPPCl spin-coated film shows the highest average gas sensing with methanol vapor (see Figure 3.3).

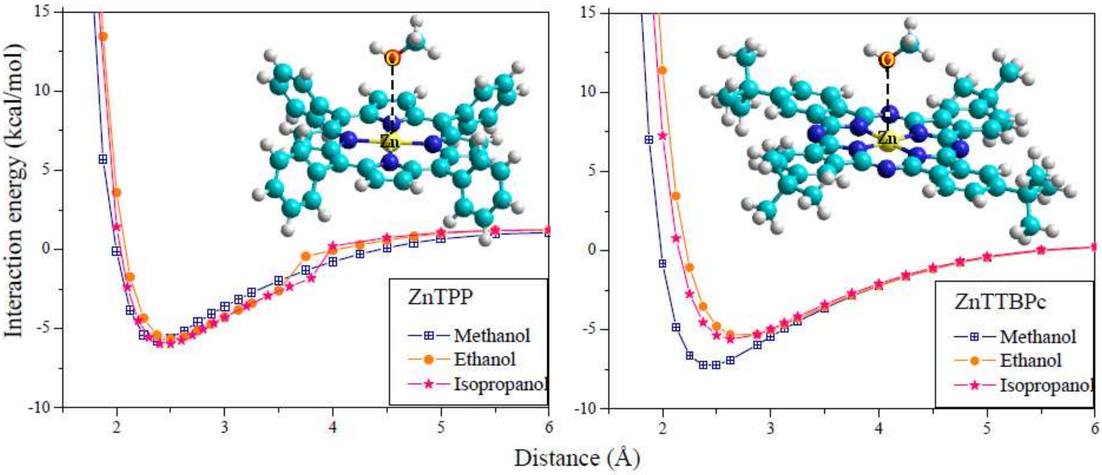

**Figure 3.9** Plot of interaction energies versus distance between oxygen atom in alcohols molecule and zinc atom in ZnTPP and ZnTTBPc molecules.

In case of ZnTPP and ZnTTBPc molecules, the interaction energy were investigated by varying the distance between oxygen atom in alcohols molecule and zinc atom in ZnTPP and ZnTTBPc molecules (see in Figure 3.9). The results reveal that ZnTPP has stronger interaction with isopropanol than methanol and ethanol at the optimized distance of 2.50 Å but ZnTTBPc has stronger interaction with methanol than ethanol and isopropanol at the optimized distance of 2.375 Å.

In addition, the binding energies and charges transfer when porphyrin or phthalocyanine interacts with alcohol molecule are reported in Table 3.1. The NBO charges at central metal atom of the optimized molecule for ZnTTBPc, ZnTPP and MnTPPCl were 1.63340 a.u., 1.61282 a.u. and 1.36981 a.u., respectively while the NBO charges at oxygen atom of methanol, ethanol and isopropanol were -0.74124 a.u., -0.75877 a.u. and -0.75311 a.u., respectively. The optimized distance between metal atom and oxygen atom shows the highest binding energy. ZnTPP show the highest binding energy with isopropanol at the distance of 2.50 Å while ZnTTBPc show the highest binding energy with methanol at the distance of 2.375 Å. From the experimental result, ZnTPP spin-coated film presents a good average gas sensing with isopropanol vapor while ZnTTBPc spin-coated film presents a good average gas sensing with methanol vapor (see in Figure 3.3). The computational result shows the agreement with the experimental result. The charges transfer between porphyrin or phthalocyanine and alcohols molecules were observed at the optimized distance. This charges normally transferred from central metal atom of porphyrin or phthalocyanine to the oxygen atom of alcohols molecule. The charge transfer between analyte molecule and sensing molecule in calculation method was corresponded to the absorption spectrum change of sensing thin film in the experiment results.

**Table 3.1** The interaction energies per one molecule; $\Delta E_{Int}$ (kcal/mol) at the optimized distance; D (Å) and the change in NBO charge for ZnTPP, ZnTTBPc and MnTPPCl.

| Interaction between | Sensing molecule | | | | | | | | | | | |
|---|---|---|---|---|---|---|---|---|---|---|---|---|
| | ZnTPP | | | | ZnTTBPc | | | | MnTPPCl (b)-(c) | | | |
| | $D$ | $\Delta E_{Int}$ | Δ Charge of | | $D$ | $\Delta E_{Int}$ | Δ Charge of | | $D$ | $\Delta E_{Int}$ | Δ Charge of | |
| | | | Zn | O | | | Zn | O | | | Mn | O |
| Methanol | 2.375 | -5.79 | 0.036 | -0.046 | 2.375 | -7.24 | 0.030 | -0.048 | 2.875 | -6.05 | 0.057 | -0.027 |
| Ethanol | 2.500 | -5.66 | 0.031 | -0.035 | 2.625 | -5.31 | 0.023 | -0.033 | 2.875 | -5.04 | 0.051 | -0.020 |
| Isopropanol | 2.500 | -5.96 | 0.031 | -0.039 | 2.625 | -5.60 | 0.023 | -0.037 | 3.125 | -5.08 | 0.044 | -0.021 |

### 3.4.4 Principal Component Analysis (PCA)

PCA is the simplest technique amongst true eigenvector-based multivariate analyses, which best accounts for the variance in the data. The principle idea of this method is start from the chemical analysis that are used more than one measurement for single sample such as volatile amine detection based on four types of nanocomposite gas sensor array [4]. Moreover, this technique has been used as the pattern recognition method in e-nose system; for example, identify the quality of food products and contamination of formaldehyde in seafood. In this work, the gas-sensing responses (S) from UV-Vis spectrophotometer were analyzed by PCA calculation. The data sets for PCA calculation were extracted from the difference of the average gas-sensing responses between a sensing vapor and the reference gas. The efficiency in VOCs discrimination of mixed layer gas sensor based on ZnTTBPc/ZnTPP/MnTPPCl was compared with its single layer gas sensor by using PCA method. Figure 3.10 shows the PCA in two-dimensional score plot related to the data from the five sensing arrays based on the optical absorption spectra region (R1-R5). The results conclude that the mixed layer of ZnTTBPc/ZnTPP/MnTPPCl more clearly classified the three types of alcohol vapor than mono layer of ZnTTBPc, ZnTPP and MnTPPCl.

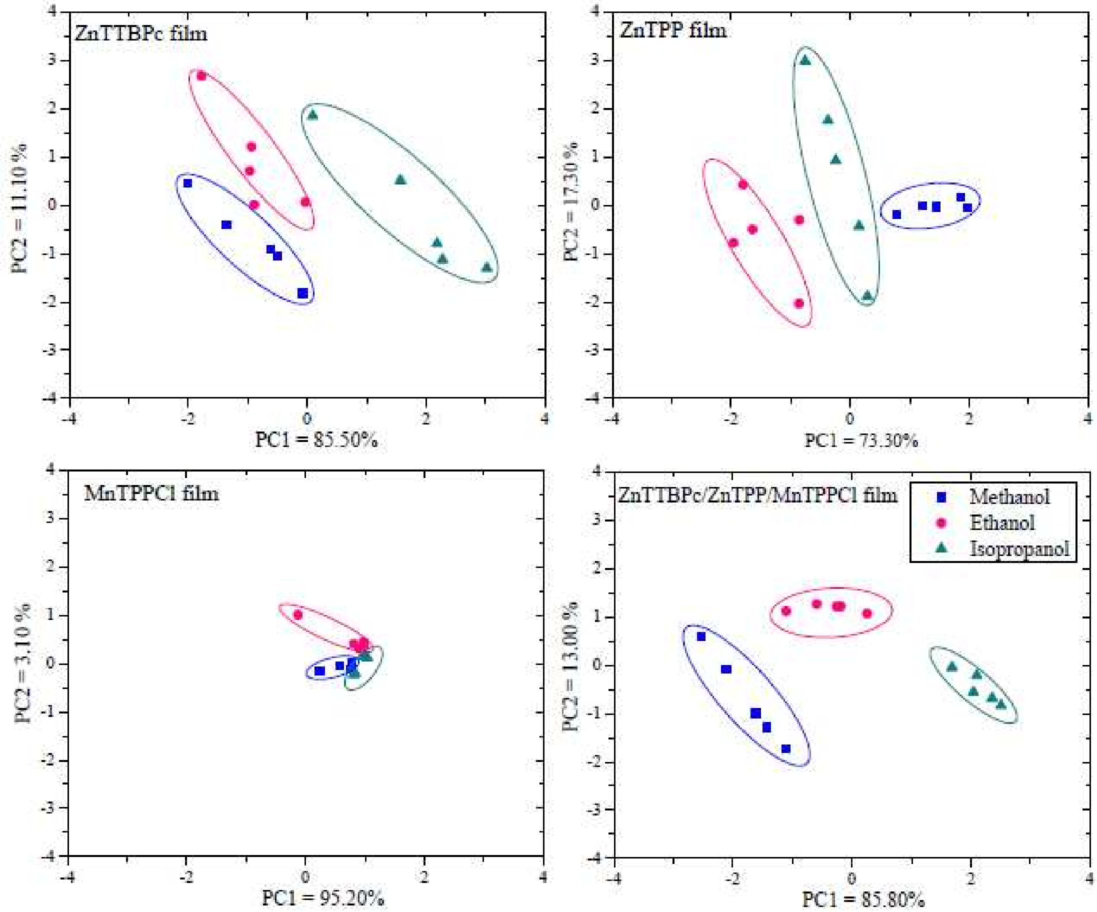

**Figure 3.10** PCA two dimensional score plot of the optical gas sensors based on ZnTTBPc, ZnTPP, MnTPPCl and ZnTTBPc/ZnTPP/MnTPPCl film.

The efficiency of mixed layer gas sensor was tested with other VOCs which are found in food and beverages odor such as acetone and acetic acid. Figure 3.11 (a) shows the classification of five vapors, namely methanol, ethanol, isopropanol, acetone (5% eq.) and acetic acid (5% eq.) for mixed layer gas sensor. Therefore, this mixed layer gas sensor was optimized for gas sensor in this optical e-nose system. Despite the classification of the different concentration of alcohol such as ethanol was interested in this work too. The ratios between ethanol and water were varied by change the volume of ethanol and water in the total volume of 50 ml. The optical sensors separate the different ratio between ethanol and water from 0 to 100% (see Figure 3.11(b)). The separation between ethanol 100% and 0% is shown clearly in PC1 axis direction. The PC1 axis that is the highest variance value of principal coordinates (81.67%) represents the almost important information of the data set. The data set of ethanol 100% stays in the left hand side of Figure 3.11(b) while the data set of ethanol 0% (or water 100%) stays in the right hand side of Fig. 11(b). It is clearly to conclude that PCA is an absolute statistical method in the electronic nose system to classify the group of vapor. This method is a high efficiency and a low demand on computing power in the system. Therefore, the optical electronic nose system based on the three types of organic compounds should be highly effective for discriminating VOCs and applicable to qualitative measurements of food and alcoholic beverage.

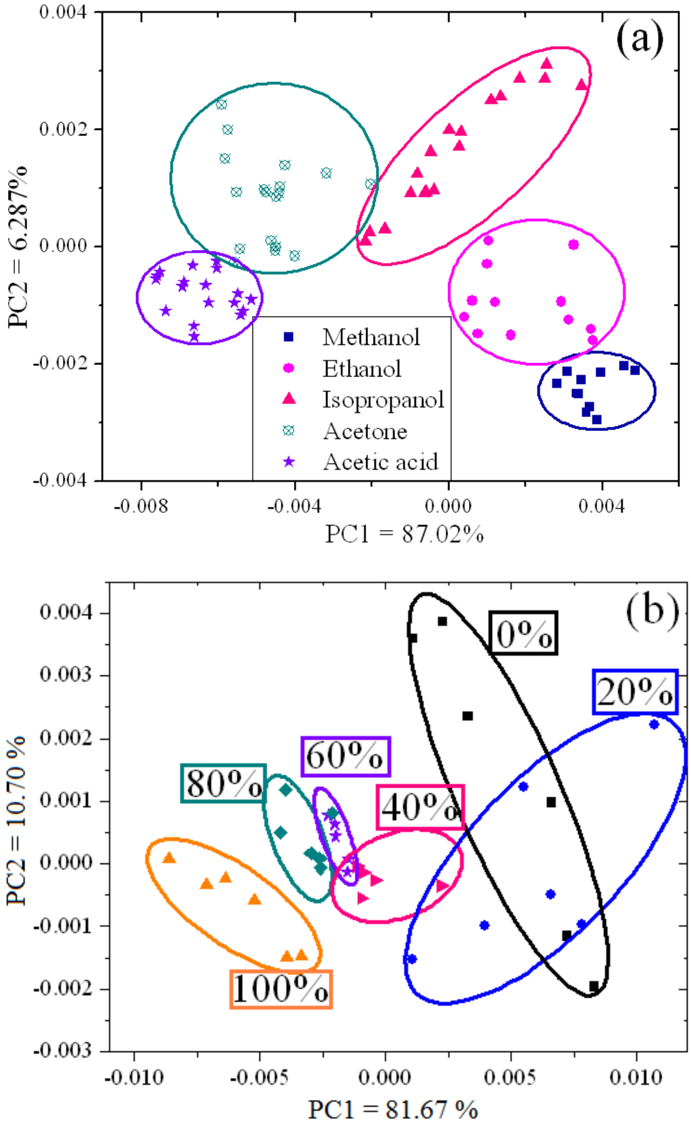

**Figure 3.11** PCA two dimensional score plot related to the five arrays optical sensor corresponding to (a) five types of VOC vapor and (b) varying concentration of ethanol in water.

## 3.5. Conclusions

The mixed layer of ZnTTBPc/ZnTPP/MnTPPCl spin-coated thin films has been demonstrated to be able to detect various kinds of VOC vapor, namely methanol, ethanol, isopropanol, acetone (5% eq.) and acetic acid (5% eq.). The AFM and XRD were used to investigate the nano crystalline structure of mixed layer spin-coated thin film. DFT method based on B3LYP6-31G* level successfully optimized the ground state structure of ZnTTBPc, ZnTPP, MnTPPCl, methanol, ethanol and isopropanol molecules. The interaction energies between sensing molecule and analyzed molecule in computational method confirmed the agreement with the gas sensing behavior in experimental result. Therefore, the optical electronic nose constructed from the mixed layer organic molecule exploits the high chemical information based on the optical absorption properties and the effective classification method based on PCA calculation.

# CHAPTER IV

# AN OPTICAL ARTIFICIAL NOSE SYSTEM FOR ODOR CLASSIFICATION BASED ON LED ARRAYS

## 4.1 Synopsis

Optical electronic nose (olfactory sensing) technologies have recently become a convenient technique to identify the quality of food and beverage products based on the odor classification. In this chapter, we reported an optical-based electronic nose system consisting of thin-film sensing materials, array of light emitting diode (LED), photo-detector and pattern recognition program. The organic mixtures thin film gas sensor was prepared by spin coating of Zinc-2,9,16,23- tetra-tert-butyl-29H,31H-phthalocyanine (ZnTTBPc), Zinc-5,10,15,20-tetra-phenyl-21H,23H-porphyrin (ZnTPP) and manganese(III)-5,10,15,20-tetraphenyl-21H,23H-porphyrin chloride (MnTPPCl) onto a clean glass substrate. The electronic nose system was developed by using the low-cost LED array as a light source. Then the light intensity that is transmitted through the organic thin film during the experiment was detected by the color light to frequency converter device (photo-detector). The ability of this system was tested by using volatile organic compound (VOCs) vapors such as methanol, ethanol, and isopropanol. Principal component analysis (PCA) has been used as the pattern recognition for this electronic nose system. The result confirms that the sensing layer that composed of the three types of organic compounds described the odor of chemical vapors, dried seafood and beers.

## 4.2 Introduction

An electronic nose is a clever instrument that functions as an olfactory system in human. The electronic nose instrument consists of an array of gas sensors, transducer, gas-flow system and pattern recognition. Several methods have been used for transduction of the sensing signals such as mass [70] and electrical transduction [51]. Optical technique is a simple and convenient method to detect the change of organic thin film gas sensor such as metallo-phthalocyanine (MPc) and metallo-porphyrin (MP) [61]. MPc and MP is the organic compound that produce the absorption spectra in UV-Vis region because the aromatic characters of these materials are related to electronic transitions within their π-aromatic system [71]. The optical electronic nose has been successfully predicted the volatile organic compound (VOC) concentrations in their binary mixtures (acetic acid and ethanol) based on spectrophotometer [72]. In addition, MPc and MP, namely ZnTTBPc, ZnTPP and MnTPPCl [41], successfully detected and classified volatile VOCs vapor such as alcohols, acetone, acetic acid and food product. Previous chapter confirmed that the organic mixtures of ZnTTBPc, ZnTPP and MnTPPCl spin-coated thin films are able to classify various VOC vapors, namely, methanol, ethanol, isopropanol, acetone (5% eq.), acetic acid (5% eq.) and methyl benzoate (5% eq.) based on UV-Vis spectrophotometer instrument [73]. In this chapter, an optical electronic nose was developed for optical measurement by using the low-cost LEDs as a light source and the organic thin film as the sensing material. The color light to frequency converter device was used as transducer to collect the changing of light intensity that transmits from the sensing layer. The organic mixtures thin film gas sensor was prepared by spin coating the mixing solution of ZnTTBPc, ZnTPP and MnTPPCl onto a clean glass substrate and annealing at 250°C under argon atmosphere. Finally, the classification of the odor was analyzed by principal component analysis (PCA) method.

## 4.3 Experimental

### 4.3.1 Optical Electronic Nose System Setup

The optical electronic nose set up comprises basic components namely, light source, sensing materials or sensor and a device for detecting light signals coming from the sensor as shown in Figure 4.1. Low-cost LED array was chosen to be a light source in this system. There was commercial photo-detector (ET-TCS230) to detect the light intensity. All of the measurements were performed at room temperature. The gas sensing capability of the organic thin films have been investigated under the dynamic gas flow through a home-built chamber that shields the light from the outside. Nitrogen (99.9%) gas was used as the reference and carrier gas to conduct headspace vapor from the sample bottle at the rate flow about 500 ml/min. The gas flow was controlled by solenoid valve to switch between the reference gas (4 minutes) and sample gas (2 minutes). The solenoid valve and LED array were controlled by LABVIEW program based on DAQ card. Each measurement consists of 5 cycles of switching between the reference and sample gas.

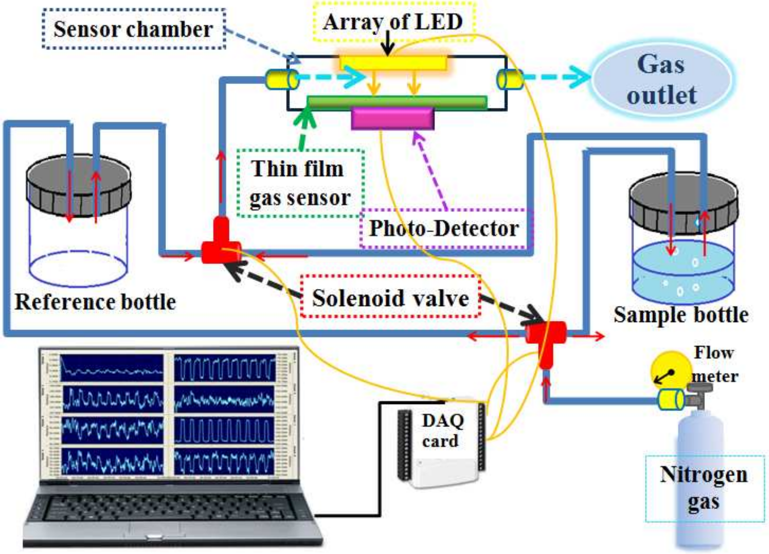

**Figure 4.1** Schematic diagram of optical electronic nose setup.

The schematic diagram for LED array and photo-detector is shown in Figure 4.1. The spectra of color LED was investigated by ocean optic instrument. The light intensity of red, yellow, green, blue, pink, and violet LED was occurred at 638, 587, 537, 457, 472 and 399 nm.  The switching between eight LEDs was controlled by a multiplexers (MAX4617CPE) device. This system consists of infrared, red, yellow, green, blue, pink, violet and white LED. Then the photo-detector that consists of photodiode array translates the light intensity to the current and frequency (f), respectively. This measurement was controlled by LABVIEW program.

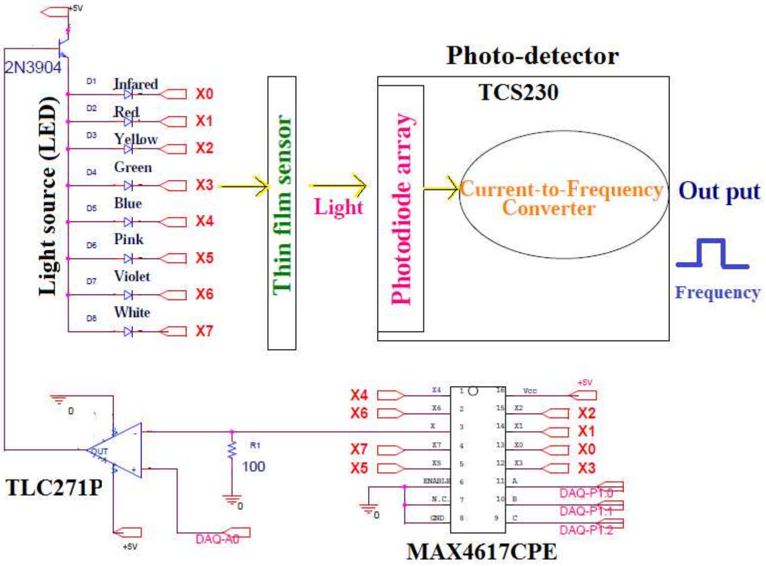

**Figure 4.2** The diagram of eight colors LED for optical sensing arrays and photo-detector device.

### 4.3.2 Sensor Fabrication

ZnTTBPc, ZnTPP and MnTPPCl were obtained from Sigma-Aldrich. The mixed solution of ZnTTBPc/ZnTPP/MnTPPCl was obtained from a 3 ml of chloroform solution containing 12 mg of ZnTTBPc, 5 mg of ZnTPP and 15 mg of MnTPPCl. Then the blended ZnTTBPc/ZnTPP/MnTPPCl thin films were obtained by spinning the solution onto a glass substrate at 1,000 rpm for 30 s. The spin-coated thin films were placed in a furnace under the argon atmosphere, heated at the rate of 5 °C per minute to reach 250 °C and then cooled down for 3 hours. The optical spectrum of annealed spin-coated film was tested under the atmosphere of methanol, ethanol and isopropanol vapor using Jenway UV-Vis spectrophotometer.

## 4.4 Results and Discussions

### 4.4.1 Optical Measurements and Sensing Characteristics

The absorption spectra of non-annealed and annealed spin-coated films are shown in Figure 4.3 (a). The mixed layer thin film shows the absorption peak at 345, 430, 480, 620 and 695 nm, in accordance with the absorption peaks of Q band and B band in the metallo-phthalocyanine (MPc) [58] and Soret bands and the Q bands in the metallo-porphyrin (MP) [59]. The main peak of annealed film was shifted. The intensity of absorption peak at 345 and 480 nm increased while the intensity of absorption peak at 620 and 695 nm decreased. And the absorption peak at 430 nm shifted to 428 nm. The absorption change of annealed film during the gas flow system is presented in Figure 4.3 (b). Methanol, ethanol and isopropanol were used as sensing vapors. The absorption changes were clearly observed at 390, 430, 480 and 695 nm. The interaction between porphyrin and oxidizing or reducing gases depend on the π-π* interaction that relate to the absorption spectra of the organic compounds [74]. Therefore, the visible light LEDs were used as the light sources and photo detector was used as transducer to detect the color change of sensing material in this chapter.

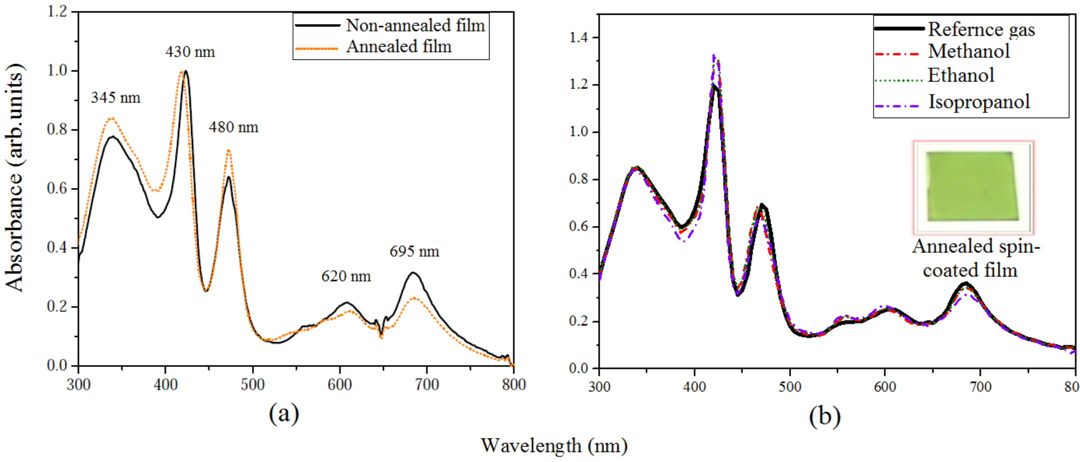

**Figure 4.3** The absorption spectra of (a) non-annealed and annealed films and (b) annealed films under reference gas, methanol, ethanol and isopropanol vapor.

Figure 4.4 show the sensing signal of blue (457 nm) and violet (399 nm) LED with methanol, ethanol and isopropanol vapor. The photo-detector collected the frequency (f) that directly proportional to the light intensity. Methanol and ethanol vapors present the faster response with gas sensor than isopropanol vapor. This result was related to the vapor pressure of alcohol because isopropanol has low vapor pressure than methanol and ethanol.

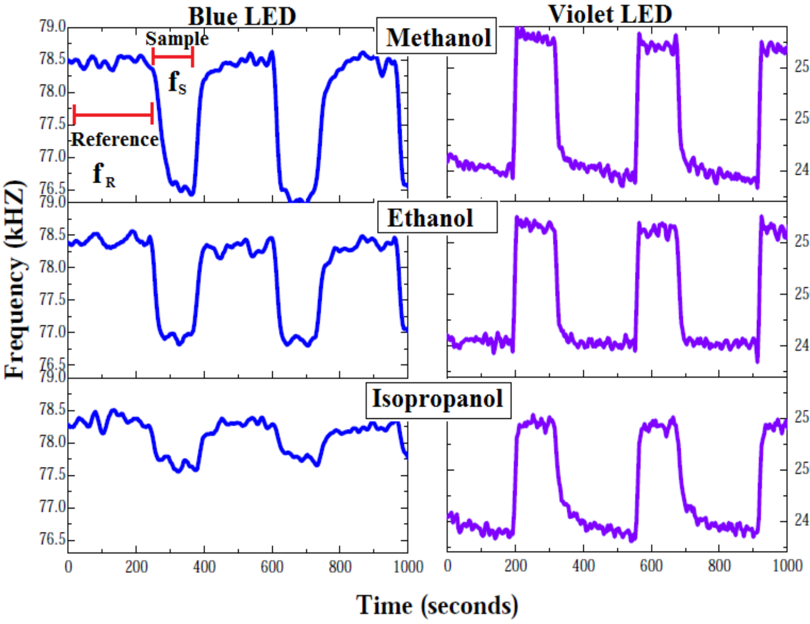

**Figure 4.4** The sensing signal of blue and violet LED with methanol, ethanol and isopropanol vapor.

The average gas sensing response of eight LED sensor array for three types of alcohol is presented in Figure 4.5. The gas sensing response (S) was calculated from equation (1)

$$S = \Delta f / f_R \qquad (4.1)$$

when $f_R$ is the average frequency during flowing reference gas and $\Delta f$ is the average of the different frequency between reference gas ( $f_R$ ) and sample gas ( $f_S$ ).

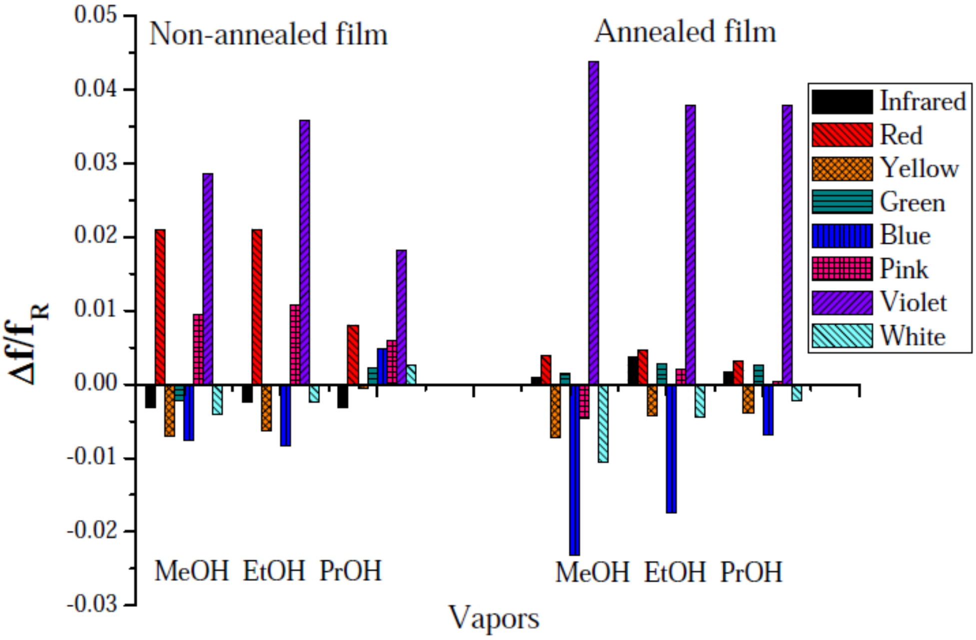

**Figure 4.5** The average gas sensing response of eight LED sensor array for three types of alcohol.

Gas sensing responses of non-annealed film and annealed film were compared (see Figure 4.5). The annealed film presented the strong gas sensing responses for all types of alcohol. Thermal annealing method developed structure of sensing layer. Violet LED presents the highest average gas sensing response with all of chemical vapor. The LED operating in the violet region which is corresponding to the absorption spectrum of porphyrin at 430 nm (see Figure 4.3) presents the highest response with analyzed gas [75].

The surface structures of non-annealed and annealed layers are investigated by atomic force microscope (AFM) (see Figure 4.6). The roughness of non-annealed and annealed film were 1.15 and 2.28 nm, respectively. Thermal annealing process changed the surface from smooth to knobbed surface. This modified surface was the optimized structure for gas detection because the gas sensing response increased for annealed film gas sensor.

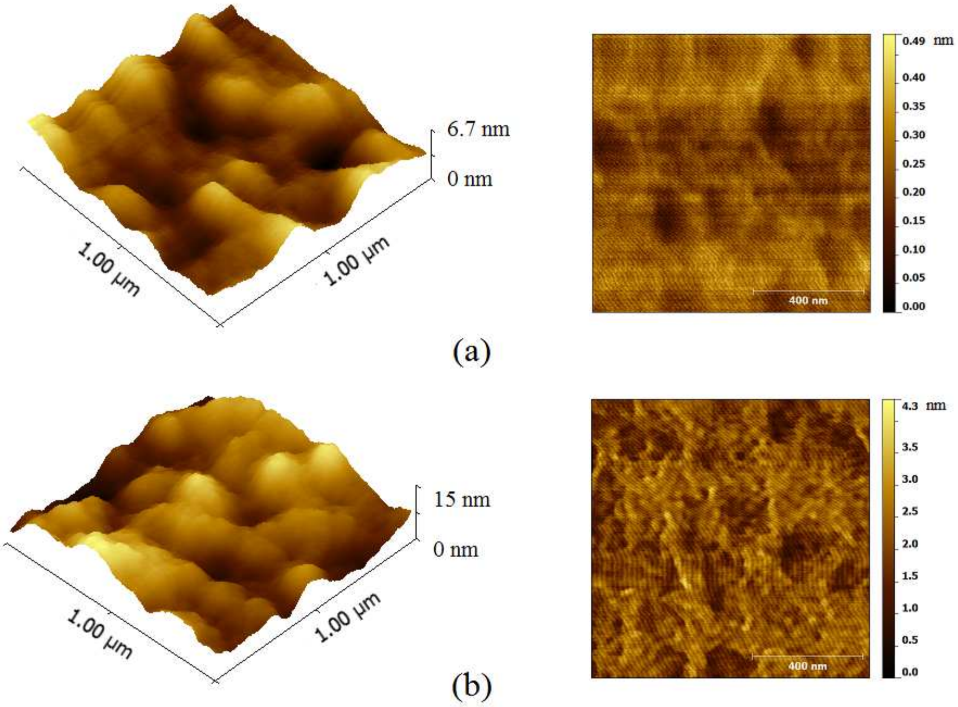

**Figure 4.6** AFM image in 3D and phase of (a) non-annealed film and (b) annealed film.

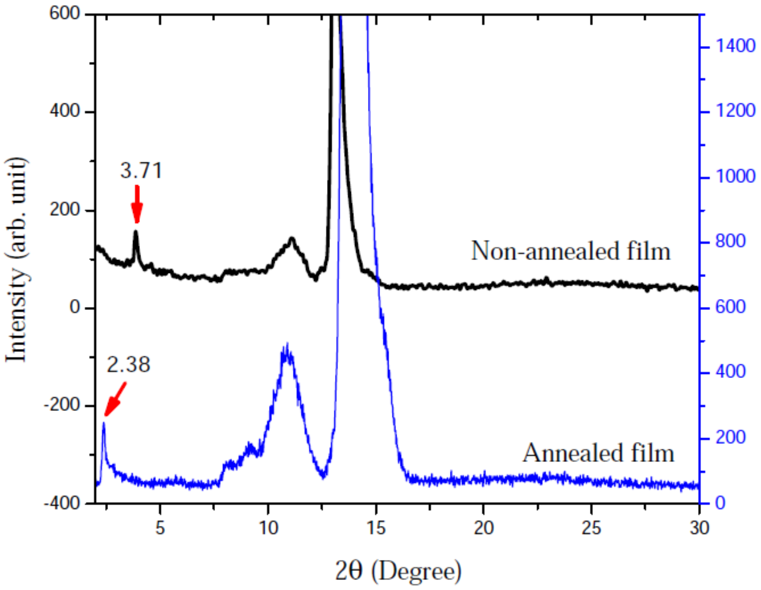

**Figure 4.7** XRD pattern of non-annealed film and annealed film.

Figure 4.7shows the corresponding intensity peaks of non-annealed and annealed ZnTTBPc/ZnTPP/MnTPPCl spin-coated films by observing a broad diffraction band from $2^{o}$ to $30^{o}$. The intensity peaks at 2θ equal to $11^{o}$ and $13^{o}$ for both films are the effect from the glass slide substrate. The intensity peaks of non-annealed and annealed film present at 2θ equal to $3.71^{o}$ and $2.38^{o}$, respectively. The interplanar distance (d) for non-annealed film is 23.79 Å while interplanar distance (d) for annealed film is 37.09 Å. The distance between crystal planes increased after thermal annealed process. Therefore, annealing at high temperature affected to the orientation of dye molecules, for example the interplanar space of ZnTTBPc evaporated film increased when temperature of substrate was increased [67].

### 4.4.2 Odor Classifications

PCA technique was used as the classification method for optical electronic nose to identify the quality of food products [37, 61]. The data sets of PCA were calculated from the difference of the average gas sensing responses between a sample vapor and the reference gas. In this electronic nose setup, there are 8 sensors based on different LED color to identify the types of chemical vapor. ZnTTBPc/ZnTPP/MnTPPCl sensor successfully detected and discriminated several four type of chemical vapor (see in Figure 4.8). There are clearly separate four types of alcohol. The data of alcohol mixtures (methanol 50% and ethanol 50%) located between methanol 100% and ethanol 100% data. In addition, this electronic nose system successfully describes various concentration of ethanol in water volume by volume (0-100% of ethanol) as shown in Figure 4.9. Food and beverages produce were classified by this e-nose system, such as Figure 4.10 show the classification of 3 dried seafood and 3 commercial beers. These results indicate that this optical electronic nose system may be used as the olfactory system to classify foods and beverages.

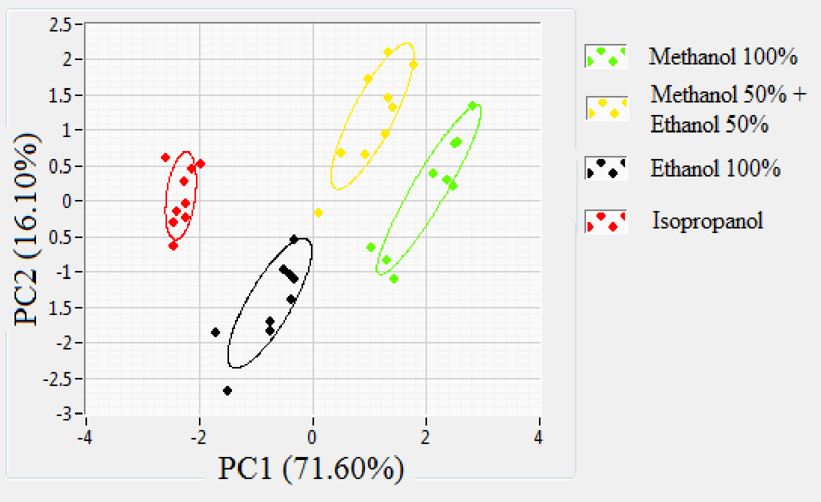

**Figure 4.8** PCA two dimensional score plot related to the eight arrays of optical sensor corresponding to several types of the alcohol vapor.

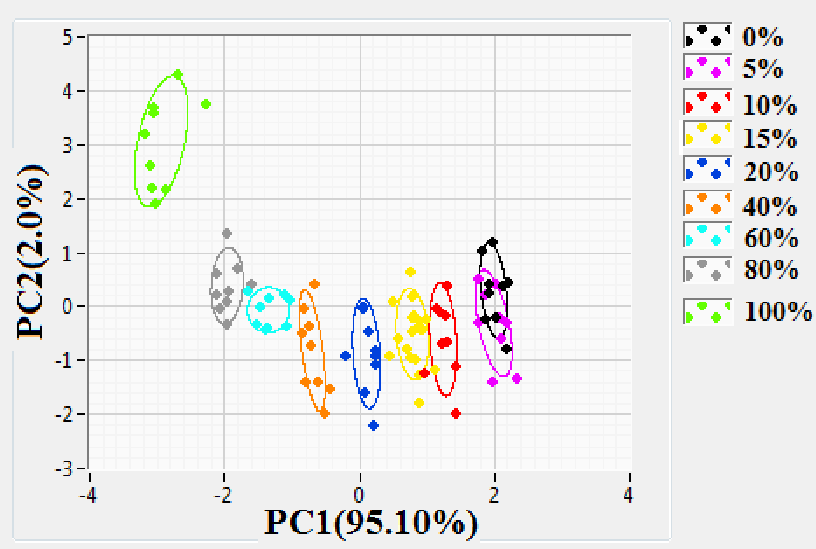

**Figure 4.9** PCA two dimensional score plot related to the eight arrays of optical sensor by varying the concentration of ethanol in water.

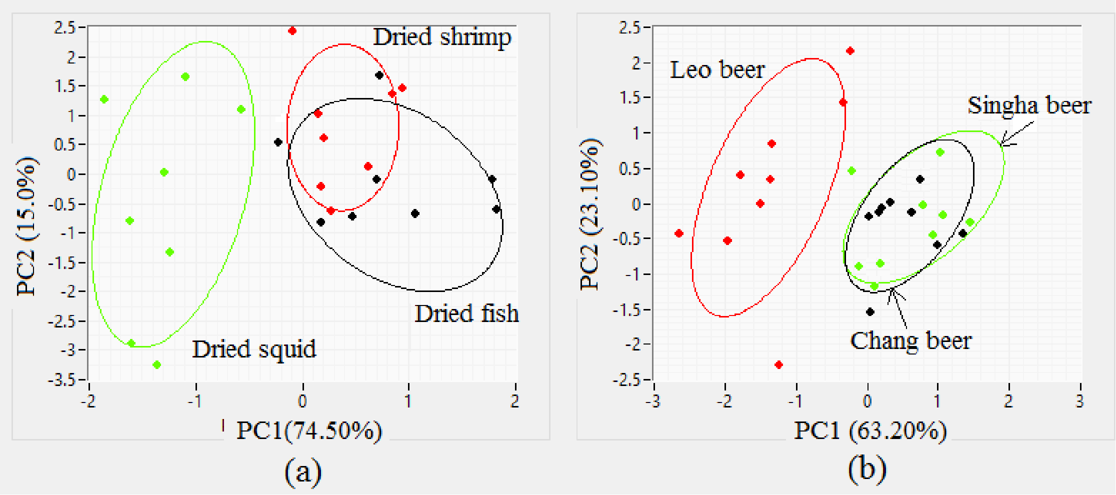

**Figure 4.10** Classification of (a) dried seafood and (b) alcoholic beverages based on PCA calculation.

## 4.5 Conclusion

The optical electronic nose was developed by using LED and photo detector as the sensor array and ZnTTBPc/ZnTPP/MnTPPCl spin-coated thin films as a sensing layer. The photo detector successfully detected the change of light intensity during the gas flow measurement. Gas sensor was developed by thermal annealing process. The annealed film presented more roughness and larger interplanar distance than non-annealed film. The annealed structure increased efficiency of gas sensor. PCA clearly separated the methanol 100%, ethanol 100%, isopropanol 100% and mixing of methanol 50%+ethanol 50%. Finally, this system detected the varying concentration of ethanol solution in water. The classification of food and beverage will test in the future work.

# CHAPTER V

# HYBRID OPTICAL-ELECTROCHEMICAL ELECTRONIC NOSE SYSTEM BASED ON Zn-PORPHYRIN AND MULTI-WALLED CARBON NANOTUBE COMPOSITE

## 5.1 Synopsis

In this chapter, we have enhanced the capability of an e-nose system based on combined optical and electrochemical transduction within a single gas sensor array. The optical part of this e-nose is based on detection of the absorption changes of light emitted from eight light emitting diodes (LEDs) as measured by a complementary metal oxide semiconductor (CMOS) photo-detector. The electrochemical part works by measuring the change in electrical resistivity of the sensing materials upon contact with the sample vapor. Zinc-5,10,15,20-tetra-phenyl-21H,23H-porphyrin (ZnTPP) and multi-walled carbon nanotube (MWCNT) composite was used as the sensing materials based on its good optoelectronic properties. This sensing layer was characterized by UV-Vis spectroscopy and atomic force microscope and tested with various VOC vapors. Density functional theory (DFT) calculations were performed to investigate the electronic properties and interaction energies between ZnTPP and analyte molecules. It can be clearly seen that this hybrid optical-electrochemical electronic nose system can classify the vapor of different volatile organic compounds.

## 5.2 Introduction

The olfactory system is an essential equipment for survival of all mammals, although nowadays human employs this critically important sense mainly for pleasure. At present, electronic nose (e-nose) has been invented to mimic this sense of smell and applied in many applications such as food safety and quality control [76], and air quality monitoring [77] etc. The main components of an e-nose system are an array of gas sensors, transducer and pattern recognition. Gas sensors can be implemented based on different sensing materials and transduction principles, for example, conducting polymer [78], metal oxide semiconductor [3], piezoelectric [40], electrochemical, and optical sensors [79]. Recently, combing different working principles to produce hybrid electronic nose is becoming an active area of e-nose research.

Porphyrins are a class of semiconductor materials that have been widely used as optical sensors to detect the volatile organic compound (VOC) based on the change of light intensity [71]. Zinc-5,10,15,20-tetra-phenyl-21H,23H-porphyrin (ZnTPP) was demonstrated to optically detect alcohol, acetone, acetic acid, methyl benzoate, and commercial alcoholic beverages [37,63]. To observe the electrical change of highly resistive ZnTPP, carbon nanotube (CNT) has been introduced to produce CNT/ZnTPP nanocomposite with moderate conductivity [80]. In addition, CNT may help to amplify the gas detection by increasing adsorption surface presented on the interior and exterior of the sidewalls [81].

In this chapter, we have constructed a hybrid e-nose system based on ZnTPP/MWCNT nanocomposite thin film and hybrid optical and electrical measurements. The eight color light emitting diodes (LEDs) and a CMOS photo-detector were used as light source and detector, respectively, for optical measurement of the absorption changes of sensing materials. In addition, change in electrical resistance of the sensing materials upon contact with the sample vapor was also recorded to complement the optical measurement. This hybrid gas sensor array was tested with different VOC groups such as alcohols, ester, ether, ammonia, ketone and acid. To understand the sensing mechanism, density functional theory (DFT) calculations were performed to investigate the electronic properties and interaction energies between ZnTPP and analyte molecules [82]. Classification of these vapors based on was successfully solved by pattern recognition based on the principal component analysis (PCA).

## 5.3 Experimental

### 5.3.1 Optical-electrochemical Electronic Nose System

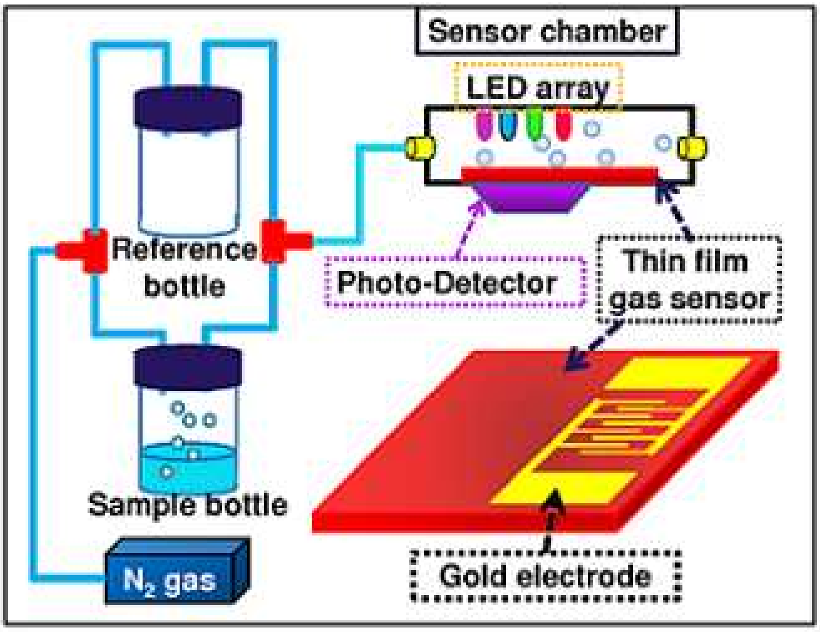

**Figure 5.1** The hybrid optical-electrochemical e-nose system based on the organic thin film.

The optical-electrochemical electronic nose comprises two basic components, namely optical and electrochemical parts as shown in Figure 5.1. The optical part is composed of eight color light emitting diodes (LEDs) and the device for detecting light signals coming from the sensor (CMOS photo-detector). The intensity peak of red, yellow, green, blue, pink, and violet LEDs was centered at 638, 587, 537, 457, 472 and 399 nm. The electrical part was constructed from the voltage divider circuit to detect the resistance change of sensing material. Both optical and electrical parts work by measuring the change in light intensity and resistance of the sensing materials upon contact with the sample vapor at room temperature. This sensing material was prepared on the clean glass substrate on top of the interdigitated gold electrodes. The gas sensing capability of the hybrid gas sensor has been investigated under the dynamic gas flow through a home-built chamber. Nitrogen (99.9%) gas was used as the reference and carrier gas to conduct headspace vapor from the sample bottle at the rate flow about 500 ml/min. The gas flow was controlled by solenoid valves to switch between the reference gas (4 minutes) and sample gas (2 minutes). Each measurement consists of 4 cycles of switching between the reference and sample gas. The experiment was repeated for three times on each sample.

### 5.3.2 Sensor Fabrication

ZnTPP was obtained from Sigma-Aldrich, whereas MWCNT was obtained from Chiang Mai University (synthesized by Dr. Phisit Singjai) [83]. MWCNT was dissolved in chloroform solution at the concentration of 2 mg/ml by using ultrasonicator and magnetic stirrer while ZnTPP was dissolved in chloroform solution at the concentration of 4 mg/ml by using ultrasonicator. Such concentration ratio yields the optimized gas sensing properties in our work. Then the solutions of MWCNT and ZnTPP were mixed together using ultrasonicator and magnetic stirrer. The hybrid gas sensor (ZnTPP-MWCNT) thin film was prepared by spinning the solution onto the specially-prepared substrate (see Figure 5.1) for optical and electrical measurement at 1,000 rpm for 30 s.

### 5.3.3 Quantum Mechanics Modeling

The geometries and electronic structure of porphyrin in ground state have been studied by density functional theory (DFT) calculation [56]. The initial structure of ZnTPP and VOCs molecules were optimized based on B3LYP/6-31G* level of theory. Then the electronic properties and the interaction energy between VOCs and ZnTPP were calculated by B3LYP/6-31G* too. The distance between the oxygen atom in VOCs molecule (nitrogen atom in ammonia molecule) and the zinc atom in porphyrin molecule at the highest interaction energy was investigated. The interaction energies between ZnTPP and VOCs molecule were calculated by equation (5.1):

$$E_{\mathrm{int}\,eraction} = E_{ZnTPP+VOC} - (E_{ZnTPP} + E_{VOC}) \tag{5.1}$$

Where $E_{ZnTPP}$ and $E_{VOC}$ is the total energy of isolated ZnTPP and VOC molecule, respectively.

## 5.4 Results and discussions

### 5.4.1 Characterization of Hybrid Gas-sensing Films

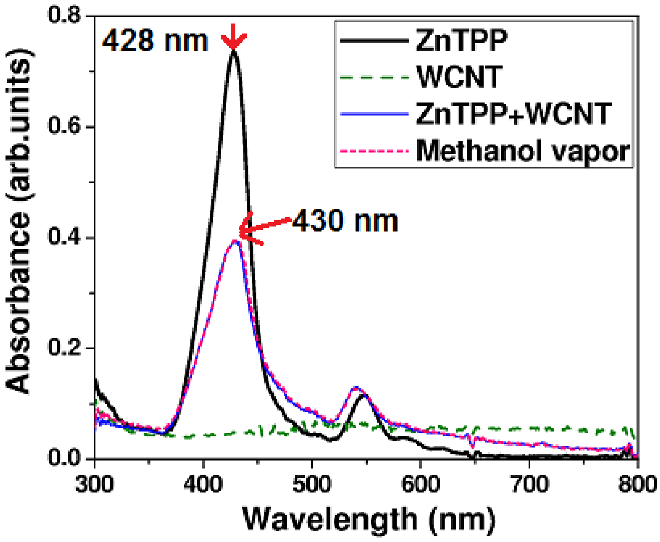

**Figure 5.2** The absorption spectra of ZnTPP, MWCNT and ZnTPP+MWCNT spin-coated thin film.

Figure 5.2 presents the UV-Vis absorption spectra of ZnTPP, MWCNT and ZnTPP-MWCNT spin-coated thin film. The absorption peak of ZnTPP was occurred at 428 nm and the non-absorption peak of MWCNT was observed [84]. This absorption spectrum is related to the Soret band (B band) around 400 nm and weak Q bands at 480-680 nm which can be determined by the transition of the electrons from ground to the excited state [85]. But after adding MWCNT into ZnTPP, the absorption spectrum was decreased and slightly shifted to 430 nm. The absorption spectrum shift corresponded to the formation of more aggregates or closer packing in porphyrin thin film [70,86] and normally occurred after the formation of the porphyrin thin film [87]. The slight red shift in Soret band is assigned to the change in the packing (stacking) between the ZnTPP molecular layers when MWCNT molecules are inserted. The blue shift in Q band can be assigned to the additional pi-pi interactions between ZnTPP and MWCNT. In the gas sensing experiment, methanol vapor effected to the absorption spectrum of hybrid gas sensor only slightly by shifting the absorption peak. The biggest spectrum shift was occurred in the range 300-360 nm.

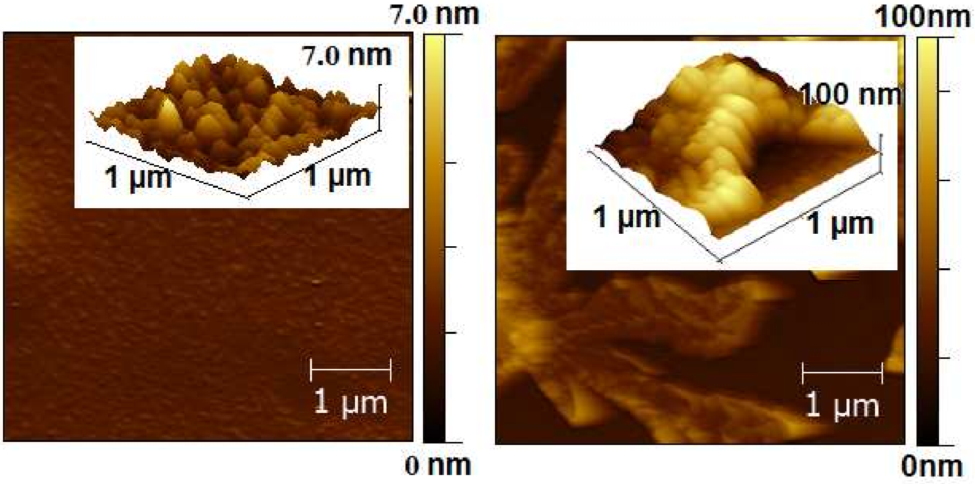

**Figure 5.3** DFM images in top views and 3D of ZnTPP (left) and ZnTPP-MWCNT (right) spin-coated film.

The effect of MWCNT in ZnTPP spin-coated film was investigated by dynamic force microscope (DFM) as shown in Figure 5.3. The average roughness for ZnTPP and ZnTPP-MWCNT spin-coated film was found to be 0.64 and 27.50 nm, respectively. Thus, the increasing grain size of ZnTPP-MWCNT corresponds to the average diameter size of MWCNT 27 nm [83]. Therefore, more surface area available for gas sensing is expected and MWCNT can act as nanochannel that help transport the analyte molecules into the deeper layers of ZnTPP, leading to enhanced sensitivity. The distribution of MWCNT is quite random and it organizes like a rope that consists of many aligned CNT due to van der Waals forces between CNT walls [88].

The sensor signals of hybrid gas sensor were investigated by measuring the change in light intensity and resistance of the material under the dynamic gas flow (see in Figure 5.4). In optical measurement, the photodiode array in CMOS photo-detector is functioning as a current to frequency convertor. This detector counts the pulse of the current as the frequency which is generated from the incident photon and related to the light intensity [89]. Therefore, the gas sensor signals of optical measurement were presented in terms of frequency values. The highest change of gas sensor signals was observed in the violet LED (399 nm) that related to the change in the absorption spectra of ZnTPP-MWCNT under methanol vapor (Figure 5.3). The same trend of sensor signal was observed in the electrical measurement, which suggests a slight charge transfers between MWCNT and the reducing gas [90].

### 5.4.2 Gas Sensing Response

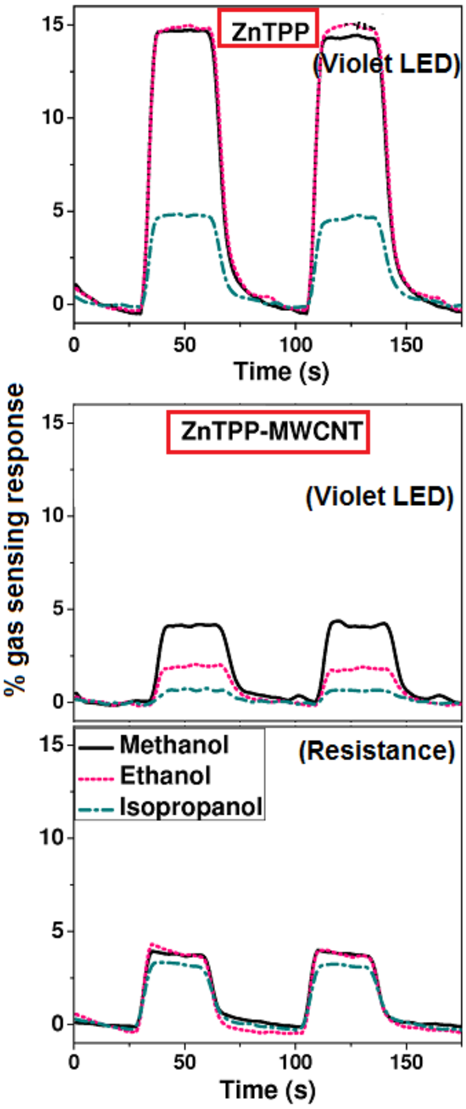

**Figure 5.4** The percentage of gas sensing response in ZnTPP, MWCNT and ZnTPP-MWCNT spin-coated film with methanol, ethanol and isopropanol vapor at room temperature.

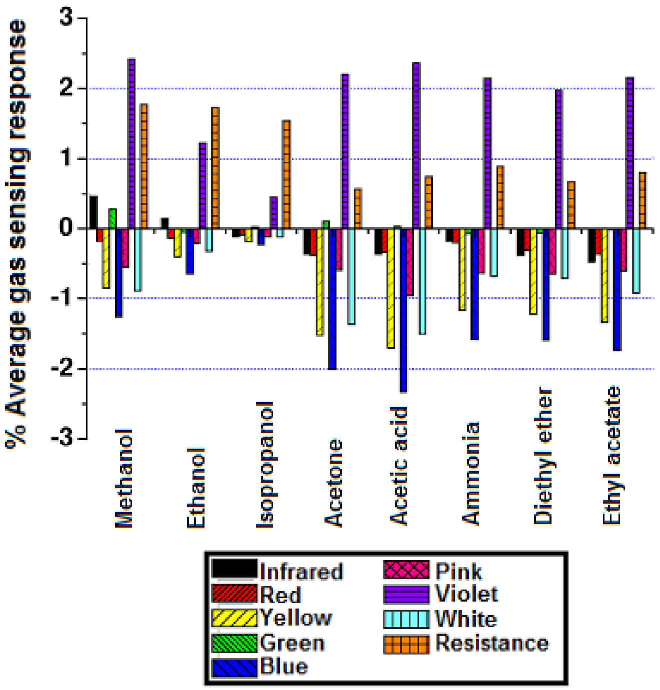

**Figure 5.5** The percentage of the average gas sensing response for nine sensor array with eight types of VOC.

The gas sensing response (S) was calculated from the $\Delta f / f_R$ where $\Delta f$ is defined from $f_S - f_R$ (see in Figure 5.4). The $f_S$ and $f_R$ represent the sensor signal upon sensing vapor and reference gas, respectively. Figure 5.5 shows the percentage of average gas sensing response for nine sensors with eight types of VOC. The sample vapors were generated from the solution of methanol (100%), ethanol (100%), isopropanol (100%) and acetone (5% aq.), acetic acid (5% aq.), ammonia (5% aq.), diethyl ether (5% aq.) and ethyl acetate (5% aq.) at ambient conditions. Based on evaporation rate at these conditions, methanol vapor presents the highest average gas sensing among alcohols. Acetic acid presented higher average gas sensing response than other VOCs (5% in aqua). It can be seen most vapor responses strongly within the green-violet region of the visible spectra. It was thus expected that this hybrid electronic nose will be efficient for most VOCs.

### 5.4.3 Sensing Mechanism

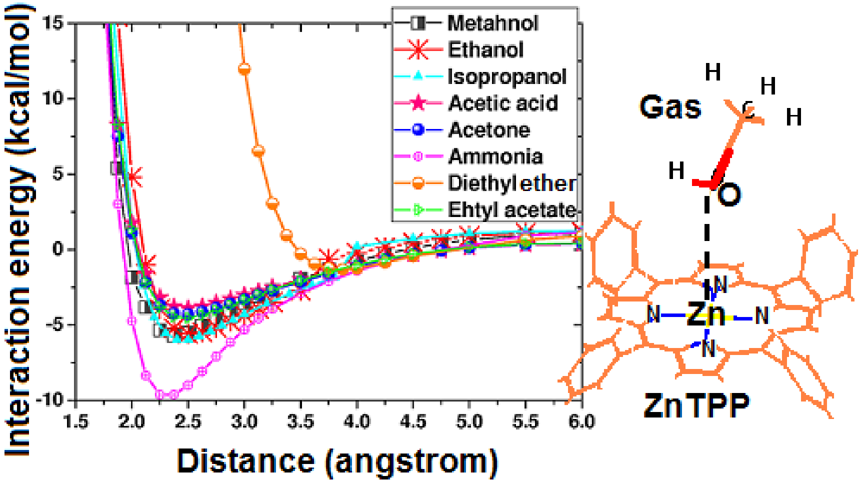

**Figure 5.6** The plot of interaction energies versus distance between oxygen atom in VOCs molecule (or nitrogen atom in ammonia) and Zinc atom in ZnTPP molecule.

To understand the mechanism of ZnTPP sensor, we have investigated the interaction energy when ZnTPP interacts with VOC molecule. Figure 5.6 plots the interaction energies versus distance (*D*) between oxygen atom in VOCs molecule (or nitrogen atom in ammonia) and Zinc atom within the center if ZnTPP molecule. Ammonia molecule presents stronger interaction energy than alcohols, ethyl acetate, acetone, acetic acid and diethyl ether. The average optimized distance for all VOC is about 2.46 Å. Table 1 indicates the change of electronic properties such as energy gap and charge exchange at the optimized distance. Electron transfer from Zinc and nitrogen atoms in the porphyrin ring to the oxygen atom in VOCs molecule was found. Such results have confirmed our experiment that the resistance of hybrid gas sensor was increased under the VOCs gas flow. In addition, VOC molecules have induced the change in energy gap responsible for the shift in absorption spectra.

**Table 5.1** Interaction energy (*IE*), energy gap change ($\Delta E_g$), and NBO charge change ($\Delta$ *NBO charge*) of ZnTPP at the minimize energy based on DFT calculation.

| **VOCs** | ***D*** **(Å)** | ***IE*** **(kcal/mol)** | **$\Delta E_g$ (eV)** | ***Δ NBO charge of*** | | |
|---|---|---|---|---|---|---|
| | | | | ***Zn*** | ***N*** | ***O*** |
| Methanol | 2.375 | -5.79 | -0.12 | 0.036 | 0.010 | -0.046 |
| Ethanol | 2.50 | -5.66 | -0.10 | 0.031 | 0.007 | -0.035 |
| Isopropanol | 2.50 | -5.97 | -0.10 | 0.031 | 0.010 | -0.039 |
| Acetone | 2.50 | -4.29 | -0.11 | 0.034 | 0.010 | -0.003 |
| Acetic acid | 2.50 | -3.89 | -0.11 | 0.034 | 0.011 | -0.048 |
| Ammonia | 2.375 | -9.62 | -0.15 | 0.041 | 0.963 | -0.056 |
| Diethyl ether | 3.875 | -1.31 | -0.07 | 0.008 | 1.232 | -0.007 |
| Ethyl acetate | 2.50 | -4.52 | -0.11 | 0.036 | 1.220 | -0.156 |

### 5.4.4 Classification of Odor

PCA is a pattern recognition method usually employed to analyze multi-dimensional data. This method was used to reduce the dimension of the data and present the new data set in the new axis (PC1 and PC2) easily visualized by human [1], as shown in Figure 5.7. The results thus confirm that the hybrid electronic nose successfully classifies several odorous molecules such as alcohols, acetone, acetic acid, diethyl ether and ethyl acetate, which are the basis of more complex odors such as foods and fragrances.

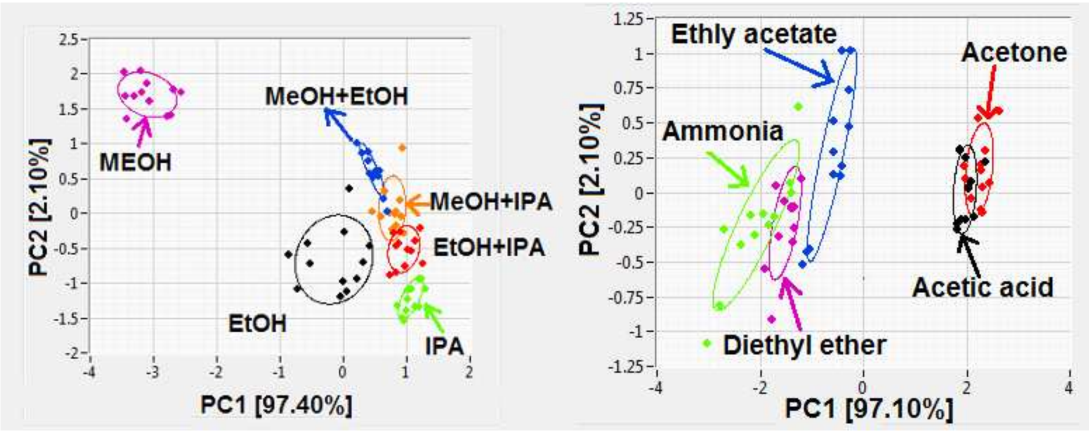

**Figure 5.7** PCA two dimensional score plot related to the nine arrays of optical sensor corresponding to several types of the VOC vapor.

## 5.5 Conclusion

The hybrid electronic nose based on hybrid ZnTPP-WMCNT sensing materials and hybrid optical-electrochemical detection was successfully demonstrate to classify various VOCs, for examples, alcohols, acetone, acetic acid, ammonia, diethyl ether and ethyl acetate. The combined theoretical (DFT calculations) and experimental (sensing measurement) approach successfully provides the sensing mechanism underlying the gas detection that based on the ion-dipole interaction with a moderate charge transfers from porphyrin to VOCs molecule. It was expected that this hybrid electronic nose should be applicable for analysis of the foods and other products that contain fraction of the detected VOC molecules.

# CHAPTER VI

# MOLECULARLY IMPRINTED POLYMER FOR OPTICAL GAS SENSOR IN ELECTRONIC NOSE

## 6.1 Synopsis

In this chapter, optical gas sensors were developed by using molecular imprinted polymer (MIP) technique base on polyurethane (PU) and dye composite. We prepared the MIP material by adding analyte or template molecules (such as 1-propanol and 1-buthanol) in the PU solution. Then dye molecule namely, zinc tetra-tert-butyl-phthalocyanine (ZnTTBPc) was dissolved in polymer solution. Spin coating technique was used to prepare the sensing layer for quartz crystal microbalance (QCM) measurement while drop coating technique was used to prepare the sensing layer for optical measurement. The gas sensor was tested by using the optical e-nose based on LED arrays (see the details in Chapter IV). This sensing layer was tested with VOC vapor in the same concentration to confirm the selectivity of gas sensor. The MIP gas sensor presented strong sensing signal for analyte gas in case of 1-buthanol. Moreover, the gas sensing response was analyzed by pattern recognition, namely, principal component analysis (PCA) in electronic nose (e-nose) application. PCA result showed that MIP technique improved the odor classification for ZnTTBPc material.

## 6.2 Introduction

E-nose is an intelligent device functioning like the human olfactory system. The key components of an e-nose system are the gas sensor array and pattern recognition. Most research topics on e-nose have been focused on searching for new types of gas sensors. In previous work, organic gas sensor thin films based on optically active compounds, namely metal-porphyrin (MP) and metal-phthalocyanine (MPc), were developed using the optical-based detection technique [40]. Quantum chemical calculations based on the density functional theory (DFT) have confirmed that the optically active molecule presents the moderate-to-strong interactions with the functional groups in volatile organic compounds (VOCs) molecule [37]. Although both MP and MPc have been practically useful detection of several VOCs, they are selective towards functional groups rather than individual molecules. Therefore, MIP method has been introduced for improving the selectivity of these gas sensors towards specific molecular shape of VOCs of interest. The imprinted gas sensor was fabricated from the polymer matrices that assemble around the template molecules. Then the template molecules were removed from the polymer matrix leaving behind cavities in size and shape of the template molecules [20]. For instance, imprinted sensors have been used for gas detection based on mass transducer technique or quartz crystal microbalance (QCM) [91]. This technique has been used to detect the mass of analyze molecule that interacts with the polymer.

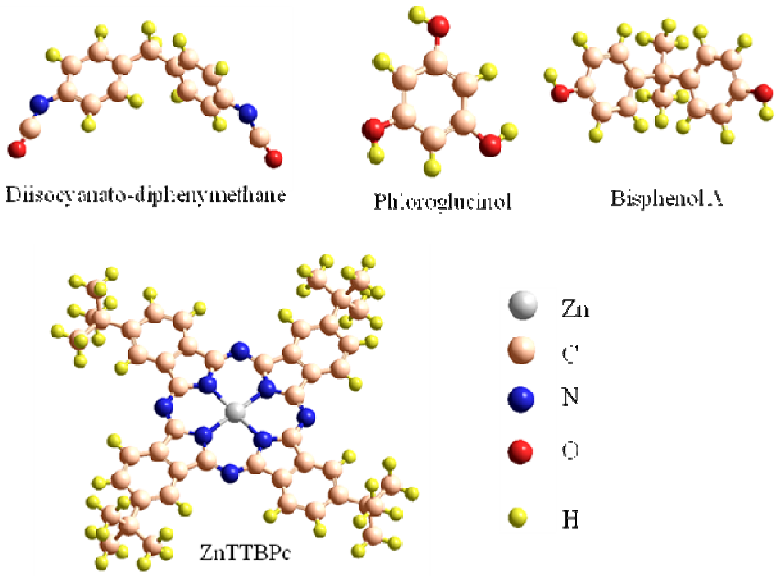

**Figure 6.1** Molecular structure of diisocyanato-diphenymethane (DPDI), phloroglucinol, bisphenol A (BPA) and ZnTTBPc

In the case of optical detection, optically active compounds, such as ZnTTBPc (see in Figure 6.1) were added into the polymer matrix during the polymerization process. In this chapter, 1-propanol (1-PrOH) and 1-buthanol (1-BuOH) were used as template molecules, while polyurethane (PU) was used as the matrix polymer. This polymer matrix was fabricated from the following monomers, namely diisocyanato-diphenylmethane (DPDI), phloroglucinol and bisphenol A (BPA) (see Figure 6.1). These monomers self-organized around the template molecule to form an optimized structure. Selective cavities were created after removing the template molecule [92]. This MIP gas sensor was investigated by QCM measurements to confirm the selectivity, while the optical properties of gas sensors were investigated in the optical e-nose setup. This commercial light emitting diodes (LED) and CMOS photo-detectors were used as the light source and light detector, respectively. The gas sensing responses were reported in the form of the absorbance data for eight color LEDs, such as infrared, red, yellow, green, violet, pink, blue and white (see in **Error! Reference source not found.**). The MIP mixed dye gas sensors were tested with the methanol (MeOH), ethanol (EtOH), 1-propanol (1-PrOH), 1-buthanol (1-BuOH), 2-propanol (2-PrOH), 2-buthanol (2-BuOH) and acetone vapors, respectively, by QCM and optical e-nose measurements. Moreover, the effect of MIP in gas sensor was analyzed by atomic force microscope (AFM) and UV-Vis spectrophotometer. AFM was operated in a dynamic force mode (DFM) or tapping mode that was used to investigate the soft material such as polymer surface [93]. UV-Vis spectrophotometer was used to analyze the absorption spectrum of phthalocyanine in matrix polymer.

## 6.3 Experimental

### 6.3.1 Sensor Fabrication

The polyurethane (PU) was prepared by mixing 50 mg diisocyanato-diphenylmethane (DPDI), 98.5 mg bisphenol A (BPA), 11 mg phloroglucinol and 100 µl tetrahydrofuran (THF) then sonicating for 30 minutes to mix all components. Analyzed molecules such as 1-PrOH and 1-BuOH were imprinted into the polymer by adding 970 µl of analyte solvent in 30 µl of PU and stirring overnight. Finally, the dye molecule, namely ZnTTBPc, was added to the polymer solution in the concentration of 10 mg/ml. The sensing layer on quartz electrode was prepared by spin coating at a spin speed of 3000 rpm. These sensing materials were hardened over night at 70 $^{o}$C to remove the analyte or templates from polymers before measurement.

The sensing layers for optical e-nose setup were prepared by spin coating and drop coating technique on clean glass substrate. Spin-coated film was spun at spin speed of 500 rpm while drop coated film was used 15 µl of MIP mixed dye solution. Both gas sensors were hardened over night at 70 $^{o}$C to remove the analyte or templates from polymers before measurement.

### 6.3.2 QCM Setup

The gold electrode pattern for QCMs measurement was produced by a screen-printing technique onto AT cut quartz blanks with a diameter of 13.9 mm. There were 2 electrodes printed on one side of each quartz plate and heated up to 400 $^{o}$C for 2 hours. Then the other side of quartz plate was printed and again heated up to 400 $^{o}$C for 4 hours. This resulted in 2 channels (Ch 1 and Ch 2) for sensing on the same quartz plate (see in Figure 6.2).

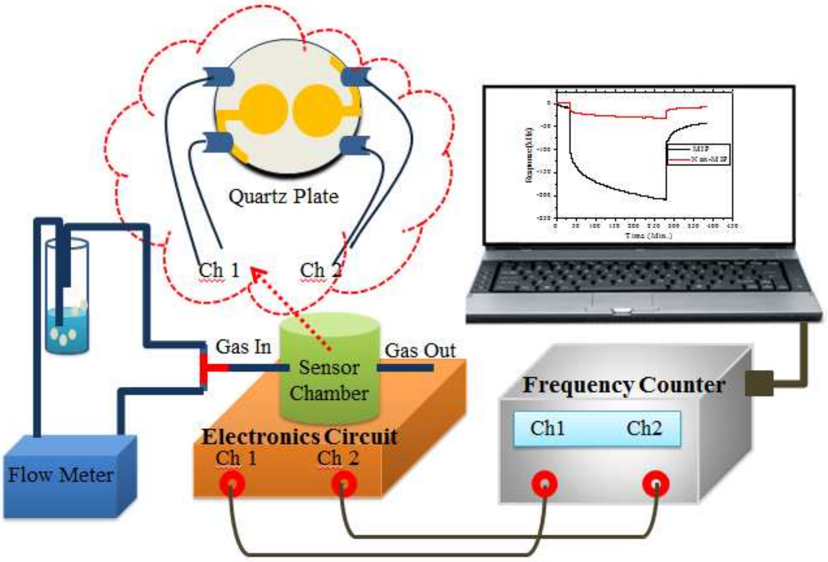

**Figure 6.2** Schematic drawing of the QCM measurement setup.

The measurement setup to obtain optimal reference for QCM is presented in Figure 6.2. The quartz plate in the sensor chamber was connected with an electronic circuit. Then frequency counter was used to characterize the QCM frequencies for both channels. The sensing vapor was evaporated from the solvent. The vapor concentration in the gas measurement setup was controlled by mixing reference gases and evaporated solvents. The total flow rate of gas was controlled to be 1 liter per minute.

### 6.3.3 Optical E-nose Setup

The optical electronic nose set up has been shown in **Error! Reference source not found.** (see Chapter IV). In this system, low-cost LED array was chosen to be a light source and photo-detector was used to detect the light intensity. The intensity peak of red, yellow, green, blue, pink, and violet LEDs was centered at 638, 587, 537, 457, 472 and 399 nm, respectively. The gas sensing response of the sensing material was investigated under dynamic gas flow through a home-built chamber that shields the chamber from outside light. Nitrogen gas was used as the reference and carrier gas to conduct headspace vapor from the sample bottle. All of components were controlled by LABVIEW program based on DAQ card.

## 6.4 Results and Discussion

### 6.4.1 Influence of MIP in QCM Technique

MIP gas sensors were tested by QCM measurement. The typical data from each electrode was measured by connecting it to a custom-made oscillator and reading out the frequency by frequency counter. The output data is reported in term of frequency change (Hz) as function of time. The frequency change was occurred from the change of fundamental oscillation frequency upon adsorption of molecules in gas phase. The frequency change ($\Delta f$) was calculated from $f_T - f_i$, where $f_T$ and $f_i$ were defined as frequency at any time and initial frequency of gas sensor, respectively.

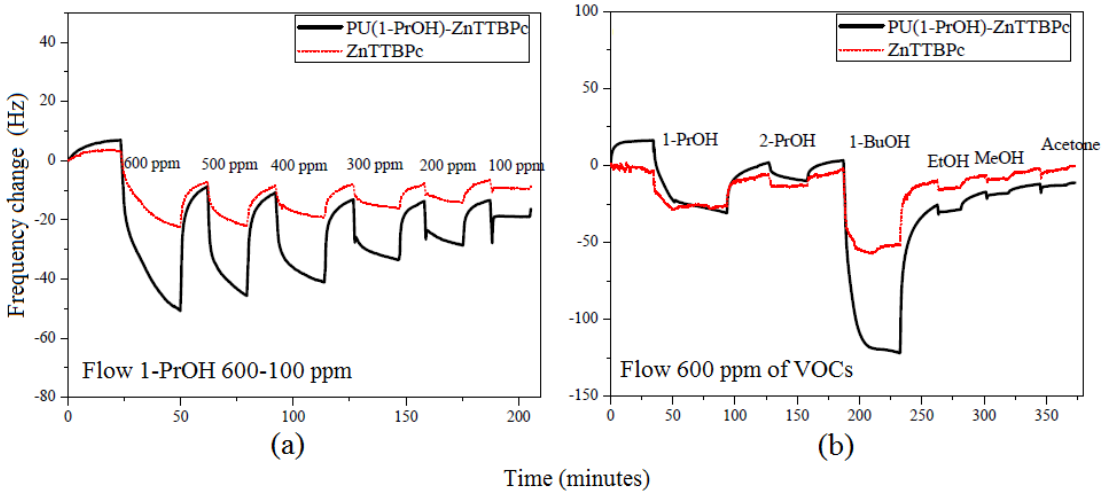

**Figure 6.3** Typical sensor signals of PU(1-PrOH)-ZnTTBPc and ZnTTBPc for (a) 1-PrOH in concentration of 100-600 ppm and (b) VOCs vapor in concentration of 600 ppm.

Figure 6.3 (a) presents the frequency change of PU imprinting with 1-PrOH mixed dye (PU(1-PrOH)-ZnTTBPc) and pure dye (ZnTTBPc) for 1-PrOH in the concentration of 100-600 ppm. PU(1-PrOH)-ZnTTBPc presented more frequency change than ZnTTBPc for all concentration. Therefore, MIP technique successfully developed the sensitivity of ZnTTBPc. The frequency change of MIP gas sensor was increased by increasing the concentration of 1-PrOH. This gas sensor detected 1-PrOH at the low concentration at 100 ppm. The selectivity of gas sensors are shown in Figure 6.3 (b). These signals were measured from the different vapor in the same concentration at 600 ppm. The highest frequency change of PU(1-PrOH)-ZnTTBPc was observed in case of the 1-BuOH that was not the template molecule (1-PrOH). Sometimes, this phenomenon was occurred because mass of template molecule less than mass of other sample molecule [94].

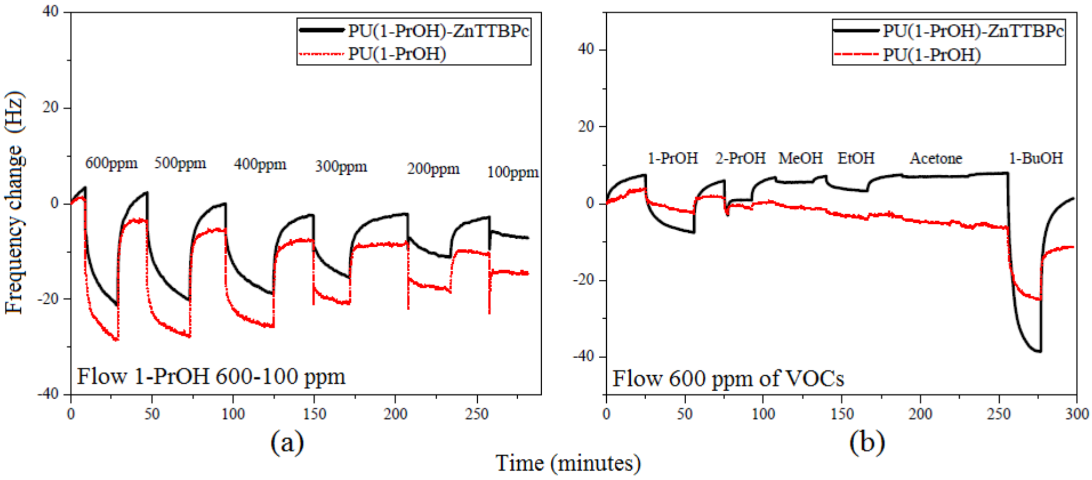

**Figure 6.4** Frequency response of PU(1-PrOH)-ZnTTBPc and PU(1-PrOH) for (a) 1-PrOH in concentration of 100-600 ppm and (b) VOCs vapor in concentration of 600 ppm.

The effect of dye compound that was added to MIP layer was investigated in Figure 6.4. Frequency change of PU(1-PrOH)-ZnTTBPc and PU(1-PrOH) was compared by varying the concentration of 1-PrOH (see Figure 6.4 (a)) and changing the sensing vapor (see Figure 6.4 (b)). MIP with dye (PU(1-PrOH)-ZnTTBPc) presented the similar frequency change in the MIP without dye (PU(1-PrOH)).

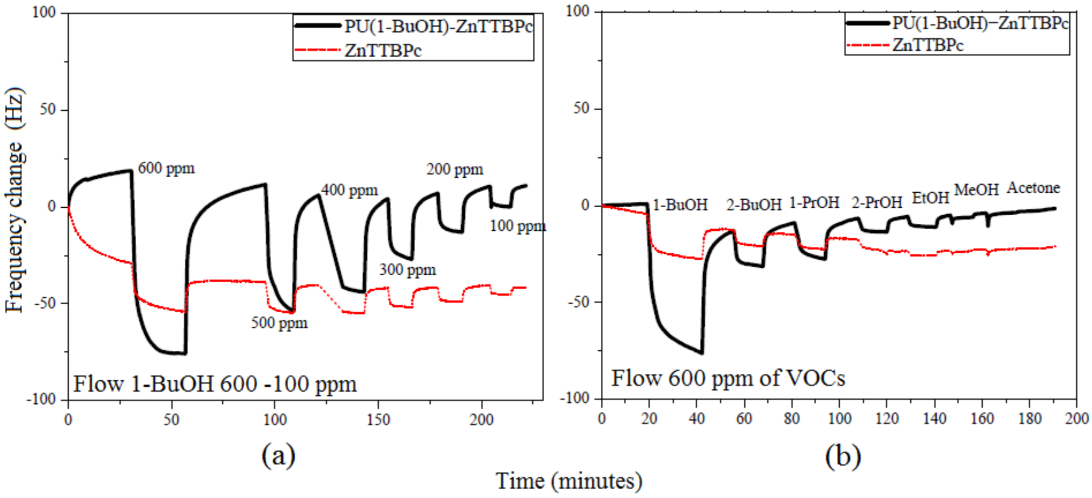

**Figure 6.5** Typical sensor signals of PU(1-BuOH)-ZnTTBPc and ZnTTBPc for (a) 1-BuOH in concentration of 100-600 ppm and (b) VOCs vapor in concentration of 600 ppm.

Figure 6.5 (a) presents the frequency change of PU imprinting with 1-BuOH mixed dye (PU(1-BuOH)-ZnTTBPc) and pure dye (ZnTTBPc) for 1- BuOH in the concentration of 100-600 ppm. PU(1-BuOH)-ZnTTBPc presented more frequency change than ZnTTBPc for all concentration of 1-BuOH. This results are agreed with the PU(1-PrOH)-ZnTTBPc (see Figure 6.3 (a)). Therefore, MIP technique successfully developed the sensitivity of dye compound for 1-PrOH and 1-BuOH detection. The frequency change of MIP gas sensor was increased by increasing the concentration of 1-BuOH. This MIP sensor was tested by VOCs at the concentration 600 ppm. The selectivity of gas sensors are shown in Figure 6.5(b). This result clearly presented that MIP gas sensor had the selectivity with template molecule (1-BuOH).

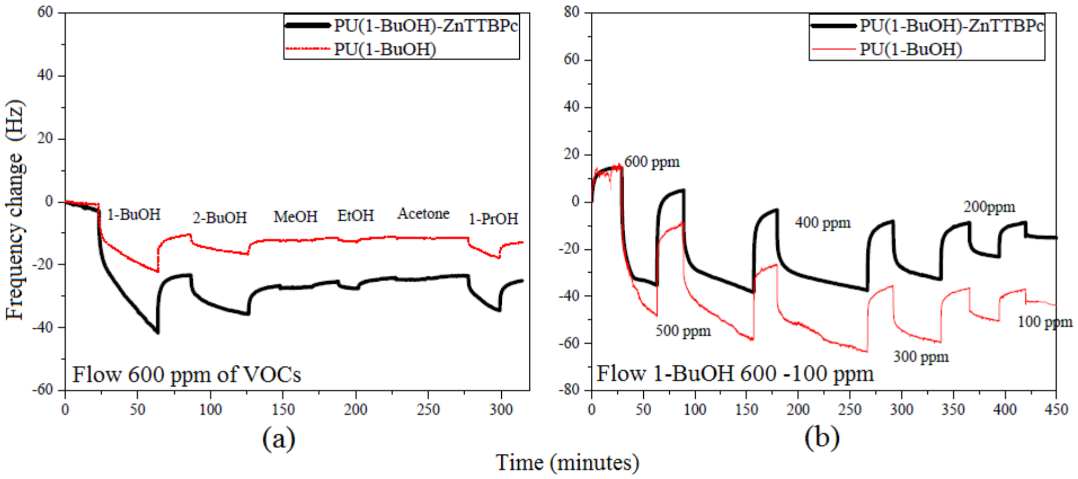

(a) (b)

**Figure 6.6** Frequency response of PU(1-BuOH)-ZnTTBPc and for PU(1-BuOH)- for (a) 1-BuOH in concentration of 100-600 ppm and (b) VOCs vapor in concentration of 600 ppm.

The effect of dye compound in MIP sensor was investigated in Figure 6.6. Frequency change of PU(1-BuOH)-ZnTTBPc and PU(1-BuOH) was compared by varying the concentration of 1-BuOH (see Figure 6.6 (a)) and changing the sensing vapor (see Figure 6.6 (b)). MIP based on dye (PU(1-BuOH)-ZnTTBPc) presented the similar frequency change in the MIP without dye (PU(1-BuOH)). Both PU(1-PrOH)-ZnTTBPc and PU(1-BuOH)-ZnTTBPc sensors confirmed that the sensing signals from QCM measurement were occurred from MIP technique.

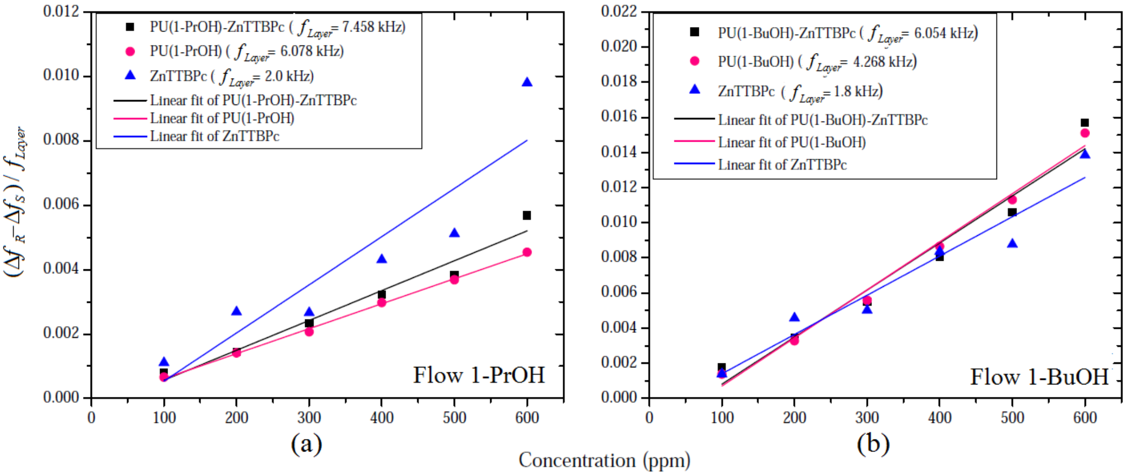

**Figure 6.7** The sensor characteristic curve that related to concentration of (a) 1-PrOH and (b) 1-BuOH.

Figure 6.7 shows the sensor characteristic curve that was calculated from sensor response $\{(\Delta f_R - \Delta f_S)/f_{Layer}\}$, where $\Delta f_R$, and $\Delta f_S$ were defined as frequency change of reference gas and sensing vapor, respectively. $f_{Layer}$ was calculated from the frequency change between frequency of empty quartz and spin coated quartz. $f_{Layer}$ was related to the thickness of sensing layer on quartz. Usman Latif et al. reported that the frequency shift of 1 kHz on the gold electrode was generated from a 40-nm thick layer [20]. A linear relationship between sensor response ($(\Delta f_R - \Delta f_S)/f_{Layer}$) and vapor concentration was plotted by using linear fit curve in the origin program. The Intercept (i) and Slope (m) of this curve was calculated.

Sensor characteristic curve for 1-PrOH was investigated in Figure 6.7 (a). The sensor response of PU(1-PrOH)-ZnTTBPc was similar to PU(1-PrOH). Sensor characteristic curves of 1-BuOH for PU(1-BuOH)-ZnTTBPc, PU(1-BuOH) and ZnTTBPc are shown in Figure 6.7 (b). Both MIP with dye and without dye presented the same sensor characteristic curve for all concentration. These results conclude that dye molecule cannot effect to polymer structure. Especially, Sensor characteristic curves of ZnTTBPc that were presented in the same trend of MIP gas sensor because of the low value $\Delta f_{Layer}$ of ZnTTBPc film. The low value $\Delta f_{Layer}$ was corresponded to the low thickness of layer.

The limit of detection (LOD) of 1-PrOH and 1-BuOH are reported in Table 6.1. LOD is used to represent the lowest of vapor concentration that sensor can be possibly detected [95]. PU(1-PrOH)-ZnTTBPc and PU(1-PrOH) present the LOD with 1-PrOH in the range of 20-38 ppm while PU(1-BuOH)-ZnTTBPc and PU(1-BuOH) present the LOD with 1-BuOH in the range of 69-74 ppm. Therefore, the LOD of 1-PrOH is lower than 1-BuOH. Both PU(1-PrOH)-ZnTTBPc and PU(1-BuOH)-ZnTTBPc can be used as gas detection at the low concentration (under 100 ppm) based on QCM setup.

**Table 6.1** Interception (i), slope (m) and limit of detection (LOD) of ZnTTBPc, PU(1-PrOH), PU(1-PrOH)-ZnTTBPc, PU(1-BuOH) and PU(1-BuOH)-ZnTTBPc with 1-PrOH and 1-BuOH.

| | **Intercept (i)** | **Slope (m)** | **Limit of detection (LOD)** |
|---|---:|---:|---:|
| **Signal for 1-PrOH** (Figure 6.7 (a)) | | | |
| PU(1-PrOH)-ZnTTBPc | $-3.60\text{x}10^{-4}$ | $9.27\ \text{x}10^{-6}$ | 38.80 |
| PU(1-PrOH) | $-1.60\ \text{x}10^{-4}$ | $7.75\ \text{x}10^{-6}$ | 20.60 |
| ZnTTBPc | $-9.60\ \text{x}10^{-4}$ | $1.50\ \text{x}10^{-5}$ | 64.10 |
| **Signal for 1-BuOH** (Figure 6.7 (b)) | | | |
| PU(1-BuOH)-ZnTTBPc | $-1.87\ \text{x}10^{-3}$ | $2.68\ \text{x}10^{-5}$ | 69.80 |
| PU(1-BuOH) | $-2.03\ \text{x}10^{-3}$ | $2.74\ \text{x}10^{-5}$ | 74.20 |
| ZnTTBPc | $-8.31\ \text{x}10^{-4}$ | $2.24\ \text{x}10^{-5}$ | 37.20 |

### 6.4.2 Development of Gas Sensor based on MIP for Optical Technique

ZnTTBPc and PU mixed with ZnTTBPc gas sensors were prepared on glass substrate and analyzed by the UV-Vis spectrophotometer in the range of 300 - 800 nm.

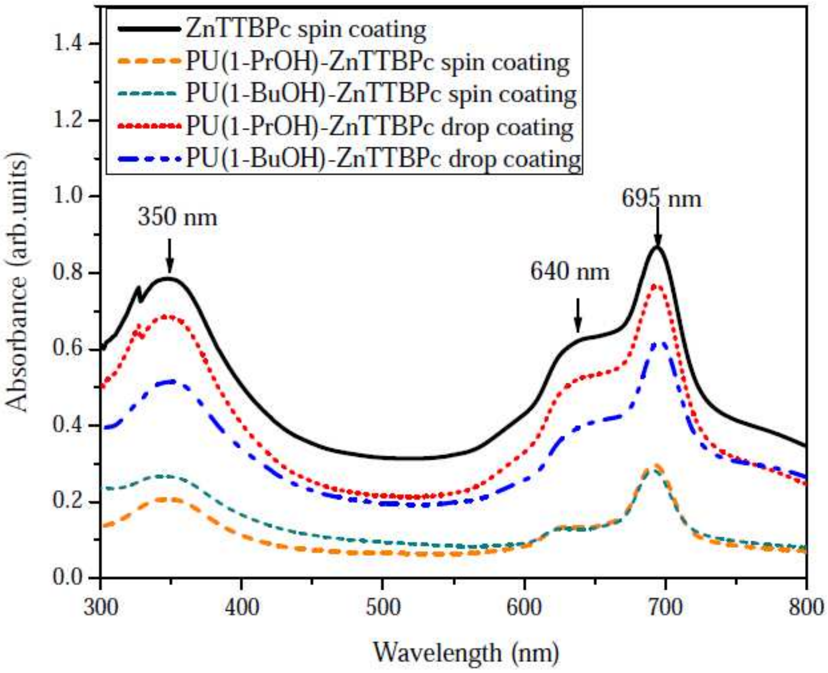

**Figure 6.8** The absorption spectra of ZnTTBPc, PU(1-PrOH)-ZnTTBPc and PU(1-BuOH)-ZnTTBPc.

Figure 6.8 shows the absorption spectra of ZnTTBPc, PU(1-PrOH)-ZnTTBPc and PU(1-BuOH)-ZnTTBPc. The Q band of ZnTTBPc, related to n-π* transition was located at 695 nm and B band, related to π-π* transition of Pc was located at 350 nm [96]. The main peak of MIP mixed ZnTTBPc were located at the same position of pure ZnTTBPc. Therefore, PU had no affect for this dye based on the spectral properties. The absorption spectra of drop coating films higher than the spectra of spin coating film. Moreover, the gas sensing signal of both spin coating and drop coating films were tested by optical properties based on optical e-nose setup.

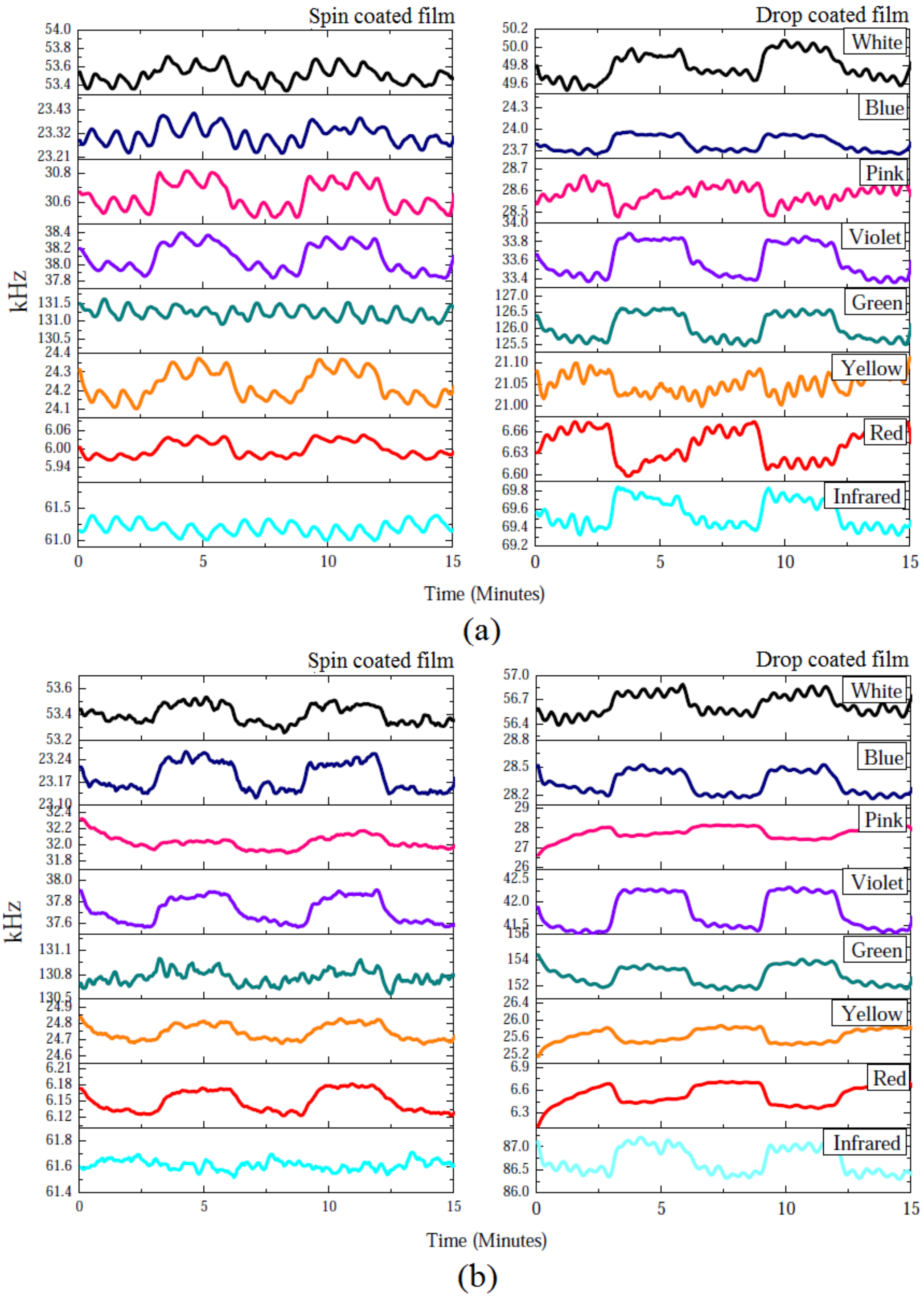

**Figure 6.9** Sensing signal from optical e-nose for (a) PU(1-PrOH)-ZnTTBPc test with 1-PrOH and (b) PU(1-BuOH)-ZnTTBPc test with 1-BuOH.

The comparison of sensing signals between spin coating gas sensor and drop coating gas sensor are shown in Figure 6.9. Each signal measured from the light intensity that transmits from gas sensor during the gas flow process. Photo-detector was used to count the frequency of photon which related to light intensity. The sensor signal was reported in the value of frequency (kHz). The drop coated films produced more stable signal than the spin coated one that produced some noises. This result was related to the thickness of sensing layer. Drop coated film presented the higher absorption spectra than spin coated film (see Figure 6.8). This means that drop coated layer had more thickness than spin coated layer. The amount of dye molecule in drop coated layer was higher than the spin coated layer. The amount of dye molecule effected to the sensor signal. Moreover, spin coating method that produced the thin layer presented the weak sensor signal and the strong noise. This noise most probably fluctuations in the gas system.

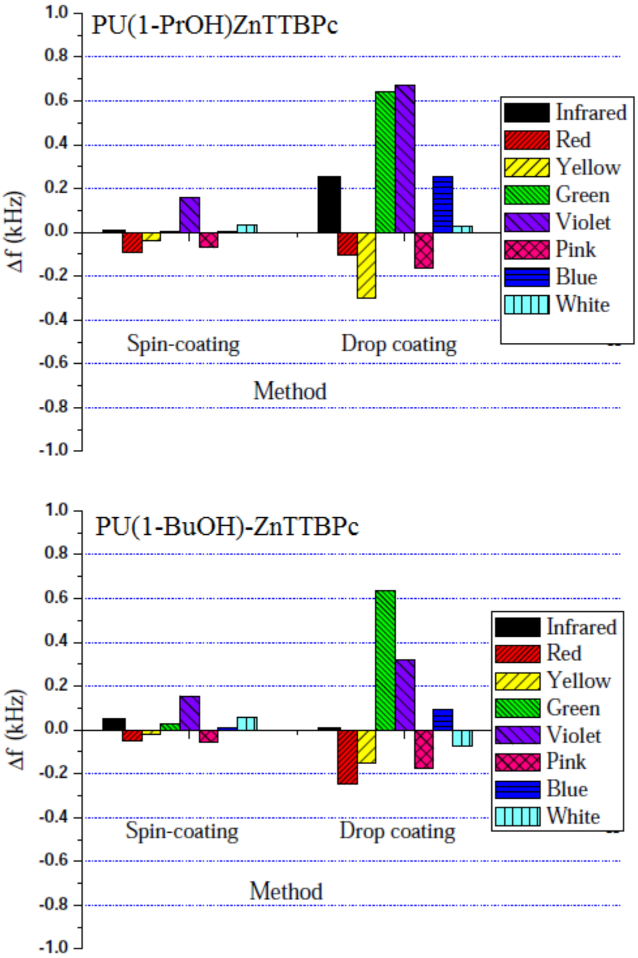

**Figure 6.10** The difference of sensing signal between sensing vapor and reference gas of spin coating and drop coating methods.

Then the difference of sensing signal between sensing vapor and reference gas of spin coated and drop coated film are investigated in Figure 6.10. $\Delta f$ is defined from $f_S - f_R$ . $f_S$ and $f_R$ represent the sensor signal upon sensing vapor and reference gas, respectively. Both PU(1-PrOH)-ZnTTBPc and PU(1-BuOH)-ZnTTBPc presented strong $\Delta f$ in green and violet LED color. Drop coated films had more sensing signal than spin coated films. Therefore, drop coating method was the suitable method to prepare the MIP mixed dye gas sensor.

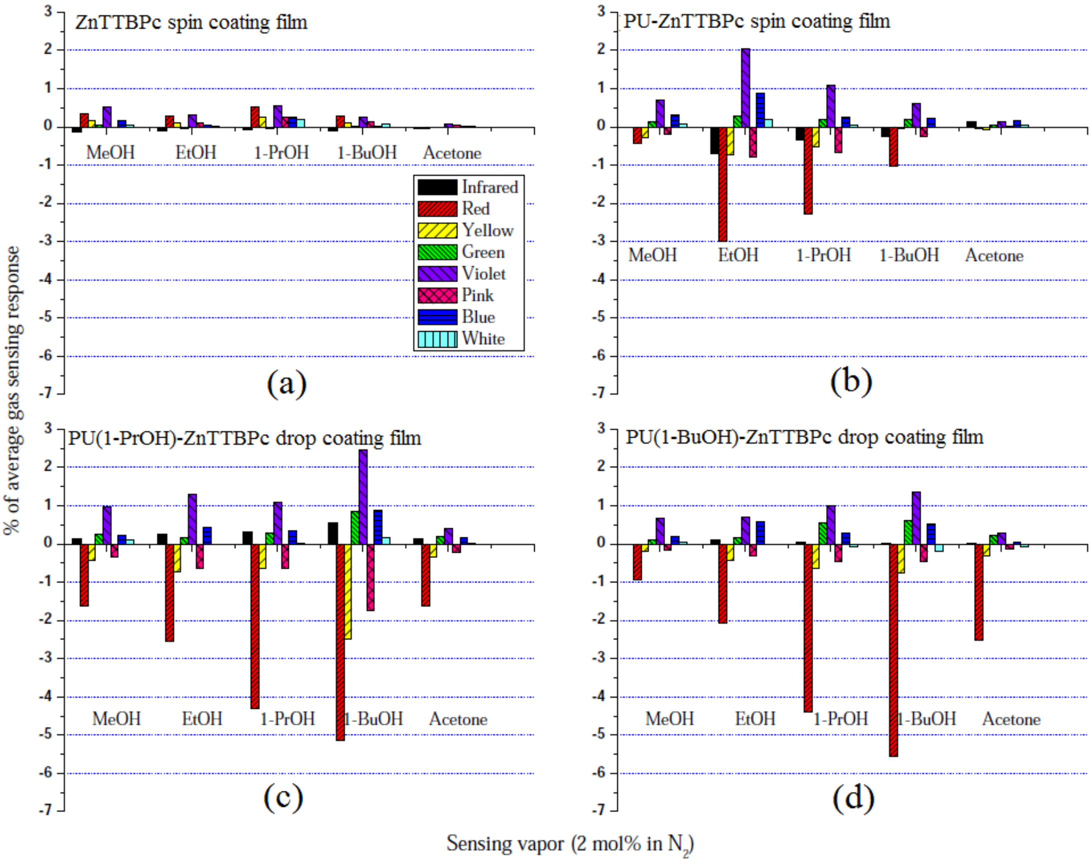

**Figure 6.11** Percentage average gas sensing response ($\%\bar{S}$) of ZnTTBPc spin coated film, PU-ZnTTBPc spin coated film, PU(1-PrOH)-ZnTTBPc drop coated film and PU(1-BuOH)-ZnTTBPc drop coated film with sensing vapor in the concentration of 2 mol% in nitrogen gas.

The effect of MIP technique in optical measurement was investigated by using the average gas sensing response ($\bar{S}$). The gas sensing response ($S$) was calculated from $\Delta f / f_R$. Percentage average gas sensing response ($\%\bar{S}$) of ZnTTBPc spin coated film, PU-ZnTTBPc spin coated film, PU(1-PrOH)-ZnTTBPc drop coated film and PU(1-BuOH)-ZnTTBPc drop coated film with sensing vapors are investigated in Figure 6.11. The concentrations of VOCs were controlled by the weight loss of solvent in nitrogen gas ($N_2$). The solvent bottle was immersed in the heat bath to control the temperature. Then $N_2$ was used as the carrier gas to conduct the solvent vapor. The concentration of vapor was calculated by finding the lost weight of solvent in the different $N_2$ flow rate. The concentration of vapor was fixed at 2 mol % in $N_2$. The effect of matrix polymer in gas sensor was analyzed by optical e-nose. $\%\bar{S}$ of ZnTTBPc was increased after using the PU as the matrix polymer (PU-ZnTTBPc) (see Figure 6.11 (a-b). Matrix polymer modified the sensitivity and response behavior of dye compound [97]. But PU-ZnTTBPc presented the highest gas sensing response with ethanol vapor. Therefore, the MIP technique was used to enhance the selectivity for other analyte vapors, such as 1-PrOH and 1-BuOH. This polymer was imprinted with 1-PrOH and 1-BuOH. Figure 6.11 (c-d) confirms that the gas sensing response of 1-PrOH and 1-BuOH vapors were increased by MIP technique. Both PU(1-PrOH)-ZnTTBPc and PU(1-BuOH)-ZnTTBPc presented strong $\%\bar{S}$ with 1-BuOH, such as red LED. $\%\bar{S}$ values of red LED for both MIP sensors (PU(1-PrOH)-ZnTTBPc and PU(1-BuOH)-ZnTTBPc) were higher than Non-MIP (PU-ZnTTBPc) about 2 (1-PrOH detection) and 4 (1-BuOH detection), respectively. The results from optical e-nose agree with the result from the QCM measurement that both gas sensors produced good sensitivity with 1-BuOH vapor. The surface of gas sensors was investigated in the next step.

### 6.4.3 Surface Analysis

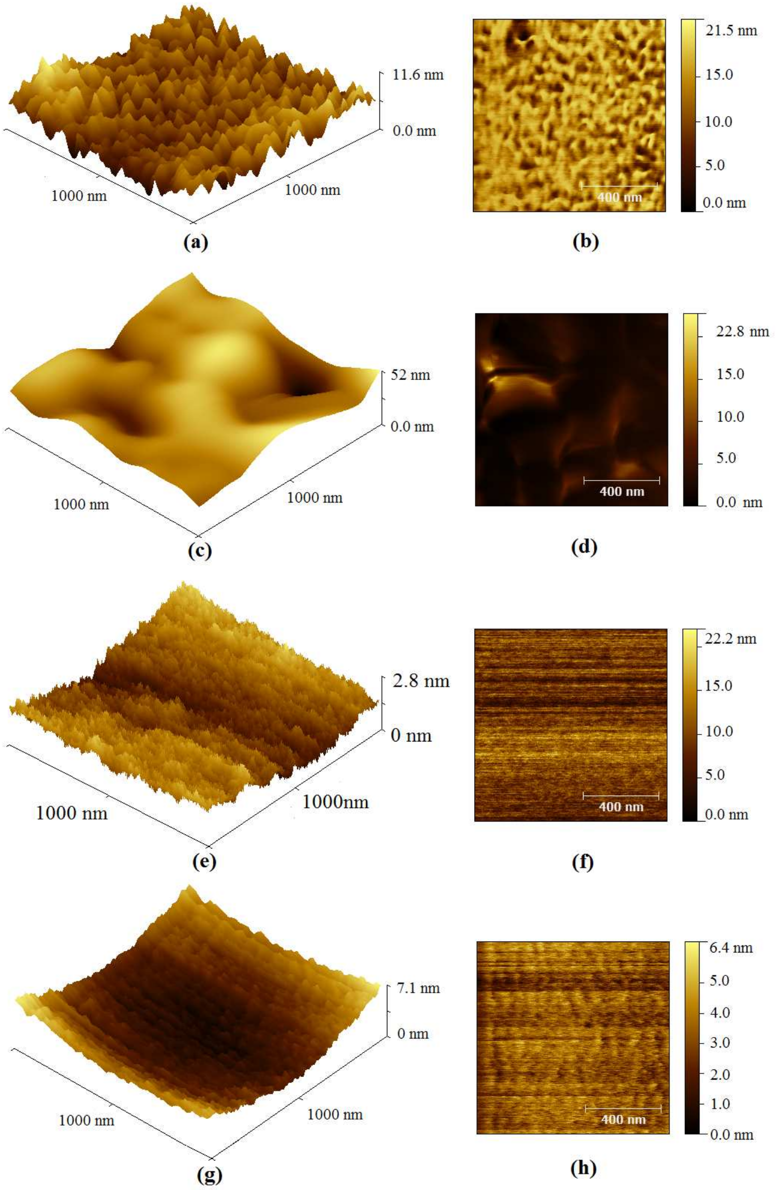

**Figure 6.12** The AFM image in 3D and top view of (a-b) ZnTTBPc spin-coated film, (c-d) PU-ZnTTBPc spin-coated film, (e-f) PU(1-PrOH)-ZnTTBPc drop-coated film and (g-h) PU(1-BuOH)-ZnTTBPc drop-coated film.

**Table 6.2** Surface roughness and thickness of ZnTTBPc, PU-ZnTTBPc, PU(1-PrOH)-ZnTTBPc and PU(1-BuOH)-ZnTTBPc

| Parameter | ZnTTBPc | PU-ZnTTBPc | PU(1-PrOH)-ZnTTBPc | PU(1-BuOH)-ZnTTBPc |
|---|---|---|---|---|
| Roughness (nm) | $2.52 \times 10^{-1}$ | $4.69 \times 10^{-1}$ | $8.96 \times 10^{-2}$ | $9.51 \times 10^{-2}$ |
| Thickness (nm) | 50 | 50 | 350 | 460 |

AFM in non-contact mode was used as the surface analysis. ZnTTBPc spin-coated film, PU-ZnTTBPc spin-coated film, PU(1-PrOH)-ZnTTBPc drop-coated film and PU(1-BuOH)-ZnTTBPc drop-coated film were measured in the area of 1000 x 1000 nm (see Figure 6.12). Roughness average and thickness of sensing layers were investigated as Table 6.2. ZnTTBPc and PU-ZnTTBPc spin-coated film presented more roughness than PU(1-PrOH)-ZnTTBPc and PU(1-BuOH)-ZnTTBPc drop-coated film. Polymer based on ZnTTBPc presented more thickness than pure ZnTTBPc. And from the optical e-nose results, MIP gas sensors based on ZnTTBPc that were fabricated by drop coating method showed the stronger absorption spectrum and average gas sensing response. Therefore, this highest thickness film will be an appropriated layer for gas sensor based on polymer. But drop coating method presented a disadvantage point, such as a curve on sensor surface (see Figure 6.12 (g)).

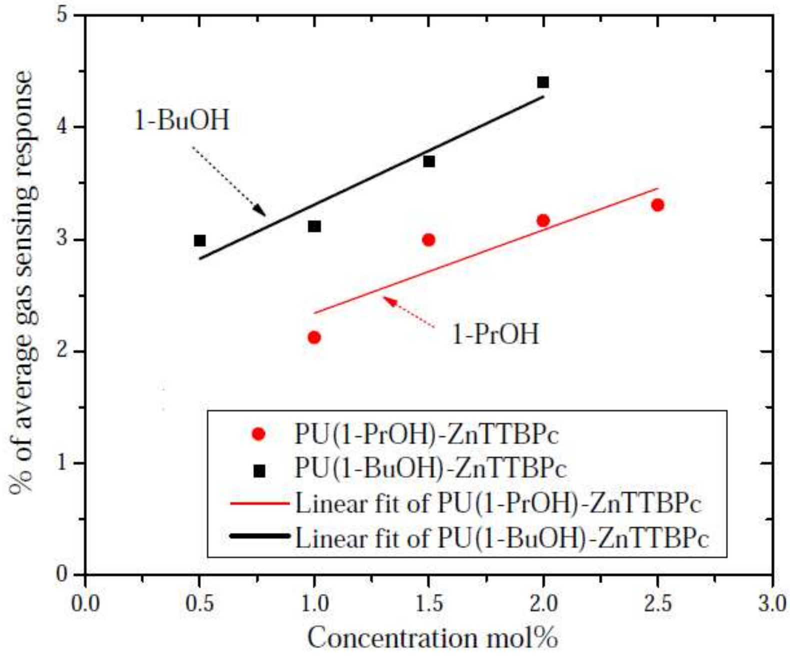

**Figure 6.13** Percentage average gas sensing response of PU(1-PrOH)-ZnTTBPc drop-coated film with 1-PrOH and PU(1-BuOH)-ZnTTBPc drop-coated film with 1-BuOH.

Sensor characteristic curve which is the relationship between percentage average gas sensing response and concentration of vapor is shown in Figure 6.13. PU(1-PrOH)-ZnTTBPc drop-coated film presented the sensing response with 1-PrOH while PU(1-BuOH)-ZnTTBPc drop-coated film presented the sensing response with 1-BuOH. Origin program was used to calculate the linear curve of both gas sensors. Slopes of linear fit for PU(1-PrOH)-ZnTTBPc and PU(1-BuOH)-ZnTTBPc are 0.743 and 0.964, respectively. MIP mixed dye produced stronger gas sensing response with 1-BuOH than 1-PrOH in the same concentration.

### 6.4.4 Odor Classification based on PCA

The benefit of MIP gas sensors were investigated by the statistical method for odor classification, namely principal component analysis (PCA). PCA was used to transform complex data to the lower dimensional data set. The new data axis was call in the term of “PC”. The first principal component (PC1) contained an almost data variable while the second principal component (PC2) contained less data variable than

PC1 [98]. This technique was used for classification purpose in e-nose, such as, food produce [88]. The data set for calculation in optical e-nose were prepared from the gas sensing response from eight colors of LED. The sensing response of PU(1-PrOH)-ZnTTBPc and PU(1-BuOH)-ZnTTBPc drop coated film were tested with evaporated solvent at the room temperature. The gas flow was controlled at 500 ml/min. Both reference gas and sensing vapor were flowed for 2 min per each experiment.

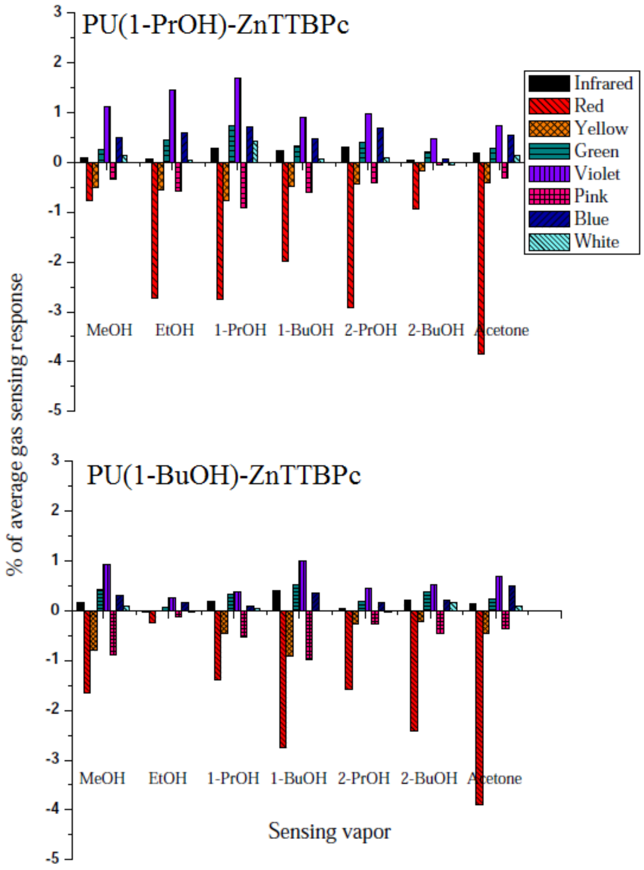

**Figure 6.14** Percentage average gas sensing response of PU(1-PrOH)-ZnTTBPc and PU(1-BuOH)-ZnTTBPc drop-coated film with sensing vapor.

The average gas sensing response pattern of MIP gas sensors are presented in Figure 6.14. Both gas sensors showed the different pattern for all vapors. Acetone vapor presented the highest $\%\overline{S}$ because acetone had higher vapor pressure than alcohols. Vapor pressures of VOCs were reported by Erik Olsen at el. [100]. The vapor pressures of alcohols were sorted from the highest value to the lowest value as MeOH, EtOH, 2-PrOH, 1-PrOH, 2-BuOH, 1-BuOH, respectively. Although MeOH and EtOH presented strong vapor pressure, but MIP based on dye presented the strong $\%\bar{S}$ with template molecule (1-PrOH and 1-BuOH).

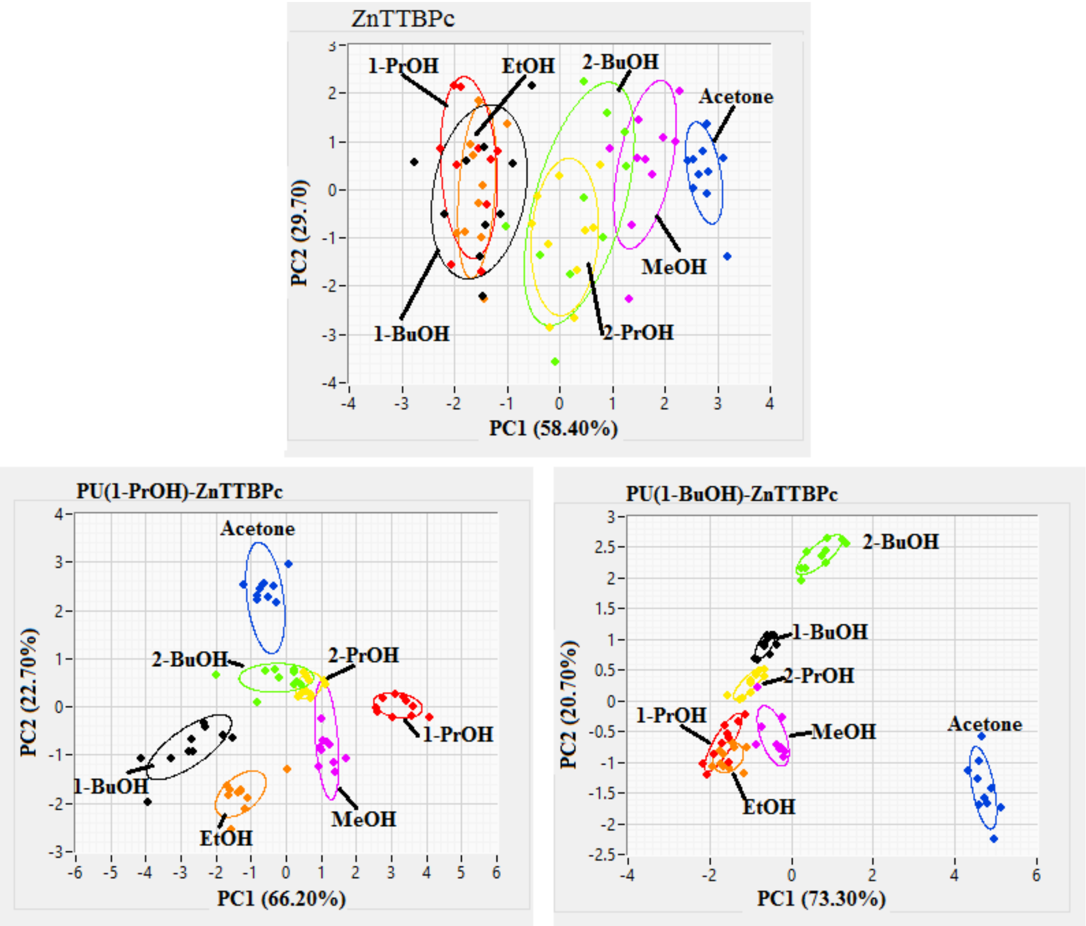

**Figure 6.15** PCA two dimensional score plot related to the eight sensor arrays of ZnTTBPc, PU(1-PrOH)-ZnTTBPc and PU(1-BuOH)-ZnTTBPc gas sensor.

The comparison between ZnTTBPc and MIP based on ZnTTBPc was investigated by PCA calculation (see Figure 6.15). ZnTTBPc thin film separated ketone group from hydroxyl group in VOC. But ZnTTBPc unclearly separated 6 types of alcohol. Then MIPs based on ZnTTBPc were calculated by PCA method. PU(1-PrOH)-ZnTTBPc clearly classify MeOH, EtOH, 1-PrOH, 1-BuOH and acetone while there is the overlap data plot between 2-PrOH and 2-BuOH. PU(1-BuOH)-ZnTTBPc clearly classify MeOH, 2-PrOH, 1-BuOH, 2-BuOH and acetone while there is the overlap data plot between EtOH and 1-PrOH. These results confirm that, the classification of gas sensor was developed by MIP technique.

## 6.5 Conclusion

The molecular imprinted polymer (MIP) based on polyurethane mixed ZnTTBPc was imprinted with 1-PrOH and 1-BuOH. QCM measurement was used as the mass transducer to investigate sensor characteristic and selectivity of this MIP. QCM results confirm that PU was imprinted with both templates. PU(1-PrOH)-ZnTTBPc and PU(1-BuOH)-ZnTTBPc gas sensor presented the sensor signal with template vapor at the low vapor concentration (100 ppm). These MIP gas sensors were tested with the sensing vapor, such as, methanol, ethanol, 1-propanol, 1-buthanol and acetone by the optical e-nose setup. All sensing vapors were prepared in the same concentration of 2 mol% in $N_2$ gas. Both PU(1-PrOH)-ZnTTBPc and PU(1-BuOH)-ZnTTBPc gas sensors presented strong gas sensing response with 1-BuOH. It was expected that this MIP method improved the gas sensor structure that suitable for the template molecule detection. Moreover, the classification of MIP mixed dye gas sensors were calculated by principal component analysis (PCA). This method confirms that MIP mixed dye gas sensor had more efficiency for odor classification than pure dye based on optical e-nose setup.

# CHAPTER VII
# CONCLUSION

In this thesis, optical technique was used as the transducer to transform the physical properties of gas sensor to the electronic signal. Two types of electronic noses (e-nose) based on optical detection, namely, e-nose based on UV-vis spectrophotometer and e-nose based on light-emitting diodes (LEDs) were investigated. The e-nose based on UV-vis spectrophotometer measures changes in the absorption spectra. This e-nose yields the sensing signals by calculating the area integral under absorption spectra. But the second type of e-nose was developed by using light-emitting diodes (LEDs) as light source and CMOS photo detector as transducer. This e-nose was fabricated in the form of portable instrument that includes gas flow system and controller unit. Finally, principal component analysis (PCA) was performed as pattern recognition to investigate the efficiency of our e-nose system.

In this thesis, the optically-active organic thin film gas sensor was fabricated from organic dyes, namely, Zinc-2,9,16,23-tetra-tert-butyl-29H,31H-phthalocyanine (ZnTTBPc), Zinc-5,10,15,20-tetra-phenyl-21H,23H-porphyrin (ZnTPP) and manganese(III)-5,10,15,20-tetraphenyl-21H,23H-porphyrin chloride (MnTPPCl). The electronic structure of organic molecules were optimized by density functional theory (DFT) calculation based on B3LYP6-31G* level. The interaction energies between sensing molecule and analyte molecule obtained from the computation are in agreement with the gas sensing behaviors as obtained from the experiments. Charge transfer from the central metal atom of porphyrin or phthalocyanine to the oxygen atom of alcohols molecule at optimized distance were observed by this calculation. Therefore, the absorption spectra changes of organic thin film were the result from charge transfer phenomena. The active site of organic molecule was observed around the central metal atom such as Zn and Mn.

Three types of optical gas sensors, namely, mixture layer of MP and MPc, nanocomposite between ZnTPP and multiwall carbon nanotube (MWCNT) and molecularly imprinted polymer (MIP) mixed ZnTTBPc gas sensors were investigated.

For the mixture layer of MP and MPc gas sensor, this sensing material was prepared by mixing three types of organic compound which possess different absorption regions. The mixture layer of ZnTTBPc/ZnTPP/MnTPPCl spin-coated thin films has been demonstrated to be able to detect various kinds of volatile organic compound (VOC) vapor, namely methanol, ethanol, isopropanol, acetone (5% eq.) and acetic acid (5% eq.). Therefore, the optical electronic nose constructed from the mixed layer organic molecule exploits the high chemical information in e-nose based on UV-vis spectrophotometer and e-nose based on light-emitting diodes (LEDs) and CMOS photo detector.

The hybrid optical-electrochemical electronic nose system was investigated by using nanocomposite between ZnTPP and multiwall carbon nanotube (MWCNT) gas sensor. The electrochemical part works by measuring the change in electrical resistivity of the sensing materials upon contact with the sample vapor. From atomic force microscope measurement, roughness of the gas sensor was increasing by adding MWCNT. It means that more surface area available for gas sensing is expected and MWCNT can act as nanochannel that help transport the analyte molecules into the deeper layers of ZnTPP, leading to enhanced sensitivity.

In case of molecularly imprinted polymer (MIP) mixed ZnTTBPc gas sensor was developed by MIP technique based on polyurethane (PU). QCM results confirm that PU mixed ZnTTBPc gas sensors were imprinted with 1-PrOH and 1-BuOH molecule. In the e-nose based on light-emitting diodes (LEDs) and CMOS photo detector system, both PU(1-PrOH)-ZnTTBPc and PU(1-BuOH)-ZnTTBPc gas sensors presented strong gas sensing response with 1-BuOH. It was expected that this MIP method improved the gas sensor structure that suitable for the template molecule detection.

The classification of three types of gas sensors were calculated by principal component analysis (PCA). This method confirms that mixtures layer of MP and MPc gas sensor has more efficiency for odor classification than mono layer of dye, nanocomposite between ZnTPP and MWCNT gas sensor successfully separated

VOC, and MIP mixed dye gas sensor had more efficiency for odor classification than pure dye.

PCA method was used to compare the efficiency for three types of gas sensor for alcohol classification as shown in Figure 7.1. Mixtures layer of MP and MPc and nanocomposite between ZnTPP and MWCNT present similar classification in the x axis. Methanol (MeOH) vapor was clearly separated from ethanol (EtOH) and isopropanol (IPA) vapor. But MIP mixed ZnTTBPc gas sensor clearly classified isopropanol from methanol and ethanol in the x axis. From the results, MIP method affects the classification process such as MIP gas sensor clearly classifying analyte alcohol vapor (propanol) from other vapor.

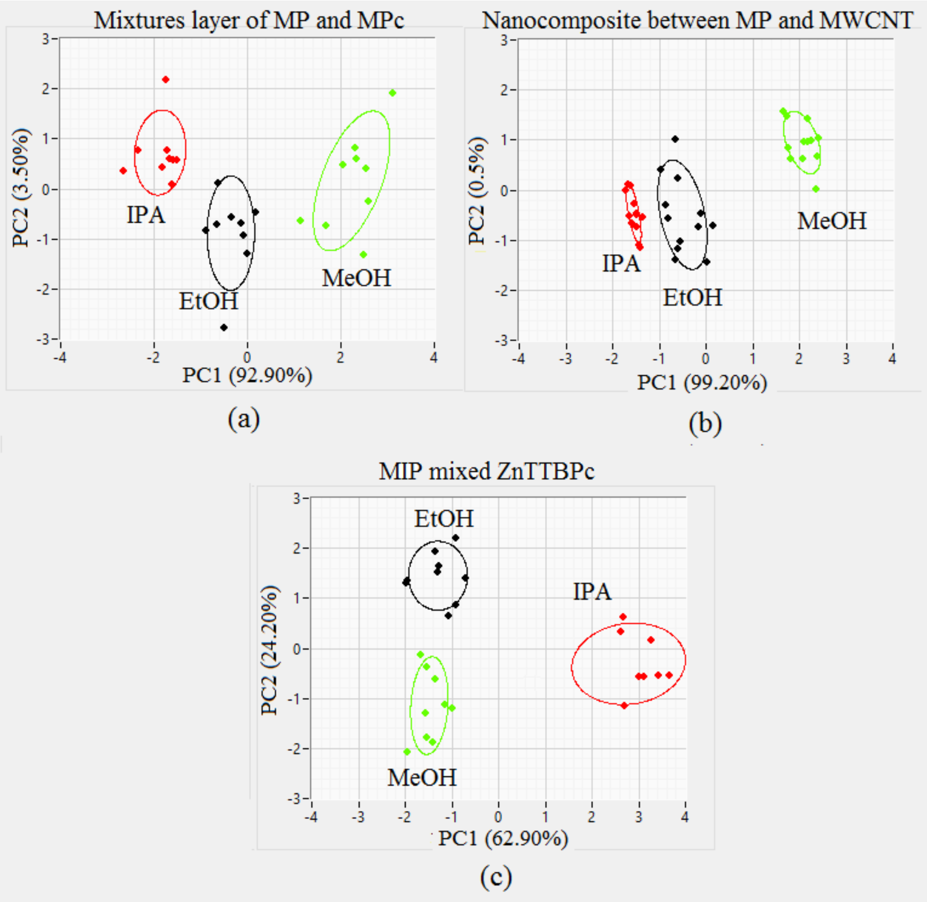

(a) (b) (c)

**Figure 7.1** PCA two dimensional score plot of (a) mixtures layer of MP and MPc, (b) nanocomposite between ZnTPP and MWCNT and (c-d) MIP mixed ZnTTBPc.

# REFERENCES

1 Pearce T. C., Schiffman S. S., Nagle H.T., et al. (2003) Handbook of machine olfaction electronic nose technology. WILEY-VCH Verlag GmbH & Co. KGaA, Weinheim.

2 Campbell M. (1997) Sensor system for environmental monitoring vol.1: sensor technologies. Blackie Academic & Professional, London.

3 Wongchoosuk C., Wisitsoraat A., et al (2010) Portable electronic nose based on carbon nanotube-SnO2 gas sensors and its application for detection of methanol contamination in whiskeys. Sens. Actuators B, 147, 392-399.

4 Lorwongtragool P., Wisitsoraat A., et al (2011) An electronic nose for amine detection based on polymer/SWNT-COOH nanocomposite. J. Nanosci. Nanotechnol., 11, 10454-10459.

5 Ding H., Erokhin V. et al (2000) A physical insight into the gas-sensing properties of copper II tetra-tert-butyl-5,10,15,20-tetraazaporphyrin Langmuir-Blodgett films. Thin Solid Films, 379, 279-286.

6 Long J., Xu J., et al (2011) A colorimetric array of metalloporphyrin derivatives for the detection of volatile organic compounds, Materials Science and Engineering B, 176, 1271– 1276.

7 Akrajas, Salleh M. M., et al. (2012) Optical Electronic Nose Based on Fe(III) Complex of Porphyrins Films for Detection of Volatile compounds. Key Engineering Materials, 495, 75-78.

8 Holonyak Jr., Bevacqua N., et al. (1962) Coherent (visible) light emission from Ga(As1-xPx) junctions. Applied Physics Letters, 1(4), 82-83.

9 Dasgupta P. K., Eom I.Y., et al. (2003) Light emitting diode-based detectors: Absorbance, fluorescence and spectroelectrochemical measurements in a planar flow-through cell. Analytica Chimica Acta, 500, 337-364.

10 Akrajas, Salleh M.M., et al. (2002) Enriching the selectivity of metalloporphyrins chemical sensors by means of optical technique. Sens. Actuators B: Chemical., 85, 191-196.

11 Spadavecchia J., Ciccarella G., et al. (2004) Spin-coated thin films of metal porphyrin-phthalocyanine blend for an optochemical sensor of alcohol vapour. Sens. Actuators B: Chemical, 100, 88-93.

12 Muthukumar P., & John S. A. (2011) Highly sensitive detection of HCl gas using a thin film of meso-tetra(4-pyridyl)porphyrin coated glass slide by optochemical method. Sens. Actuators B, 159,238-244.

13 Spadavecchia J., Ciccarella G., et al. (2003) Metallophthalocyanines thin films in array configuration for electronic optical nose applications. Sens. Actuators B, 96, 489-497.

14 Nguyen K.A., & Pachter R. (2001) Ground state electronic structures and spectra of zinc complexes of porphyrin, tetraazaporphyrin, tetrabenzoporphyrin, and phthalocyanine:A density functional theory study. J. Chem. Phys., 114, 10757-10767.

15 Saini, G. S. S., Singh, S., et al. (2009) Zinc phthalocyanine thin film and chemical analyte interaction studies by density functional theory and vibrational techniques. J. Phys. Condens. Matter, 21, 225006.

16 Zhang S., Xie C., et al. (2009) Spoiling and formaldehyde-containing detections in octopus with an E-nose. Food Chemistry 113, 1346-1350.

17 Roderick W. R. (1966) Current ideas on the chemical basis of olfaction. J. Chemical Education, 43(10), 510-520.

18 De La Presa Owens, Schlich C., et al. (1998) Using sensory and instrumental data to interpret the effect of storage at elevated temperatures on aroma of Chardonnay wines. Annals of the New York Academy of Sciences, 855, 854-859.

19 Mecea V. M. (2005) From quartz crystal microbalance to fundamental principles of mass measurements. Analytical Letters, 38, 753-767.

20 Latif U., Rohrer A., et al. (2011) QCM gas phase detection with ceramic materials VOCs and oil vapors. Anal Bioanal Chem, 400, 2457-2462.

21 Dickert F. L., Lieberzeit P. A., et al. (2004) QCM array for on-line-monitoring of composting procedures. Analyst, 129, 432-437.

22 Korposh S., Selyanchyn R., et al. (2010) Nano-assembled thin film gas sensors. IV. Mass-sensitive monitoring of humidity using quartz crystal microbalance (QCM) electrodes. Sens. Actuators B, 147, 599-606.

23 Barochi G., & Rossignola J., et al. (2011) Development of microwave gas sensors. Sens. Actuators B, 157, 374-379.

24 Zhang C., Bailey D. P., et al. (2006) Colorimetric sensor arrays for the analysis of beers: a feasibility study. J. Agric. Food Chem., 54, 4925-4931.

25 Zhang C., & Suslick K. S. (2007) Colorimetric sensor array for soft drink analysis. J. Agric. Food Chem., 55, 237-242.

26 Zhang C., & Suslick K. S. (2005) A colorimetric sensor array for organics in water. J. AM. Chem. Soc., 127, 11548-11549.

27 Barsan N., & Weimar U. (2012) Fundamentals of metal oxide gas sensors. The 14th international meeting on chemical sensors (IMCS 2012), 618-621.

28 Francia G. D., Alfano B., et al. (2009) Conductometric gas nanosensors, 2009, Article ID 659275, 18 pages.

29 Smith K. M. (1975) Porphyrin and metalloporphyrins. Elsevier Scientific Pub. Co., Newyork.

30 Moser F. H., & Thomas A. L. (1963) Phthalocyanine compounds. Reinhold, London.

31 Seo K. D., Lee M. J., et al (2012) Novel D-p-A system based on zinc porphyrin dyes for dye-sensitized solar cells: Synthesis, electrochemical, and photovoltaic properties. Dyes and Pigments, 94, 143-149.

32 Zou C., & Wu C.D. (2012) Functional porphyrinic metal-organic frameworks: crystal engineering and applications. Dalton Trans., 41, 3879-3888.

33 Ghasemi-Varnamkhasti M., Rodríguez-Méndez M. L., et al. (2012) Monitoring the aging of beers using a bioelectronic tongue. Food Control, 25, 216-224.

34 Li Y., Chen S., et al. (2012) Deposition-pressure-induced optimization of molecular packing for high-performance organic thin-film transistors based on copper phthalocyanine. J. Phys. Chem. C, 116, 4287-4292.

35 Berg K., Selbo P. K., et al. (2005) Porphyrin-related photosensitizers for cancer imaging and therapeutic applications. J. Microscopy, 218, 133-147.

36 Wang B., Zuo X., et al. (2007) Preparation, characterization and gas sensing properties of lead tetra-(tert-butyl)-5,10,15,20-tetraazaporphyrin spin-coating films. Sens. Actuators B, 125, 268-273.

37 Kladsomboon S., Pratontep S., et al. (2011) An artificial nose based on M-porphyrin (M = Mg, Zn) thin film and optical spectroscopy. J. Nanosci. Nanotechnol., 11, 10589-10594.

38 Richardson T.H., Dooling C.M., et al. (2002) Gas sensing properties of porphyrins assemblies prepared using ultra-fast LB deposition. Colloids and Surfaces A., 198-200, 843-857.

39 Li X.Y., Shen S.Y., et al. (1998) The gas response behavior of spin-coated phthalocyanine films to $NO_2$. Thin Solid Films, 324, 274-276.

40 Arshad S., Salleh M.M, et al. (2007) Detection of volatile organic compounds using titanium dioxide coated with dye-porphyrins thin films in bulk acoustic system. Solid State Sci. and Technol., 15, 175-181.

41 Salleh M.M., Umar A. A., et al. (2002) Optical sensing of capsicum aroma using four porphyrins derivatives thin films. Thin Solid Films, 417, 162-165.

42 Piletsky S.A., & Whitcombe M.J. (2013) Designing receptors for the next generation of biosensors. Springer Series on Chemical Sensors and Biosensors, 12, 167-187,

43 Humphris A. D. L., Miles M. J., et al. (2005) A mechanical microscope: High-speed atomic force microscopy. Applied Physics Letters, 2005, 86.

44 Arafat H. N., Nayfeh A. H., et al. (2008) Modal interactions in contact-mode atomic force microscopes. Nonlinear Dyn, 54, 151-166.

45 Parker T.C., Tang F., et al. (2008) Non-contact atomic force microscopy characterization of micro-cantilevers and piezo electric transducers with frequencies up to the tens of MHz. Sens. Actuators B: Chemical, 148, 306-310.

46 Zhang X., Zhang Y., et al. (2005) Infrared spectra of metal-free, N/,N-dideuterio, and magnesium porphyrins: density functional calculations. Spectrochimica Acta Part A, 61, 2576-2583.

47 Poveda L. A., Ferro V. R., et al. (2000) Molecular modeling of highly peripheral substituted Mg- and Zn-porphyrins. J. Physical Chemistry Chemical Physics , 2, 4147-4156.

48 Fernandez M. J., Fontecha J. L., et al. (2007) Discrimination of volatile compounds through an electronic nose based on ZnO SAW sensors. Sens. Actuators B, 127, 277-283.

49 Brereton R.G. (2003) Chemometrics data analysis for the laboratory and chemical plant. John Wiley & Sons, Ltd.

50 http://neurobot.bio.auth.gr.

51 Manno D., Micocci G., et al. (1999) Gas sensing properties of meso,meso-buta-1,3-diyne-bridged Cu(II) octaethylporphyrin dimer Langmuir–Blodgett films. Sens. Actuators B: Chemical, 57, 179-182.

52 Montmeat P., Madonia S., et al. (2005) Metalloporphyrins as sensing material for quartz-crystal microbalance nitroaromatics sensors. IEEE sens. J., 5, 174-179.

53 Jing L., Jianhua X., et al. (2011) Volatile organic compound colorimetric array based on zinc porphyrin and metalloporphyrin derivatives. Energy Procedia, 12, 625-631.

54 Słota R., Broda M. A., et al. (2011) Structural and molecular characterization of meso-substituted zinc porphyrins: A DFT supported study. Molecules, 16, 9957-9971.

55 Uttiya S., Kerdcharoen T., et al. (2008) Effect of structural transformation on the gas-sensing properties of phthalocyanine thin films. J. Korean Phys. Soc., 52, 1575-1579.

56 Asghari-Khiavi M., & Safinejad F. (2010) Theoretical studies on metal porphyrin halides: geometrical parameters and nonlinear optical responses. J. Mol. Model., 16, 499-503.

57 Lozano J., Santos J. P., et al. (2008) Enrichment sampling methods for wine discrimination with gas sensors. J. Food Compos. Anal., 21, 716-723.

58 Liu C.H. J., & Lu, W.C. (2007) Optical amine sensor based on metallophthalocyanine. J. Chin. Inst. Chem. Eng., 38, 483-488.

59 Shoji A., Tsukada N., et al. (2007) Plasma polymerization of manganese chloride tetraphenylporphyrin and evaluation of the thin film. J. Photopolym. Sci. Technol., 20, 241-244.

60 Zhang Y., Luo X., et al. (2012) Colorimetric artificial nose and pattern recognition methods for the concentration analysis of $NH_3$. Water Air Soil Pollut, 223, 2969-2977.

61 Spadavecchia J., Ciccarella G., et al. (2004) Variation in the optical sensing responses toward vapors of a porphyrin/phthalocyanine hybrid thin film. Chem. Mater., 16, 2083-2090.

62 Roales J., Pedrosa J. M., et al. (2011) Optimization of mixed Langmuir-Blodgett films of a water insoluble porphyrin in a calixarene matrix for optical gas sensing. Thin Solid Films, 519, 2025-2030.

63 Spadavecchia J., Rella R., et al. (2005) Optochemical vapour detection using spin coated thin film of ZnTPP. Sens. Actuators B, 115, 12-16.

64 Senthilarasu S., Hahn Y. B., et al. (2007) Structural analysis of zinc phthalocyanine (ZnPc) thin films: X-ray diffraction study. J. Appl. Phys., 102, 043512-043512-6.

65 Oku T., Takeda A., et al. (2010) Fabrication and characterization of fullerene-based bulk heterojunction solar cells with porphyrin, $CuInS_2$, diamond and exciton-diffusion blocking layer. Energies, 3, 671-685.

66 El-Nahass M.M., El-Khalek H.M., et al. (2012) Topological, morphological and optical properties of Gamma irradiated Ni (II) tetraphenyl porphyrin thin films. Opts. Communs., 285, 1872-1881.

67 Senthilarasu S., Hahn Y. B., et al. (2007) Structural analysis of zinc phthalocyanine (ZnPc) thin films: X-ray diffraction study. J. Appl. Phys. 102, 043512.

68 Kment S., Kluson P., et al. (2009) Preparation of thin phthalocyanine layers and their structural and absorption properties. Thin Solid Films, 517, 5274-5279.

69 Bevilaqua R. C.A., Zanella I., et al. (2010) Chlorophyll a and pheophytin a as gas sensors of $CO_2$ and $O_2$ molecules. Chem. Phys. Letters, 496, 310-315.

70 Ding H., Erokhin V., et al. (2000) A physical insight into the gas-sensing properties of copper II tetra-tert-butyl-5,10,15,20-tetraazaporphyrin Langmuir-Blodgett films. Thin Solid Films, 379, 279-286.

71 Umar A. A., Salleh M. M., et al. (2002) Enriching the selectivity of metallo porphyrins chemical sensors by means of optical technique. Sens. Actuators B, 85, 191-196.

72 Amamcharla J. K., & Panigrahi S. (2010) Simultaneous prediction of acetic acid/ethanol concentrations in their binary mixtures using metalloporphyrin based opto-electronic nose for meat safety applications. Sens. & Instrumen. Food Qual., 4, 51-60.

73 Kladsomboon S., Pratontep S., et al. (2010) Optical Electronic Nose Based on Porphyrin and Phthalocyanine thin films. proceeding of the electrical engineering/electronic computer telecommunication and information technology conference (ECTI2010), 565-568.

74 Sales N. F. d., & Mansur H. S. (2008) Chemsensor of $NO_2$ gas based on porphyrin of 5, 10, 15, 20-tetraphenylporphyrin LB films and LS films. Materials Research, 11(4), 477-482.

75 Natale C. D., Salimbeni D., et al. (2010) Porphyrins-based opto-electronic nose for volatile compounds detection. Sens. Actuators B, 65, 220-226.

76 Szkudlarz S. M., & Jelen H.H. (2010) Detection of olive oil adulteration with rapeseed and sunflower oils using mos electronic nose and SMPE-MS. J. Food Quality, 33, 21-41.

77 Zampolli S., Elmi I., et al. (2004) An electronic nose based on solid state sensor arrays for low-cost indoor air quality monitoring applications. Sens. Actuators B, 101, 39-46.

78 Srivastava S., Sharma S.S., et al. (2010) Study of chemiresistor type CNT doped polyaniline gas sensor. Synthetic Metals, 160, 529-534.

79 Dunbar A. D. F., Richardson T. H., et al. (2006) Investigation of free base, Mg, Sn, and Zn substituted porphyrin LB films as gas sensors for organic analytes. J. Phy. Chem., 110, 16646-16651.

80 Consales M., & Campopiano S. (2006) Carbon nanotubes thin films fiber optic and acoustic VOCs sensors: performances analysis. Sens. Actuators B, 118, 232-242.

81 Shih Y., & Li M. (2008) Adsorption of selected volatile organic vapors on multiwall carbon nanotubes. J. Hazardous Materials, 154, 21-28.

82 Kladsomboon S., Pratontep S., et al. (2009) Investigation of thermal and methanol-vapor treatments for MgTPP as an optical gas sensor. Proceedings of the 4th IEEE-NEM, 843-847.

83 Singjai P., Changsarn S., et al. (2007) Electrical resistivity of bulk multi-walled carbon nanotubes synthesized by an infusion chemical vapor deposition method. Mater. Sci. Eng. A, 443, 42-46.

84 Zhang X., Zang J., et al. (2005) Tubular composite of doped polyaniline with multi-walled carbon nanotubes. Appl. Phys. A, 80, 1813-1817.

85 Tonezzer M., Quaranta A., et al. (2006) Optical sensing responses of tetraphenyl porphyrins toward alcohol vapours: A comparison between vacuum evaporated and spin-coated thin films. Sens. Actuators B, 122, 620-626.

86 Song X., Miura M., et al. (1996) Langmuir-Blodgett films of stearic acid containing octakis ((methoxycarbonyl) methyl) – mesotetrakis (((eicosanyloxy)carbonyl)phenyl)porphyrin. Langmuir, 12, 2019-2027.

87 Castillero P., Sa´nchez-Valencia J. R., et al. (2010) Active and optically transparent tetracationic porphyrin/TiO2 composite thin films. Appl. Mater. Interfaces, 2(3), 712-721.

88 Wang Q., & Johnson J. K. (1999) Molecular simulation of hydrogen adsorption in single-walled carbon nanotubes and idealized carbon slit pores. J. Chem. Phys., 110(1), 577-586.

89 Bolton E. K., Sayler G. S., et al. (2002) Integrated CMOS photodetectors and signal processing for very low-level chemical sensing with the bioluminescent bioreporter integrated circuit. Sens. Actuators B, 85, 179-185.

90 Penza M., Rossi R., et al. (2010) Metalloporphyrins-modified carbon nanotubes networked films-based chemical sensors for enhanced gas sensitivity. Sens. Actuators B, 144, 387-394.

91 Dickert F. L., Lieberzeit P. A., et al. (2003) Chemical sensors from molecules complex mixtures to cells supramolecular imprinting strategies. Sensors, 3, 381-392.

92 Dickert F. L., Tortschanoff M., et al. (1999) Molecularly imprinted sensor layers for the detection of polycyclic aromatic hydrocarbons in water. Anal. Chem., 71, 4559-4563.

93 Liu W., Yan Y., et al. (2012) Study on the nano machining process with a vibrating AFM tip on the polymer surface. Appl. Surf. Sci., 258, 2620-2626.

94 Dickert F. L., Besenböck H., et al. (1998) Molecular imprinting through van der waals interactions: fluorescence detection of PAHs in water. Adv. Mater., 10(2) 149-151.

95 Kladsomboon S., & Kerdcharoen T. (2012) A method for detection of alcohol vapours based on optical sensing of MgTPP thin film by an optical. Anal. Chim. Acta., 757, 75-82.

96 Topal S. Z., Atilla D., et al. (2012) Investigation of optical and electrochemical properties as well as metal ion sensitivities of different number of crown ether appended phthalocyanines. J. Porphyrins Phthalocyanines, 16, 1-9.

97 Itagaki Y., Deki K., et al. (2005) Toxic gas detection using porphyrin dispersed polymer composites. Sens. Actuators B, 108, 393-397.

98 Ouyang Q., Zhao J., et al. (2013) Classification of rice wine according to different marked ages using a novel artificial olfactory technique based on colorimetric sensor array. Food Chemistry, 138, 1320-1324.

99 Lewis E., Sheridan C., et al. (2007) Principal component analysis and artificial neural network based approach to analyzing optical fiber sensors signals. Sens. Actuators A, 136, 28-38.

100 Olsen E., & Nielsen F. (2001) Predicting vapour pressures of organic compounds from their chemical structure for classification according to the VOC directive and risk assessment in general. Molecules, 6, 370-389.

# APPENDIX

## INTERNATIONAL PUBLICATIONS

1. Kladsomboon S., Pratontep S., Puntheeranurak T., and Kerdcharoen T., An Artificial Nose Based on M-Porphyrin (M = Mg, Zn) Thin Film and Optical Spectroscopy, Journal of Nanoscience and Nanotechnology, 11, 10589-10594, 2011.
2. Kladsomboon S., Lutz M., Pogfay T., Puntheeranurak T., and Kerdcharoen T., Hybrid Optical-Electrochemical Electronic Nose System Based on Zn-Porphyrin and Multi-Walled Carbon Nanotube Composite, Journal of Nanoscience and Nanotechnology, 12, 5240-5244, 2012.
3. Kladsomboon S. and Kerdcharoen T., A Method for Detection of Alcohol Vapors Based on Optical Sensing of MgTPP Thin Film by Optical Spectrometer and Principal Component Analysis, Analytica Chimica Acta, 757, 75–82, 2012.
4. Kerdcharoen T. and Kladsomboon S., Application of Nanomaterials in Sensors and diagnostic : Optical Chemical Sensor and Electronic Nose based on Porphyrin and Phthalocyanine, Springer Series on Chemical Sensors and Biosensors, 14, 237-255,2013.

## PATENT

1. Kerdcharoen T. and Kladsomboon S., Portable Optical-Electrochemical Electronic Nose based on Light Emitting Diode, Thai patent 1201002073, 3 May 2012.

# BIOGRAPHY

| | |
|---|---|
| **NAME** | Miss Sumana Kladsomboon |
| **DATE OF BIRTH** | February 3, 1984 |
| **PLACE OF BIRTH** | Samutsongkhram, Thailand |
| **INSTITUTION ATTENDED** | Bachelor of Science (Physics),<br>Kasetsart University, 2006<br>Grad. Dip (Teaching Science Profession),<br>Kasetsart University, 2007<br>Master of Science (Physics),<br>Mahidol University, 2009<br>Doctor of Philosophy (Physics),<br>Mahidol University, 2013 |
| **SCHOLARSHIP** | CHE-Ph.D.-SW-INV Scholarship from the Commission of Higher Education |
| **HOME ADDRESS** | 24/4 Moo4 Thai-Hard Sub-District,<br>Meang District, Samutsongkhram,<br>Thailand, 75000<br>Tel. +66-3476-7483 (home)<br>+66-9119-4147 (mobile) |
| **E-MAIL** | kl_sumana@yahoo.com<br>kladsomboon.sumana@gmail.com |